

Role of Topological Defects in Breaking and Enhancing Discrete Symmetries

By
Soumyadeep Bhattacharya
PHYS10201004008

The Institute of Mathematical Sciences, Chennai

A thesis submitted to the
Board of Studies in Physical Sciences
In partial fulfillment of requirements
For the Degree of
DOCTOR OF PHILOSOPHY

of
HOMI BHABHA NATIONAL INSTITUTE



June, 2016

Homi Bhabha National Institute

Recommendations of the Viva Voce Board

As members of the Viva Voce Board, we certify that we have read the dissertation prepared by Soumyadeep Bhattacharya entitled “Role of Topological Defects in Breaking and Enhancing Discrete Symmetries” and recommend that it may be accepted as fulfilling the dissertation requirement for the Degree of Doctor of Philosophy.

_____ Date:

Chairman - Balachandran Sathiapalan

_____ Date:

Guide/Convener - Purusattam Ray

_____ Date:

Examiner - Chandan Dasgupta

_____ Date:

Member 1 - Rajesh Ravindran

_____ Date:

Member 2 - Ronojoy Adhikari

Final approval and acceptance of this dissertation is contingent upon the candidate's submission of the final copies of the dissertation to HBNI.

I hereby certify that I have read this dissertation prepared under my direction and recommend that it may be accepted as fulfilling the dissertation requirement.

Date:

Place:

Guide

STATEMENT BY AUTHOR

This dissertation has been submitted in partial fulfillment of requirements for an advanced degree at Homi Bhabha National Institute (HBNI) and is deposited in the Library to be made available to borrowers under rules of the HBNI.

Brief quotations from this dissertation are allowable without special permission, provided that accurate acknowledgement of source is made. Requests for permission for extended quotation from or reproduction of this manuscript in whole or in part may be granted by the Competent Authority of HBNI when in his or her judgement the proposed use of the material is in the interests of scholarship. In all other instances, however, permission must be obtained from the author.

Soumyadeep Bhattacharya

DECLARATION

I, hereby declare that the investigation presented in the thesis has been carried out by me. The work is original and has not been submitted earlier as a whole or in part for a degree / diploma at this or any other Institution / University.

Soumyadeep Bhattacharya

ACKNOWLEDGEMENTS

I thank Purusattam Ray for suggesting that I examine the phase diagram of spin models with discrete symmetries as a part of my research work towards a thesis and for helpful discussions regarding the topic. I also thank the members of the Doctoral Committee for their lasting patience in allowing me to work on the present topic at my own pace.

I thank Rajesh Ravindran for introducing me to a variety of computational techniques in statistical physics, Ronojoy Adhikari for discussions on the fundamentals of thermodynamics, renormalization and the role of topological defects in classical systems, Syed Hassan for discussions on the physics of quantum phase transitions beyond the Landau paradigm, Deepak Dhar for discussions on the percolation properties of domain walls and Kedar Damle for discussions on the role of defects in spin models with higher symmetries.

I also thank Bikas Chakrabarti, Parongama Sen, Chandan Dasgupta, Satya Majumder, Krishnendu Sengupta, Subir Sachdev, Ganapathy Baskaran, Ganapathy Murthy, Naina Shah, Gabriel Aeppli, Mukul Laad, David Mukamel, Christophe Chatelain, Tim Garoni, Martin Weigel, Wolfhard Janke, Ramesh Anishetty, Sanatan Digal, Biswanath Layek, Ajit Srivastava, Pushan Majumdar, Subhash Karbelkar, Diptarka Das, Suman Sinha and Joyjit Kundu for interesting discussions on various aspects of the present topic.

I also thank Mangala Pandi, Malladi Ramakrishna and Tejaswi Nanditale for discussions on methods for optimizing the numerical techniques used in simulation of spin models.

Abstract

Phase transitions accompanied by spontaneous breaking of continuous symmetries have been studied extensively in condensed matter and high energy physics. In this thesis we investigate the spontaneous breaking of discrete symmetries, specifically in spin models with three-fold, four-fold and higher discrete symmetries. We show that an interplay between the topological defects - domain walls and vortices - in these models drives the discrete symmetry to be completely broken, partially broken and even enhanced to a continuous $U(1)$ symmetry. We show that in two dimensions, percolation of domain walls drives a transition from a symmetry broken ordered phase to a symmetry enhanced quasi long range ordered phase which, in turn, undergoes a transition to the symmetry restored disordered phase when vortices proliferate. We highlight a flaw in the standard method for calculating winding numbers and propose a new method which correctly identifies vortices. We show that suppression of vortices in models with even number of states leads to an intermediate partially ordered phase and that additional suppression of domain walls, separating opposite spin states, is required to manifest the symmetry enhanced phase. We show that spin models with three or higher number of states exhibit a partial symmetry broken phase instead of symmetry enhanced phase in three dimensions as individual types of domain walls are able to percolate on their own. We also obtain a variety of phases by suppressing defects belonging to subgroups of the model's symmetry. Upon enhancing the formation of vortices instead of suppressing them, we obtain a vortex-antivortex lattice phase in two dimensions and a vortex condensate phase in three dimensions.

List of Publications arising from the thesis

- Journal

1. “Quasi-Long-Range Order and Vortex Lattice in the Three-State Potts Model”

Soumyadeep Bhattacharya and Purusattam Ray

Physical Review Letters, **2016**, 116, 097206.

- Conferences

1. “Emergence of U(1) symmetry in Z(q) clock model”

Soumyadeep Bhattacharya and Purusattam Ray

AIP Conference Proceedings, **2012**, 1447, 91.

- Others

1. “U(1) Emergence versus Chiral Symmetry Restoration in the Ashkin Teller Model”

Soumyadeep Bhattacharya

arXiv:1601.02755.

2. “Partial Breaking of Three-Fold Symmetry via Percolation of a Domain Wall”

Soumyadeep Bhattacharya and Purusattam Ray

arXiv:1608.05901.

List of Conferences Attended

1. FracMeet 2011

The Institute of Mathematical Sciences, Chennai, January 2011

2. DAE Symposium on Solid State Physics

SRM University, Chennai, December 2011

3. FracMeet 2012

The Institute of Mathematical Sciences, Chennai, January 2012

4. INCF Workshop on Neuroinformatics of Sensory-Motor Integration

The Institute of Mathematical Sciences, Chennai, November 2012

5. Bayes by the Bay

Pondicherry, January 2013

6. Diversity and Complexity

Saha Institute of Nuclear Physics, Kolkata, January 2013

7. FracMeet 2013

The Institute of Mathematical Sciences, Chennai, January 2013

8. Thermalization: From Black Holes to Glasses

International Centre for Theoretical Sciences, Bengaluru, June 2013

9. Growing Length Scale Phenomena in Condensed Matter Physics

Jawaharlal Nehru Centre for Advanced Scientific Research, Bengaluru, October 2015

List of changes as suggested by Examiners

Overall

- Added missing page numbers.
- Made some of the figure captions more self-contained.
- Corrected some cross-references within the document.

Chapter 1

- Modified the description of phases in models of crystal surfaces in Sec. 1.1 to highlight the equilibrium nature of the roughening and pre-roughening transition.
- Added clarification about dimensionality in Sec. 1.1: The models show only these two phases **on the square lattice** when $n \leq 4$.
- Changed snapshots of typical spin configurations in Fig. 1.2 from that of the \mathbb{Z}_4 ferromagnet to that of the \mathbb{Z}_6 ferromagnet, as the latter model exhibits an intermediate U(1) phase without the need for vortex suppression.
- Added clarification about ordering in the 2D XY model, in Sec. 1.5.5: Since the model does not exhibit symmetry breaking at any **non-zero** temperature, . . .

Chapter 2

- Added clarification regarding the n -fold symmetric order parameter distribution in Sec. 2.1.3: The n -fold symmetry in the distribution appears because the distribution is an accumulation of results from an **ensemble of simulations**, each starting from a completely ordered configuration belonging to one of the n states.

- Added clarification in Sec. 2.2.2 regarding the gradual variation of order-parameter and possibility of a higher-order transition in the \mathbb{Z}_3 ferromagnet with weak suppression of vortices.
- Added quantitative estimates of transition temperatures and defect proliferation temperatures in Sec. 2.2.3, Sec. 3.5.
- Added clarification in Sec. 2.3.1 that the domain wall percolation temperature in the vortex suppressed \mathbb{Z}_3 ferromagnet on the square lattice is estimated to be **very close**, but not necessarily equal to, the thermodynamic transition between the symmetry enhanced and symmetry restored phases.
- Added discussion on the change in behavior of specific heat in Sec. 2.2.3 as the order-disorder transition in the 2D \mathbb{Z}_3 model splits into two transitions with suppression of vortices.

Chapter 3

- Added plots for two-point correlations establishing the QLRO nature of the intermediate phase uncovered by vortex (and $\pm\pi$ domain wall) suppression: in the 2D \mathbb{Z}_5 ferromagnet in Fig. 3.6, in the 2D \mathbb{Z}_4 ferromagnet in Fig. 3.7 and in the 2D \mathbb{Z}_6 ferromagnet in Fig. 3.9.
- Added clarification regarding the use of the new method for calculating winding number in Sec. 3.3.3 and Sec. 1.5.3.
- Added text in Sec. 3.8 stating that the disordered phase for $\lambda = 0$ occurs for $T > 0$.

Chapter 4

- Added text in the introduction of Chapter 4 to highlight the study of models in three dimensions.

- Added $\lambda = 0$ to the caption of Fig. 4.1.
- Changed color scheme to better distinguish between the three spin states in Fig. 4.1a, Fig. 4.1b and Fig. 4.5b.
- Added analysis of percolation properties for (0 | 1) domain walls in the QLRO phase of the 2D \mathbb{Z}_3 ferromagnet in Sec. 4.4.4, establishing the percolation threshold behavior across all temperatures in that phase.

Chapter 5

- Modified the text in Sec. 5.1.2 to show how the six-fold states map onto the effective three-fold states and how the corresponding six-fold angles θ map onto the effective three-fold angles θ_3 .

Chapter 7

- Added a table summarizing the different phases obtained by manipulating the defects in all the models discussed in this thesis.

Contents

1	Introduction	39
1.1	Symmetry Enhancement	40
1.2	Partial Symmetry Breaking	43
1.3	Continuum Theory for Models with \mathbb{Z}_n Symmetries	45
1.4	Topological Defects	49
1.5	Defects in Models with \mathbb{Z}_n Symmetries	51
1.5.1	Domain Walls	52
1.5.2	Domain Wall Driven Phase Transitions	52
1.5.3	Vortices	55
1.5.4	Relationship Between Vortices and Domain Walls	56
1.5.5	Vortex Driven Phase Transitions	57
1.5.6	Energy versus Entropy Balance for Defects	58
1.6	Outline of the Thesis	62
2	Symmetry Enhancement via Domain Wall Percolation	65
2.1	\mathbb{Z}_3 Clock Ferromagnet on the Square Lattice	66

2.1.1	Hamiltonian	66
2.1.2	Monte Carlo Simulation Algorithm	66
2.1.3	Order Parameter	68
2.1.4	Thermodynamic Observables	69
2.1.5	Phase Diagram	69
2.2	Vortex Suppression	71
2.2.1	Increased Cost of Computation	71
2.2.2	Weak Suppression of Vortices	72
2.2.3	Strong Suppression of Vortices	74
2.3	Symmetry Enhanced Intermediate Phase	76
2.3.1	Domain Wall Percolation	76
2.3.2	Two-Point Correlations	79
3	Vortex Winding Number and Role of $\pm\pi$ Domain Walls	81
3.1	\mathbb{Z}_4 Clock Ferromagnet on the Square Lattice	82
3.1.1	Hamiltonian	82
3.2	Phase Diagram	82
3.3	Winding Number Calculation	85
3.3.1	Standard Method	85
3.3.2	Violation of Modular Arithmetic	86
3.3.3	Modified Method	87

3.4	\mathbb{Z}_4 Clock Ferromagnet on the Square Lattice Revisited	89
3.5	\mathbb{Z}_5 Clock Ferromagnet on the Square Lattice	91
3.6	Role of $\pm\pi$ Domain Walls	94
3.7	\mathbb{Z}_6 Clock Ferromagnet on the Square Lattice	97
3.8	\mathbb{Z}_3 Antiferromagnet on the Square Lattice	100
4	Partial Symmetry Breaking via $(0 1)$ Domain Wall Percolation	105
4.1	\mathbb{Z}_3 Ferromagnet on the Simple Cubic Lattice	106
4.1.1	Hamiltonian	106
4.1.2	Order Parameter Distribution	107
4.2	Percolation of Domain Walls and Vortex Strings	107
4.2.1	Phase Diagram	110
4.3	Suppression of Vortex Strings	110
4.3.1	Weak Suppression	110
4.3.2	Strong Suppression	112
4.4	Partial Symmetry Broken Intermediate Phase	114
4.4.1	Order Parameter	114
4.4.2	Proliferation Pattern of Domain Walls	116
4.4.3	Relative Relabelling of Spin States	117
4.4.4	Percolation Properties of $(a b)$ Domain Walls	118
4.4.5	Percolation of $(0 1)$ Domain Walls	121

4.5	\mathbb{Z}_4 Clock Ferromagnet on the Simple Cubic Lattice	122
5	Role of Subgroup Defects	127
5.1	\mathbb{Z}_6 Clock Ferromagnet on the Simple Cubic Lattice	128
5.1.1	Suppression of \mathbb{Z}_6 Vortex Strings and $\pm\pi$ Domain Walls	129
5.1.2	Restoration of \mathbb{Z}_3 Symmetry	131
5.1.3	Percolation of $(a b)$ Domain Walls	136
5.1.4	Suppression of \mathbb{Z}_3 Vortex Strings	136
5.1.5	Suppression of $\pm 2\pi/3$ Domain Walls	138
5.2	\mathbb{Z}_3 Antiferromagnet on the Simple Cubic Lattice	139
6	Melting of Vortex-Antivortex Lattice	141
6.1	\mathbb{Z}_3 Clock Ferromagnet on the Square Lattice	142
6.2	Weak Enhancement of Vortices	142
6.2.1	Strong Enhancement of Vortices	144
6.3	Vortex-Antivortex Lattice	144
6.3.1	Non-ergodic Nature of Single Spin-Flip Algorithm	146
6.3.2	Wang-Landau Algorithm for Defects	148
6.4	Phase Diagram of the \mathbb{Z}_3 Ferromagnet on the Square Lattice	149
6.5	Defect Based Order Parameter	150
6.6	Melting in n -state Potts Ferromagnets on the Square Lattice	152
6.7	\mathbb{Z}_3 Ferromagnet on the Simple Cubic Lattice	152

Synopsis

Different phases of matter can be classified according to the manner in which the symmetry of the constituent microscopic atoms manifests itself at the macroscopic scale. Commonly studied systems usually exhibit phases where the symmetry gets spontaneously broken or remains fully restored. Systems with discrete symmetries, on the other hand, exhibit richer variety of intermediate phases where the symmetry can get partially broken [1,2] or even enhanced to a continuous one [3-8]. The manifestation of these intermediate phases in statistical and quantum condensed matter models has triggered exciting advances in materials science and their manifestation in lattice gauge models has provided key insights into high energy physics.

While the notion of symmetry serves as a useful tool for characterizing phases and tracking transitions between them, it does not provide an answer to the question of what leads to the formation of the phases or what drives the transitions. Transitions characterized by spontaneous breaking of continuous symmetries have been shown to be driven by the proliferation of topological defects. Defects are regions of singularity in the system which cannot be removed by continuous deformations [9-11]. Depending on the symmetry and dimensionality of the system, these regions can appear as points (vortices, monopoles), lines (vortex strings) or, in some cases, even extend throughout the system (skyrmions, textures). The superfluid-normal transition, for example, is driven by the proliferation of vortices in thin films of superfluid [12] and by the proliferation of vortex strings in bulk superfluid [13,14]. The onset of paramagnetism in the Heisenberg ferromagnet is driven

by the proliferation of monopoles [15]. Phase transitions in superconductors [16] and liquid crystals [17] are also driven by the proliferation of defects. Extensive investigations into these systems have highlighted the important role played by topological defects in governing many-body physics. However, most of the studies have remained restricted to the role of a single type of defect. Models with discrete symmetries sustain domain wall defects in addition to the defects of their continuous symmetric counterparts. The interplay between the multiple defects can drive a variety of phase transitions and lead to a rich phase diagram [18,19]. A systematic study of this intriguing possibility is lacking as defects in systems with discrete symmetries have not received as much attention as those in systems with continuous symmetries.

In this thesis, we study the role played by defects in some simple spin models with discrete symmetries. The systems under consideration sustain domain wall and vortex defects. We show that phase transitions in the models, which have hereto been extensively characterized using symmetry based observables, are driven either by the proliferation of a single type of defect or by the simultaneous proliferation of multiple types of defects. Additionally, we demonstrate that manipulation of these defects can shift or split the phase transitions and lead to the formation of new phases which have not been reported before. Here, we briefly outline the work presented in the thesis.

Quasi-Long- Range Order Via Proliferation of Domain Walls

We begin our investigation by considering the simplest spin model which can sustain domain walls and vortices: the three state Potts ferromagnet on a square lattice. We show that the order-disorder transition in this model is driven by a simultaneous proliferation of the two types of defects. When we increase the core energy of the vortices, their formation gets suppressed and the transition is observed to shift towards higher temperatures. Above a certain threshold of suppression, the simultaneous proliferation decouples and the vortices proliferate at a temperature higher than that of the domain walls. This decoupling is shown to split the order-disorder transition and open up an intermediate phase

where the three-fold symmetry enhances to $U(1)$ and the order becomes quasi-long-range. We demonstrate that the transition from the symmetry broken ordered phase to the symmetry enhanced phase is driven by the proliferation of domain walls while the transition from the symmetry enhanced to the symmetry restored disordered phase is driven by the proliferation of vortices. Does this picture carry over to n -state models for all values of n ? Such a scenario seems plausible because energy versus entropy balance [18-19], renormalization group [3] and Monte Carlo [6-8] calculations suggest that n -state clock models exhibit an intermediate quasi-long-range ordered phase for large n . We show that the models, for higher n , indeed exhibit such an intermediate phase due to the proliferation of domain walls. However, the disordering transition for models with even values of n is no longer driven solely by the proliferation of vortices. We show that domain walls separating opposite pairs of spin states play a crucial role along with the vortices in driving the transition. The significance of these opposite state domain walls decreases for large n . In the $n \rightarrow \infty$ limit (XY model), the disordering transition is found to be driven solely by the proliferation of vortices as expected [12]. In presenting this result, we also point out a fundamental flaw in the current procedure for calculating winding numbers on lattices. This flaw, which results in the identification of unphysical vortices, arises because a rule of modular arithmetic is satisfied. We propose a modified method for calculating the winding number which violates the rule and is, therefore, able to identify the correct vortices.

Partial Order via Percolation of a Single Domain Wall

The formation of a symmetry enhanced phase via domain wall proliferation raises an important question: can the same mechanism lead to symmetry enhancement in higher dimensions? We consider the three state Potts ferromagnet on a simple cubic lattice and find that the order-disorder transition in the model is also driven by a simultaneous proliferation of domain walls and vortex strings. Suppression of the vortex strings shifts the transition to higher temperatures and above a certain threshold, splits the transition into

two. Interestingly, however, we find that the intermediate phase in this case is not symmetry enhanced. Even though domain walls proliferate in the intermediate phase while vortex strings do not, the three-fold symmetry is broken, albeit in a manner different from that in the ordered phase, which leads to partial order. This phase poses an interesting question: how can domain wall proliferation lead to symmetry enhancement in two dimensions but symmetry breaking in three dimensions? We investigate the proliferation pattern of the domain walls in terms of percolation observables. We find that a single type of domain wall percolates on its own in the symmetry broken phase and stabilizes the partial order. Such a stabilizing mechanism is found to be absent in the two dimensional system as the domain wall appears to remain at a percolation threshold throughout the symmetry enhanced phase. A similar picture is obtained for the four-state Ashkin-Teller model in three dimensions. The order-disorder transition in the model is found to be driven by the simultaneous proliferation of domain walls and vortex strings. When the vortex strings and opposite state domain walls are suppressed, the transition splits and opens up the partially ordered intermediate phase.

Partial Order Via Proliferation of Subgroup Defects

Following the results obtained in the previous section, we would expect that the order-disorder transition in n -state models with larger n will split and make way for a partially ordered intermediate phase when vortices (and opposite state domain walls for even n) is suppressed. Surprisingly, however, this expectation does not hold true even for the next simplest model with even n : the six state ferromagnet. Suppression of the two types of defects destroys the disordering transition but the model appears to exhibit an intermediate region where the six-fold symmetry is broken in a manner similar to that in the ordered phase. This intermediate region, as we show, is a prime example of how defects belonging to symmetry subgroups can drive new types of phase transitions. The six state model can be decomposed into an Ising and a three state model. Naturally, the relevant defects in the system are domain walls belonging to the Ising model, domain walls and vortices

belonging to the three state model and vortices belonging to the six state model as a whole. We show that suppression of the six state vortices and opposite state domain walls leaves the vortices and domain walls of the three state model to proliferate and form a three state disordered intermediate phase. Interestingly, this intermediate phase appears to break the same symmetry as that broken in the ordered phase. We show that the phase transition from the ordered phase to the intermediate phase is missed when using the standard six state order parameter but is clearly captured using an effective three state order parameter. Following this observation, we demonstrate that the six state model can exhibit a rich cascade of phases where the Ising model is disordered but the three state model is ordered and vice versa.

Role of Defects in Antiferromagnets

In the previous sections, we restricted ourselves to the physics of ferromagnets. A variety of statistical and quantum systems, on the other hand, are modelled by discrete spin models with antiferromagnetic interactions. Antiferromagnets on bipartite lattices, in particular, are particularly interesting because their physics can be effectively mapped onto that of certain ferromagnets. Specifically, n -state antiferromagnets map onto n -state ferromagnets for even n and $2n$ -state ferromagnets for odd n . Does the defect driven mechanism discussed so far for the ferromagnets carry over to the antiferromagnets as well? We start with the three state Potts antiferromagnet and show that its phase diagram can be explained in terms the interplay between defects of the six state ferromagnet. In particular, we show that the antiferromagnet on a square lattice exhibits disorder at all non-zero temperatures because the six state vortices begin to proliferate near zero temperature. In three dimensions, the antiferromagnet exhibits a disordering transition at a non-zero temperature from a broken sublattice symmetry phase at low temperatures. We show that this phase corresponds to the three state vortex proliferated intermediate phase in the six state ferromagnet and is, therefore, an example of a partially ordered phase. We also show how the manipulation of domain walls and vortices opens up phases discovered

for the six state ferromagnet in this antiferromagnet as well.

Melting of Vortex-Antivortex Lattice

A major portion of this thesis has focussed on the effect of suppressing vortices. In a variety of systems, superfluids and superconductors in particular, the core energy of vortices can be quite low. The resulting enhancement of vortex formation can lead to a qualitatively different set of phases. We revisit the three state Potts model on the square lattice and show that the order-disorder transition becomes sharper when the vortex core energy is decreased. Below a certain threshold of decrease, the transition splits and an intermediate phase opens up in which the vortices and antivortices pile up into alternate sublattice sites and form a vortex-antivortex lattice of their own. As the core energy is decreased further, the transition from the ordered phase to this intermediate phase is pushed towards zero temperature while the lattice melting transition from the intermediate phase to the disordered phase is pushed towards higher temperature. We show that this melting transition cannot be captured by a conventional symmetry based order parameter as the spin texture in the intermediate phase involves an equal proportion of all spin states, albeit in a weave pattern. However, the transition is shown to be clearly captured by a dilute antiferromagnetic Ising order parameter in terms of the vortices. Demonstration of vortex-antivortex lattice formation in the even state models, on the other hand, is shown to be quite tricky because it requires the simultaneous enhancement of vortices as well as opposite state domain walls. In three dimensions, characterization of the phase in even the three state Potts model is shown to be quite difficult as the vortices and antivortices cannot form a perfect lattice due to geometrical constraints. The presence of voids in the lattice pattern results in a large ground state entropy and the system appears to form a vortex string condensate instead. Response functions indicate a phase transition from this phase to the disordered phase but an order parameter capturing the transition remains as an open problem.

[1] R. V. Ditzian, J. R. Banavar, G. S. Grest and L. P. Kadanoff Phys. Rev. B **22**, 2542

(1980).

[2] N. Todoroki, Y. Ueno and S. Miyashita Phys. Rev. B **66**, 214405 (2002).

[3] J. V. José *et al.*, Phys. Rev. B **16**, 1217 (1977).

[4] S. Elitzur, R. Pearson and J. Shigemitsu, Phys. Rev. D **19**, 3698 (1979).

[5] J. Fröhlich and T. Spencer, Commun. Math. Phys. **83**, 411 (1982).

[6] C. M. Lapilli, P. Pfeifer and C. Wexler, Phys. Rev. Lett. **96**, 140603 (2006).

[7] S. K. Baek, P. Minnhagen and B. J. Kim, Phys. Rev. E **80**, 060101 (2009).

[8] O. Borisenko *et. al.*, Phys. Rev. E **85**, 021114 (2012).

[9] N. D. Mermin, Rev. Mod. Phys. **51**, 591 (1979).

[10] P. M. Chaikin and T. C. Lubensky, *Principles of Condensed Matter Physics* (Cambridge University Press, 2000).

[11] A. Vilenkin and E. P. S. Shellard, *Cosmic Strings and Other Topological Defects* (Cambridge University Press, 2000).

[12] J. M. Kosterlitz and D. J. Thouless, J. Phys. C, **6**, 1181 (1973).

[13] G. Kohring, R. E. Shrock and P. Wills, Phys. Rev. Lett. **57**, 1358 (1986).

[14] S. R. Shenoy, Phys. Rev. B **42**, 8595 (1990).

[15] M. Lau and C. Dasgupta, J. Phys. A **21**, L51 (1988).

[16] S. C. Zhang, Phys. Rev. Lett. **71**, 2142 (1993).

[17] P. E. Lammert, D. S. Rokhsar and J. Toner, Phys. Rev. Lett. **70**, 1650 (1993).

[18] M. B. Einhorn, R. Savit and E. Rabinovici, Nucl. Phys. B **170**, 16 (1980).

[19] G. Ortiz, E. Cobanera and Z. Nussinov, Nucl. Phys. B **854**, 780 (2012).

List of Figures

1.1	Typical cross sections showing equilibrium texture of crystal surfaces at (a) low and (b) high temperatures.	41
1.2	Typical spin configurations in different phases of a \mathbb{Z}_6 ferromagnet on the square lattice.	42
1.3	Partial symmetry breaking leads to (a) an up-down-up-down texture for layers of crystals, and (b) dominance of two consecutive spin directions in a three dimensional \mathbb{Z}_4 ferromagnet (a two dimensional slice is shown here).	44
1.4	Schematic of the potential (above) for the complex scalar theory in the presence of symmetry breaking perturbations for $n = 4$ is shown with projection of the potential minima on the order parameter space (below) at different values of the renormalized parameters, corresponding to (a) the \mathbb{Z}_4 symmetry restored phase, (b) the \mathbb{Z}_4 symmetry broken phase, (c) the partial symmetry broken phase, (d) the emergent \mathbb{Z}_8 phase, and (e) the emergent U(1) phase.	47
1.5	Superfluid-normal phase transition driven by the proliferation of vortex (blue) and antivortex (red) strings in three dimensions. Top layers show two dimensional slices of field configurations belonging to the XY model of superfluid at each temperature T	51

1.6	Domain walls (gray) residing on elements of the dual lattice (dashed lines) are shown for configurations of \mathbb{Z}_4 spins on (a) the square lattice, and (b) the simple cubic lattice.	53
1.7	Proliferation of domain walls (black) across the order-disorder transition of the Ising model in (a) two dimensions, and (b) three dimensions. . . .	54
1.8	Vortices (blue) and antivortices (red) residing on elements of the dual lattice (dashed lines) are shown for configurations of \mathbb{Z}_4 spins on (a) the square lattice, and (b) the simple cubic lattice.	56
1.9	Phase transition in the XY model driven by proliferation of vortices (red) and antivortices (blue) on a square lattice.	58
2.1	Typical spin configurations obtained on a $L = 16$ square lattice for the \mathbb{Z}_3 ferromagnet at different temperatures T overlaid with domain wall (black), vortex (blue) and antivortex (red) defects. The order parameter distribution obtained for a $L = 32$ system is also shown at the corresponding temperatures.	67
2.2	Top Panel: The density of domain walls and vortices increases simultaneously across the order-disorder transition captured by the decay in magnetization and the peak in magnetic susceptibility. Bottom Panel: Upon slightly raising the core energy of the vortices by an amount λ , proliferation of the two types of defects as well as the transition shift to a higher temperature. System sizes correspond to $L = 16$ (circle), $L = 32$ (square) and $L = 64$ (triangle).	70

2.3	With strong suppression of vortices, the vortices proliferate at a temperature higher than that of domain wall proliferation. This decoupling of defect proliferation forces the order-disorder transition to split and admit an intermediate phase. The split is evidenced by a two-step decay in the magnetization $ m $ and double peaks in the susceptibility χ . The transition from the intermediate phase to the disordered phase shifts to higher temperatures with increasing λ . System sizes correspond to $L = 16$ (circle), $L = 32$ (square) and $L = 64$ (triangle).	73
2.4	Variation of specific heat in the 2D \mathbb{Z}_3 ferromagnet at different values of λ . System sizes correspond to $L = 16$ (purple), $L = 32$ (green) and $L = 64$ (red).	75
2.5	The intermediate phase uncovered using strong suppression of vortices ($\lambda = 100$) reveals (a) an emergent U(1) symmetry in the order parameter distribution obtained at $T = 5$ for a $L = 32$ system, and (b) proliferation of domain walls but absence of vortices in typical spin configurations obtained at the same temperature.	77
2.6	Measurement of standard percolation observables for geometric domain walls show that (a) the percolation strength P_{dw} increases in the intermediate phase $T > 2.2$, (b) the spanning probability Π_{dw} saturates to unity in that phase and (c) the average size of domain walls χ_{dw} peaks near the transition from the ordered phase to the intermediate phase. System sizes correspond to $L = 16$ (circle), $L = 32$ (square) and $L = 64$ (triangle). . . .	78
2.7	Measurement of two-point correlation for a $L = 256$ system shows a power-law decay whose exponent η changes with temperature, thus confirming the QLRO nature of the phase.	80

3.1	<p>Top panel: The magnetization m decays across the order-disorder transition in the \mathbb{Z}_4 clock ferromagnet on a square lattice, accompanied by a simultaneous increase in the densities of domain walls ρ_{dw} and vortices ρ_{vx}. Bottom panel: With extreme suppression of vortices, the order-disorder transition splits and the disordering transition recedes to very high temperatures. The system shows a single transition order-QLRO transition accompanied by the proliferation of domain walls. Data has been obtained for system sizes $L = 16$ (circle), $L = 32$ (square) and $L = 64$ (triangle).</p>	83
3.2	<p>Typical spin and defect configurations obtained for the \mathbb{Z}_4 clock ferromagnet on a $L = 16$ lattice and the order parameter distribution obtained for a $L = 32$ system obtained in the ordered phase (a),(d); in the disordered phase (b),(e); in the intermediate symmetry enhanced phase (c),(f). Note the unusual dominance of vortices (blue) over antivortices (red) in the disordered phase. A vortex with winding number +2 (green) is also present in the configuration for that phase.</p>	84
3.3	<p>Vortex defects identified using the standard method in (a) the anticlockwise sense and (b) the clockwise sense for a configuration of \mathbb{Z}_4 spin states. Red, blue and green denote defects with winding number -1, +1 and +2, respectively.</p>	86
3.4	<p>Vortex defects identified using the modified method in (a) the anticlockwise sense and (b) the clockwise sense for a configuration of \mathbb{Z}_4 spin states. Red, blue and green denote defects with winding number -1, +1 and +2, respectively.</p>	88
3.5	<p>Revision of the data displayed in Fig. 3.1 and Fig. 3.2, arising due to the simulation being reperformed using our modified method for calculating winding number.</p>	90

3.6 Top panel: The decay of $m_{5\phi}$ marks the onset of symmetry enhancement and the decay of magnetization marks the disordering transition in the \mathbb{Z}_5 clock ferromagnet on a square lattice. The former is accompanied by an increase in the density of domain walls ρ_{dw} while the latter is accompanied by increase in vortex density ρ_{vx} . Middle panel: With extreme suppression of vortices, the disordering transition recedes to very high temperatures. The system shows a single transition order-QLRO transition accompanied by the proliferation of domain walls. System sizes are the same as those in (Fig. 3.1). Bottom panel: Two-point correlations at different temperatures in the QLRO phase for a $L = 256$ system with $\lambda = 100$ 93

3.7 Extreme suppression of vortices and $\pm\pi$ domain walls in the \mathbb{Z}_4 clock ferromagnet on the square lattice removes the disordered phase and leaves the model with a single order-QLRO transition, which is accompanied by the rise in the density of the remaining domain walls. In the QLRO phase at $T = 3.0$, (d) the order parameter distribution obtained for a $L = 32$ system shows emergence of U(1) symmetry and (e) typical spin configurations show the proliferation of domain walls. System sizes are the same as those in (Fig. 3.1). (f) The specific heat peak accompanying the order-QLRO transition does not show any system size dependence, the sizes reported here being $L = 16$ (purple), $L = 32$ (green) and $L = 64$ (red). The QLRO nature of the phase is established by the power-law decay of two-point correlations obtained at different temperatures for a $L = 256$ system with $\lambda = 100$ and $\delta\epsilon_{\pm\pi} = 100$ 96

3.8 The \mathbb{Z}_6 clock ferromagnet on a square lattice shows an order-QLRO transition accompanied by increase of domain wall density and a QLRO-disorder transition accompanied by increase in the densities of vortices and $\pm\pi$ domain walls. Upon extreme suppression of domain walls, the system shows a single transition from the ordered phase to a partially symmetry broken phase. When $\pm\pi$ domain walls are also suppressed, the system exhibits a single order-QLRO transition driven by the proliferation of the remaining vortices. System sizes are the same as those in (Fig. 3.1). 98

3.9 The QLRO nature of the intermediate phase obtained by suppression of vortices and $\pm\pi$ domain walls in the 2D \mathbb{Z}_6 ferromagnet is established by observing the power-law decay of the two-point correlation function (a) for a $L = 256$ system at different temperatures in that phase. (b) The exponent η of the power-law continues to increase with temperature and saturates around $\eta \approx 0.52$ at large temperatures. 99

3.10 For even values of n , the fraction of spin configurations on a plaquette for which the standard method identifies unphysical vortices is shown in (a), while the net vorticity for a $L = 32$ square lattice with periodic boundary conditions, averaged over 10^4 random configurations, is shown in (b). 99

3.11 Schematic spin configuration showing \mathbb{Z}_3 spin states for the antiferromagnetic model which get mapped onto effective spins states of a \mathbb{Z}_6 ferromagnetic model. Vortices and domain walls are identified using the \mathbb{Z}_6 representation. 101

3.12 The \mathbb{Z}_3 antiferromagnet on the square lattice displays disorder at all non-zero temperatures due to proliferation of \mathbb{Z}_6 vortices. When the vortices are suppressed, the model shows a partial symmetry broken phase in which $\pm\pi$ domain walls of the \mathbb{Z}_6 representation proliferate. When the formation of these types of domain walls is suppressed as well, the model shows enhancement to U(1) symmetry in the effective \mathbb{Z}_6 order parameter space. System sizes are the same as those in (Fig. 3.1). The \mathbb{Z}_6 order parameter distribution is shown for the different cases of suppression at $T = 4$ for a $L = 16$ system. 103

4.1 Typical spin configurations obtained on a $L = 16$ simple cubic lattice for the \mathbb{Z}_3 ferromagnet in (a) the ordered phase at $T = 1.5$ and (b) the disordered phase at $T = 2.5$. The results have been obtained using $\lambda = 0$, i.e. without suppressing the formation of vortices. The order parameter distribution obtained at the corresponding temperatures are shown in (c) and (d). The largest vortex strings and domain walls obtained for each of the spin configurations are shown in (e) and (f). 108

4.2 Measurement of standard percolation observables show that the percolation strength P and the spanning probability Π of the defects rise rapidly at $T \approx 1.8$. The average defect size for both types show a peak at that temperature as well. The data has been obtained for system sizes $L = 8$ (circle), $L = 12$ (square) and $L = 16$ (triangle). 109

- 4.3 Top panel: The simultaneous decay of magnetization and $m_{3\phi}$ across $T \approx 1.8$ in the \mathbb{Z}_3 ferromagnet on the simple cubic lattice is accompanied by a peak in the magnetic susceptibility and a simultaneous increase of defect densities. Bottom panel: Weak suppression of vortex strings shifts the simultaneous proliferation of defects and the decay of magnetization as well as $m_{3\phi}$ to a higher temperature $T \approx 2.2$. System sizes correspond to those in Fig. 4.2. 111
- 4.4 With strong suppression, the simultaneous proliferation of the defects decouples and the rise in vortex string density shifts to higher temperature along with the decay in magnetization and the second peak of susceptibility. The decay of $m_{3\phi}$ and the rise of domain wall density continues to occur at $T \approx 3.0$. For extreme suppression, the model shows a single transition from the ordered phase to the intermediate phase. System sizes correspond to those in Fig. 4.2. 113
- 4.5 The order parameter distribution for a $L = 8$ system at $T = 6$, in the intermediate phase obtained via extreme suppression of vortex strings with $\lambda = 100$, shows a three-fold symmetry breaking, offset from the spin angles by $\pi/3$ while defect configurations obtained at the same temperature show that domain walls proliferate in the absence of vortex strings. This behavior is captured by the percolation properties of the domain walls as well. System sizes correspond to those in Fig. 4.2. 115
- 4.6 Spin and domain wall configurations obtained in (a) the partially symmetry broken phase of the three-dimensional model at $T = 6$ (a two-dimensional slice is shown here), and (b) the symmetry enhanced QLRO phase of the two-dimensional model at $T = 4$. Both configurations have been obtained from the models with extreme suppression of vortices with $\lambda = 100$ 116

4.7	Percolation properties of (0 1) domain walls. Top panel (a,b,c) shows the behavior for the three-dimensional model. The spanning probability saturates to unity and the average size peaks at the percolation transition at $T \approx 2.5$. Bottom panel (d,e,f) shows the behavior for the two-dimensional model. The spanning probability saturates to a value around 0.42. The percolation strength decays and the average size increases with system size throughout the QLRO phase, representative of behavior at a percolation threshold. System sizes correspond to those in Fig. 4.2.	119
4.8	System size dependence of percolation observables at different temperatures in the QLRO phase of the 2D \mathbb{Z}_3 ferromagnet obtained by suppressing vortex formation with $\lambda = 100$	121
4.9	The order-disorder transition in the \mathbb{Z}_4 clock ferromagnet on a simple cubic lattice, captured by the decay in magnetization at $T \approx 2.2$, is accompanied by a simultaneous proliferation of domain walls and vortex strings (a,b,c). Upon extreme suppression of the vortex strings and $\pm\pi$ domain walls, the system shows a transition from the ordered phase to a partially symmetry broken phase (d,e,f).	123
4.10	The order parameter distribution shows how the four-fold symmetry which is broken in (a) the ordered phase is offset by $\pi/4$ in (b) the partially symmetry broken phase. The latter phase also shows percolation of (0 1) domain walls (c,d,e).	125

5.1 The \mathbb{Z}_6 clock ferromagnet on the simple cubic lattice shows an intermediate region below the order-disorder transition where the order parameter distribution obtained for a $L = 8$ system exhibits apparent emergence of U(1) symmetry and $m_{6\phi}$ become zero. The density of vortex strings rises near the disordering transition whereas the density of domain walls rises near the decay of $m_{6\phi}$. Upon suppression of the vortex strings and $\pm\pi$ domain walls, $m_{6\phi}$ continues to decay at the temperature where domain walls begin to proliferate. The data has been obtained for system sizes $L = 8$ (circle), $L = 12$ (square) and $L = 16$ (triangle). 130

5.2 Suppression of vortex strings and $\pm\pi$ domain walls leaves the model with an ordered phase (a) and a high temperature region (b) where three consecutive spin states appear in equal proportion. The \mathbb{Z}_3 magnetization decays in this region (c) and the decay grows sharper (d) when the energy cost between the three states is made degenerate to mimic a Potts potential. The order parameter distribution obtained at $T = 2.0$ for the degenerate Hamiltonian shows \mathbb{Z}_6 symmetry breaking with increasing system size. 132

5.3 Top panel: Measurement of spanning probability show that two types of domain walls (0 | 1) and (0 | 5) percolate in the intermediate region, while a third type (1 | 5) appears to remain on a percolation threshold. Bottom panel: In the disordered phase of the \mathbb{Z}_3 ferromagnet on the simple cubic lattice, all the three types of domain walls percolate. 135

5.4	<p>Top panel: When \mathbb{Z}_3 vortex strings are suppressed, $m_{6\phi}$ saturates at unity along with the magnetization. None of the individual types of domain walls percolate in this region. Bottom panel: When $\pm 2\pi/3$ domain walls are also suppressed, the system exhibits a transition from the ordered phase to a partially symmetry broken phase in which only the $(0 1)$ domain walls begin to percolate again.</p>	137
5.5	<p>Top panel: The \mathbb{Z}_3 antiferromagnet on the simple cubic lattice exhibits a single transition from the BSS phase to the disordered phase, which is accompanied by the proliferation of \mathbb{Z}_6 vortex strings, \mathbb{Z}_3 vortex strings and $\pm\pi$ domain walls. Bottom panel: Upon suppressing the formation of the \mathbb{Z}_6 vortex strings, the system shows a partially symmetry broken phase due to the proliferation of the $\pm\pi$ domain walls.</p>	140
6.1	<p>The order-disorder transition of the \mathbb{Z}_3 clock ferromagnet on the square lattice, which is accompanied by a simultaneous proliferation of vortices and domain walls (top panel), shifts to a lower temperature when the vortices are weakly enhanced (bottom panel). The rise in the defect densities and the decay of magnetization becomes sharper as well. Data has been obtained for system sizes $L = 16$ (circle), $L = 32$ (square) and $L = 64$ (triangle).</p>	143
6.2	<p>For strong suppression of vortices, the decay of magnetization shifts to lower temperatures but the specific heat reverses its trend and starts shifting to higher temperatures. The density of vortices is observed to rise sharply to a value higher than that of domain walls before coming down to a lower value at a higher temperature. In the intermediate region, the vortices and antivortices are found to display a sublattice ordering. System sizes correspond to those in Fig. 6.1.</p>	145

6.3	Values of the thermodynamic observables obtained by simulating the model with a $v\bar{v}l$ as the initial spin configuration at each temperature. System sizes correspond to those in Fig. 6.1.	147
6.4	Densities of domain walls and vortices and the specific heat obtained using Wang-Landau algorithm for a $L = 16$ system is shown over the parameter space of temperature T and suppression strength λ	150
6.5	Variation of the $v\bar{v}l$ order parameter across temperature for different values of λ . In cases (a) and (b), the initial configuration at each temperature was a completely ordered one, while a complete $v\bar{v}l$ was used for (c). System sizes correspond to those in Fig. 6.1.	151
6.6	Melting transition from the $v\bar{v}l$ phase to the disordered phase obtained with $\lambda = -2$ for n -state Potts models on the square lattice. System sizes correspond to those in Fig. 6.1.	152
6.7	Densities of domain walls and vortex strings and the specific heat obtained using Wang-Landau algorithm for the \mathbb{Z}_3 ferromagnet on a $L = 4$ simple cubic lattice is shown over the parameter space of temperature T and suppression strength λ	153
6.8	Upon initializing the three dimensional \mathbb{Z}_3 ferromagnet on the simple cubic lattice in a manner such that it exhibits a flux lattice structure for the vortex strings (a), the lattice structure breaks down into a vortex condensate (b) over the course of Monte Carlo simulation at $T = 0.5$ with $\lambda = -1.2$. The vortex condensate clearly has more structure than the arrangement of vortex strings at $T = 2.0$ in the disordered phase (c). The panels below the configurations show two dimensional slices along the three different axes of the corresponding configurations.	154

Chapter 1

Introduction

It is a remarkable aspect of nature that a collection of inanimate microscopic molecules possess the ability to rearrange themselves and drastically change their collective behavior when subjected to different ambient conditions. A glass of water turns into solid ice or steam depending on the temperature. Liquid helium suddenly loses its viscosity and begins to flow past, and even over, obstacles when cooled below a certain temperature. A number of physical properties characterizing a material undergo drastic change when the material transitions from one phase to another. From the physicist's point of view, the fundamental property which changes across a phase transition is the manifested symmetry [1].

Water molecules, for example, shoot around in a nearly arbitrary fashion and distribute themselves homogeneously across space when existing in the liquid phase. This ensures that the results obtained from a physical measurement made at a particular location appears identical to that obtained from any other location in the container. Such an invariance is possible because the liquid phase manifests a continuous translational symmetry. When the temperature is lowered and the liquid freezes to form ice, the invariance no longer holds true. In the ice phase, the molecules rearrange themselves into the periodic structure of a crystalline lattice. The presence of molecules at certain points in space and

their absence at other points breaks the continuous symmetry to a discrete translational symmetry¹. Phase transitions of this kind, characterized by the spontaneous breaking of a continuous symmetry, have been studied extensively because ubiquitous symmetries like rotation and translation, as well as those describing the fundamental interactions in the Standard Model of particle physics, are continuous in nature [2].

Symmetries characterizing parity, charge conjugation and time reversal are, however, discrete in nature. Furthermore, a wide variety of systems, which possess continuous symmetries at the microscopic scale, are effectively described by simpler models possessing discrete symmetries. The deconfinement of quarks and gluons, from a bound state in hadrons to a free plasma, is effectively described by a model possessing a three-fold symmetry [3]. Numerical algorithms used to simulate the formation of cosmic strings during cooling in the early universe also use a model with three-fold symmetry [4]. Models with three-fold and four-fold symmetries are studied to obtain insights into the possibility of deconfined phase transitions in quantum antiferromagnets [5–7]. The formation of a phase, where ferromagnetism and ferroelectricity coexists, in multiferroic hexagonal manganite is described by a model with six-fold symmetry [8, 9]. A fascinating feature of systems possessing a discrete symmetry is that they can, in addition to spontaneous breaking, also exhibit a spontaneous enhancement of the discrete symmetry [10–12].

1.1 Symmetry Enhancement

One of the simplest examples of symmetry enhancement can be observed in the equilibrium texture of crystal surfaces [13]. Each surface atom tends to pull other atoms in a small neighborhood around itself to its own height. At low temperature, the surfaces tend to be flat and maintain an average height in integer multiples of the atom size. Therefore,

¹The ice phase is called the symmetry broken phase and the liquid phase is called the symmetry restored or fully symmetric phase. The later phase is termed as the fully symmetric one because it fully manifests, at the macroscopic scale, the continuous translational symmetry possessed by the microscopic molecules.

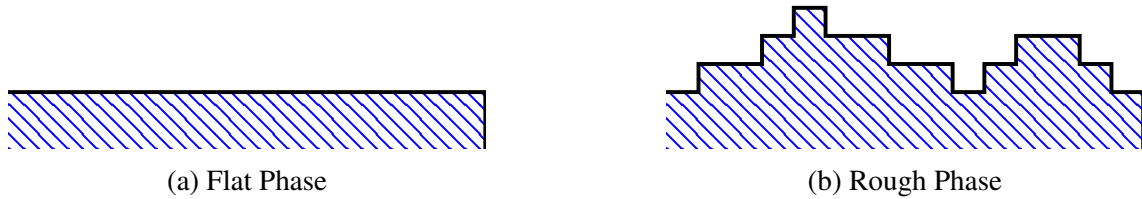


Figure 1.1: Typical cross sections showing equilibrium texture of crystal surfaces at (a) low and (b) high temperatures.

the various possible values of the average height correspond to elements in the group of integers \mathbb{Z} . However, the layer chooses a particular average height for a given instance and breaks the \mathbb{Z} symmetry in this flat phase (Fig. 1.1a). At high temperature, on the other hand, the layers tend to be rough. The average layer height no longer takes values in integer multiples of the atom size but covers a continuum of fractional values (Fig. 1.1b). The symmetry in this rough phase is, therefore, enhanced to a continuous symmetry \mathbb{R} .

Another example of symmetry enhancement is provided by n -state models of ferromagnets [10, 11]. The microscopic constituents of these models are spin vectors which can orient along one of n equispaced angles between zero and 2π . Each spin prefers to align itself along the orientation of its neighbors while thermal fluctuations attempt to arbitrarily orient them along any of the n directions. At low temperature, a majority of the spins on the square lattice align along a common direction and maintain long range order (Fig. 1.2a). By choosing a particular direction among the n possibilities, the system breaks a \mathbb{Z}_n symmetry, which is associated with the group of integers closed under addition modulo n . At high temperature, where the thermal fluctuations are strong enough to align each spin arbitrarily, the \mathbb{Z}_n symmetry gets restored and the system exhibits a disordered phase (Fig. 1.2c). The models show only these two phases on the square lattice when $n \leq 4$. When $n > 4$, the aligning tendency and the thermal fluctuations balance each other out across an intermediate range of temperatures in a manner such that the spins remain correlated but gradually change their orientation over large distances (Fig. 1.2b). As a result the average orientation of the system keeps fluctuating uniformly over a continuum of angles between zero and 2π . In effect, a continuous $U(1)$ symmetry emerges in

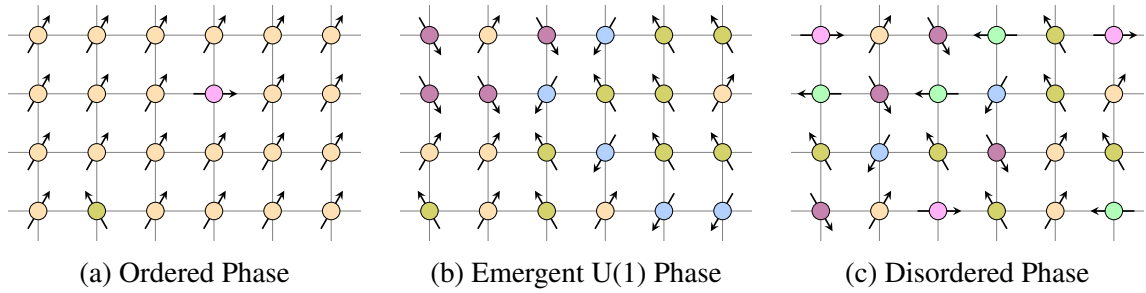


Figure 1.2: Typical spin configurations in different phases of a \mathbb{Z}_6 ferromagnet on the square lattice.

this intermediate phase [12].

While the consequences of symmetry enhancement on the physical properties of the system has been the subsequent topic of investigation in the literature [12, 14–19], a few fundamental questions have remained relatively unexplored.

1. What determines the extent of the symmetry enhanced phase?
2. What stops the $n \leq 4$ models from exhibiting symmetry enhancement?
3. What is the general criterion that determines whether a discrete symmetry (\mathbb{Z} , \mathbb{Z}_n or otherwise) exhibits enhancement to a continuous symmetry.

Since these questions have not been answered clearly, the existence of a symmetry enhanced phase in \mathbb{Z}_n models has itself become a topic of debate [20–27]. On the simple cubic lattice no robust signature of an emergent U(1) phase has been obtained for any value of n . The $n \leq 4$ models exhibit a single order-disorder transition. The $n > 4$ models exhibit an apparent U(1) emergence at intermediate temperatures in Monte Carlo simulations. However, this intermediate region continues to shrink with increasing system size [27]. This has led to proposals for three alternate scenarios:

1. The apparent U(1) emergence is a finite size effect which will vanish in the thermodynamic limit, leaving a simple order-disorder phase diagram for all n in three dimensions [20–24, 27].

2. The intermediate region will stop shrinking above a certain system size and a stable $U(1)$ phase will emerge in the thermodynamic limit [25–27].
3. An intermediate phase might be present but it will not exhibit an emergent $U(1)$ symmetry [23, 25].

If we successfully figure out a general criterion which determines the possibility of symmetry enhancement, we will be able to choose the correct candidate between the first two scenarios in a straightforward manner. However, the third scenario brings in a very different possibility amidst this debate. What kind of a phase exists at intermediate temperatures but does not exhibit symmetry enhancement?

1.2 Partial Symmetry Breaking

A simple example of an intermediate phase which does not exhibit symmetry enhancement is, again, provided by the texture of crystal surfaces. Suppose the property of the crystal atoms are modified in a manner such that each surface atom pulls nearby atoms to its own height across a larger neighborhood around itself [13, 28]. This modified system exhibits an intermediate disordered flat phase, between the flat and rough phases, where the atoms display an up-down-up-down height profile (Fig. 1.3a). The average layer height is, therefore, limited to half-integer multiples of the atom size. These heights again correspond to the elements of the group \mathbb{Z} and for a given layer, a \mathbb{Z} symmetry is broken. However, the fact that the average values in this phase are offset from that in the flat phase by half of the atom size makes the transition between the two phases quite fascinating. What kind of symmetry gets broken across this transition? A layer, in the process of formation, always has an implicit up-down symmetry. It is this two-fold symmetry which remains broken in the flat phase but gets restored in the disordered flat phase [29]. Since only a part of the symmetry characterizing the system gets restored and the remaining part stays broken, this phase is known as a partially symmetry broken

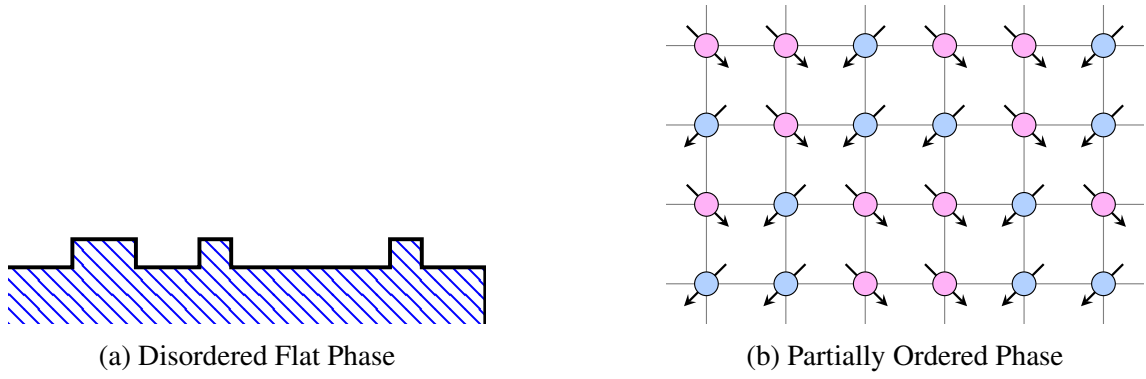


Figure 1.3: Partial symmetry breaking leads to (a) an up-down-up-down texture for layers of crystals, and (b) dominance of two consecutive spin directions in a three dimensional \mathbb{Z}_4 ferromagnet (a two dimensional slice is shown here).

phase.

Similar examples of partially symmetry broken phases have been reported for \mathbb{Z}_n models as well. The \mathbb{Z}_6 model on a square lattice, as mentioned earlier, exhibits a low temperature ordered phase, an intermediate emergent $U(1)$ phase and a high temperature disordered phase. This phase diagram is obtained when each spin interacts only with its nearest neighbors. When the range of interaction is increased to include next-nearest-neighbors and the interaction potential is modified a little, the intermediate phase shows a partially ordered or incompletely ordered phase [30]. In three dimensions, when the potential of the \mathbb{Z}_4 model is modified a little, the single order-disorder transition splits and an intermediate phase appears in which half of the spins align along one direction and the other half align along an adjacent direction [31, 32]. This makes the average orientation of the system lie midway between the n original directions, i.e. offset from the original angles by π/n (Fig. 1.3b). In a manner similar to that of the disordered flat phase (Fig. 1.3a), the texture of this phase results from the restoration of an implicit symmetry. In this case, the implicit symmetry can be exposed clearly by decomposing the \mathbb{Z}_4 model into a $\mathbb{Z}_2 \times \mathbb{Z}_2$ model [33]. The partially order appears because one of the \mathbb{Z}_2 symmetries gets restored and the other remains broken. Similar phases, where a \mathbb{Z}_2 symmetry gets restored, have been obtained for a \mathbb{Z}_6 model [34] and a \mathbb{Z}_3 model [35] in three dimensions. In the latter case, however, the \mathbb{Z}_2 restoration is explicitly driven by an external magnetic field in order

to model the effect of dynamical quarks on deconfinement.

The appearance of these partially symmetry broken intermediate phases serves to compound our questions even further:

1. What determines if an intermediate phase will be symmetry enhanced or partially symmetry broken?
2. What determines the extent of the partially symmetry broken phase?
3. Can symmetry enhanced and partially symmetry broken phases exist side by side in \mathbb{Z}_n models as it does in the texture of crystal surfaces?

Are there other types of intermediate phases in the \mathbb{Z} and \mathbb{Z}_n models? In order to answer this question, it would be useful to chart out the maximal set of phases that can appear in these models. It is also fascinating to observe how each phase in the \mathbb{Z} model has a counterpart in the \mathbb{Z}_n models. The reverse, however, does not hold true. The latter model exhibits a fully symmetric disordered phase which is absent in the former. Since the disordered phase acts as a natural boundary, demarcating the extent of the intermediate phases, we will primarily focus on the \mathbb{Z}_n models, hereafter. Once our queries have been answered satisfactorily for these models, we can map our answers to the \mathbb{Z} model as well. However, we note that the close similarity between the phases present in the two models is not a coincidence. Both models are described by very similar theories in the continuum limit [23, 29]. And the continuum theory for the \mathbb{Z}_n models is a good place to start a systematic characterization of the different types of possible phases.

1.3 Continuum Theory for Models with \mathbb{Z}_n Symmetries

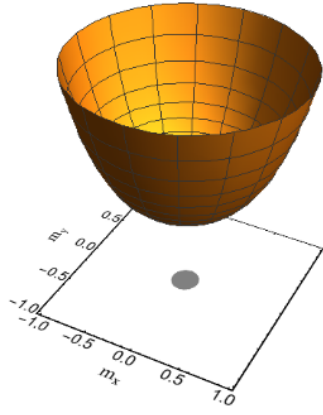
The continuum theory represents the coarse-grained description of the model which, up till now, we have considered placed on a lattice. Since the spins are two dimensional unit

vectors, their coarse-grained counterparts at each point x in the continuum space can be represented as two component vectors, whose magnitude can vary due to coarse-graining and averaging effects. They can also be represented, equivalently, as complex numbers $\Phi(x)$. The continuum theory for $\Phi(x)$ is the well-known complex scalar theory [36]. The \mathbb{Z}_n symmetry is factored in by perturbing the theory using n -fold symmetry breaking fields [23]. The perturbed action is given by

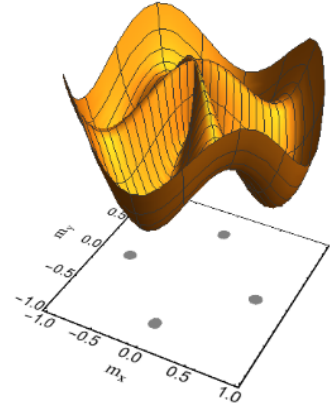
$$\begin{aligned} \mathcal{S} &= \int dx [|\nabla\Phi|^2 + V(\Phi)] \\ V(\Phi) &= a|\Phi|^2 + b|\Phi|^4 - h_n(\Phi^n + \bar{\Phi}^n) - h_{2n}(\Phi^{2n} + \bar{\Phi}^{2n}) \end{aligned} \quad (1.1)$$

We will restrict ourselves to cases where $b > 0$. While the h_{2n} term is ignored in most calculations reported in the literature [10, 23, 37], we have included it here because it can lead to the formation of an exotic phase where a \mathbb{Z}_{2n} symmetry emerges. Approximate recursion relations, describing how the initial or bare parameters of the action renormalize with scale, have been developed for the theory in two dimensions [10]. In addition, an approximate picture for the renormalization flow has been suggested for the three dimensional theory using scaling arguments [23, 24]. Instead of going through the specific details of these calculations, we briefly summarize their salient features with particular focus on the symmetry manifest at each fixed point governing the different phases. For ease of visualization, we have plotted the shape of the potential $V(\Phi)$ at representative values of the renormalized parameters along with a projection of their minima on the complex order parameter space $m_x + im_y$ (Fig. 1.4). Although the plots are shown for $n = 4$ perturbations, some of them are realized for higher values of n .

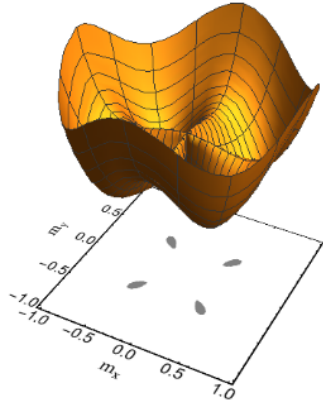
1. When the perturbations become irrelevant, i.e. their renormalized values are $h_n = 0$ and $h_{2n} = 0$, the action corresponds to that of the unperturbed complex scalar theory. This unperturbed theory has a fixed point at $a = 0$, which corresponds to the symmetry restoring transition. Both h_n and h_{2n} remain irrelevant at $a = 0$ for $n > 4$ in two dimensions and for $n \geq 4$ in three dimensions. Therefore a U(1) symmetry is



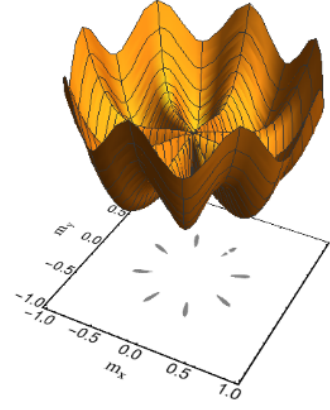
(a) $a = 0.5, h_n = -0.15, h_{2n} = 0$



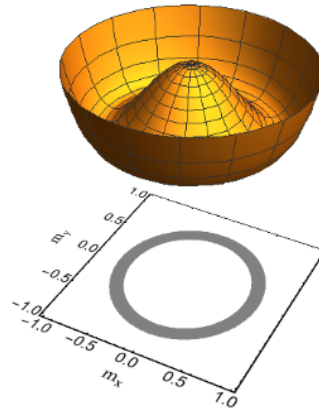
(b) $a = -1, h_n = -0.15, h_{2n} = 0$



(c) $a = -0.5, h_n = -0.15, h_{2n} = 0$



(d) $a = -0.5, h_n = 0, h_{2n} = -0.15$



(e) $a = -1, h_n = 0, h_{2n} = 0$

Figure 1.4: Schematic of the potential (above) for the complex scalar theory in the presence of symmetry breaking perturbations for $n = 4$ is shown with projection of the potential minima on the order parameter space (below) at different values of the renormalized parameters, corresponding to (a) the \mathbb{Z}_4 symmetry restored phase, (b) the \mathbb{Z}_4 symmetry broken phase, (c) the partial symmetry broken phase, (d) the emergent \mathbb{Z}_8 phase, and (e) the emergent $U(1)$ phase.

expected to emerge at the disordering transition in \mathbb{Z}_n ferromagnets for these values of n .

2. For $a > 0$, the system renormalizes to the infinite temperature fixed point, independent of whether h_n and h_{2n} are relevant or not. This fixed point governs the disordered phase of the ferromagnets and the potential shows a single minima at $m_x = 0, m_y = 0$ (Fig 1.4a).
3. For $a < 0$, the behavior of the renormalization flow is quite varied. When h_n renormalizes to a positive value, the system flows to the zero temperature fixed point where the \mathbb{Z}_n symmetry is broken and the potential shows n discrete minima at angles $\{0, 2\pi/n, \dots, 2\pi(n-1)/n\}$ (Fig 1.4b). This fixed point governs the ordered phase of the ferromagnets. It has been argued that h_n renormalizes to a positive value below the disordering transition temperature for all n in three dimensions. In two dimensions, h_n renormalizes to a positive value below the transition temperature when $n \leq 4$. For $n > 4$, h_n renormalizes to a positive value only at low temperatures $a < a^*$, where a^* depends on n .
4. If, in some cases, h_n starts with a bare positive value but renormalizes to a negative value, then the potential displays n discrete minima located at intermediate angles $\{\pi/n, 3\pi/n, \dots, \pi(2n-1)/n\}$ (Fig. 1.4c). This would correspond to a partially symmetry broken phase.
5. If h_n becomes irrelevant but h_{2n} remains relevant, then the potential displays $2n$ discrete minima located at angles $\{2\pi\alpha/n \mid \alpha \in \{0, 1/2, 1, \dots, n-1/2\}\}$ if the renormalized $h_{2n} < 0$ or at angles $\{2\pi\alpha/n \mid \alpha \in \{1/4, 3/4, 5/4, \dots, n-1/4\}\}$ if the renormalized $h_{2n} > 0$ (Fig. 1.4d). Although this possibility has not been discussed for \mathbb{Z}_n models, it has been mentioned in the context of the crystal surface model, which has a similar action (a real scalar field theory perturbed by periodic symmetry breaking fields) [29]. In this case, the system will exhibit an emergent \mathbb{Z}_{2n} symmetry.

6. Finally, when both h_n and h_{2n} become irrelevant for $a < 0$, the potential shows an emergent U(1) symmetry with a continuum of transverse minima (Fig 1.4e). This represents the ordered phase of the unperturbed theory in three dimensions where the system sustains a massless Goldstone mode. However, it has been argued that the h_n perturbation is always relevant at this Nambu-Goldstone fixed point. Therefore, the system flows over to the zero temperature \mathbb{Z}_n symmetry broken fixed point and the emergent U(1) phase is never realized in three dimensions. In two dimensions, however, both h_n and h_{2n} become irrelevant across an intermediate range of temperatures $a^* < a < 0$ for $n > 4$ and the system exhibits an emergent U(1) phase extending across that range.

While the renormalization picture for the continuum theory lists out a set of possible phases, it effectively describes the behavior of ferromagnets with clock or Villain potentials [10]. However, most of the partially symmetry broken phases have been reported for ferromagnets with potentials modified away from the clock form [30–32, 34, 38–40]. The renormalization group calculation discussed above fails to capture the phase diagram of these ferromagnets and, instead, merely provides a plausibility argument for their existence of a partially symmetry broken phase or a \mathbb{Z}_{2n} symmetric phase. In addition, it does not provide an answer to one of our fundamental questions: What is the physical mechanism which drives the phase transitions and leads to the formation of these intermediate phases?

In this thesis, we demonstrate that symmetry restoration, partial symmetry breaking and symmetry enhancement in \mathbb{Z}_n models are all driven by the proliferation of topological defects.

1.4 Topological Defects

Topological defects are regions of singularity in the order parameter field which cannot be removed by continuous deformations [41–44]. Depending on the symmetry of the order parameter and the dimensionality of the system, these regions can appear as points (vortices, monopoles), lines (domain walls, vortex strings) or, in some cases, even extend throughout the system (skyrmions, textures). Formally, the existence of topological defects is determined by the non-trivial homotopy groups of the local order parameter associated with each point in the system [41]. Due to the numerous possible ways of placing them in a system, defects carry a high configurational entropy. The triumph of entropy over energy as a criterion for the onset of a phase transition, therefore, manifests itself via the proliferation of defects.

Defect driven phase transitions, particularly those which restore spontaneously broken continuous symmetries, are known to occur in superfluids [45–60], superconductors [61–68], solids [69–74], liquid crystals [75–82], Heisenberg ferromagnets [83–85], gauge theories [86–93] and the early universe [44, 94]. In bulk superfluids, for example, vortex string defects appear as small closed loops at low temperatures. When the temperature is raised above a certain value, the loops grow large and proliferate across the system. This restores the broken $U(1)$ symmetry of the superfluid order parameter and turns the superfluid into a normal fluid (Fig. 1.5). The order-disorder transition which restores a broken $O(3)$ symmetry in bulk Heisenberg ferromagnets is driven by the proliferation of monopole defects. One of the most popular examples of defect driven transitions, however, is the Berezinskii-Kosterlitz-Thouless transition in thin films of superfluids driven by the unbinding and proliferation of point vortices. A special feature of this transition is that it occurs between two phases where the $U(1)$ symmetry remains unbroken [47, 48].

While the role of topological defects in systems with continuous symmetries has received a lot of attention, the role of defects in systems with discrete symmetries has remained relatively unexplored. Discrete symmetries sustain the defects of their continuous sym-

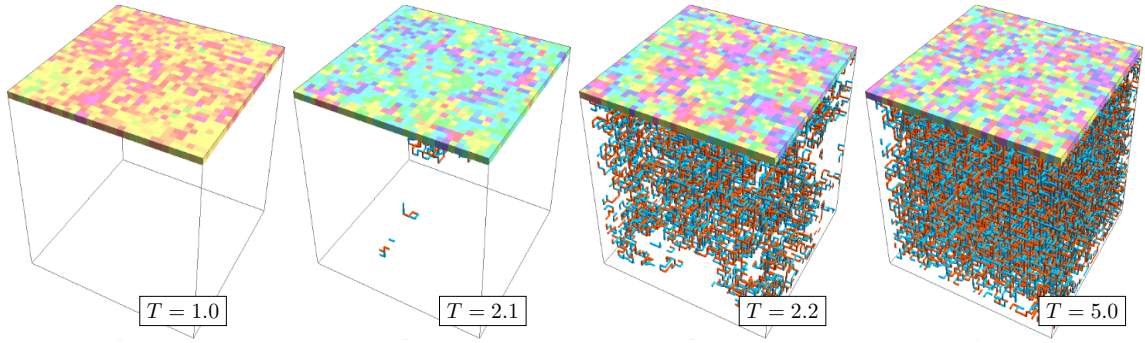


Figure 1.5: Superfluid-normal phase transition driven by the proliferation of vortex (blue) and antivortex (red) strings in three dimensions. Top layers show two dimensional slices of field configurations belonging to the XY model of superfluid at each temperature T .

metric counterparts. In addition, they also exhibit domain wall defects. The interplay between domain walls and the other types of defects raises the possibility of obtaining multiple phase transitions and, consequently, a rich phase diagram. Furthermore, the formation of the defects can be manipulated to change the location of the associated phase transitions, which in turn, can alter the phase diagram itself.

In this thesis, we will consider \mathbb{Z}_n models which exhibit simple order-disorder phase diagrams that have been studied extensively. By manipulating the formation of defects which appear in these models, we will open up new phases that have not been reported before. This would also allow us to map the proliferation of each type of defect to the corresponding phase that it generates.

1.5 Defects in Models with \mathbb{Z}_n Symmetries

Consider a \mathbb{Z}_n spin model on a lattice Λ . Each spin at vertex $i \in \Lambda$ can orient itself at an angle $\theta_i = 2\pi s_i/n$, where the integer value of the state s_i is taken from the set $\{0, 1, \dots, n-1\}$. The spins can be addressed using the angular representation θ_i or the state representation s_i , in an equivalent manner.

While the spins reside on the vertices of Λ , the defects reside on the dual lattice Λ' . If Λ is an integer lattice, then Λ' is also the same integer lattice but shifted from Λ by half a

lattice spacing along each axis. The cyclic nature of the \mathbb{Z}_n symmetry allows us to map the n angles to elements of $U(1)$, for which the first homotopy group is non-trivial [42]. This allows formation of vortices, or rather discrete versions of vortices, in the \mathbb{Z}_n models ². The discrete nature of \mathbb{Z}_n , on the other hand, allows formation of domain wall defects which correspond to the zeroth homotopy group.

1.5.1 Domain Walls

Domain walls are defects with codimension one. This implies that if the spins reside on the vertices of a d -dimensional lattice Λ , domain walls appear as $d - 1$ dimensional elements on Λ' .

Definition. If a pair of neighboring spins on the vertices of Λ are in states a and b , then a domain wall segment of unit size bearing a label $(a | b)$ appears on the $d - 1$ dimensional element of Λ' which separates the two spins.

For example, if the two spins reside on a square lattice Λ' , then a domain wall segment appears on the edge in Λ' separating the spins (Fig. 1.6a). For ferromagnets, it is implied that a domain wall segment is valid only when $a \neq b$. This may not be the case for antiferromagnets. When referring to a particular type of domain wall, we will always mention the two states it separates in the form $(a | b)$. Since we will not consider chiral interactions, a domain wall of type $(a | b)$ is equivalent to one of type $(b | a)$. If the states are not mentioned, it is implied that we are referring to the collection of all types of valid domain walls that can appear in the model under consideration.

²The only exception is the case $n = 2$ (Ising model). This model does not support vortices because the \mathbb{Z}_2 angles are mapped onto \mathbb{R} and not to $U(1)$ [95]. This mapping also explains why the Ising model does not show symmetry enhancement to $U(1)$.

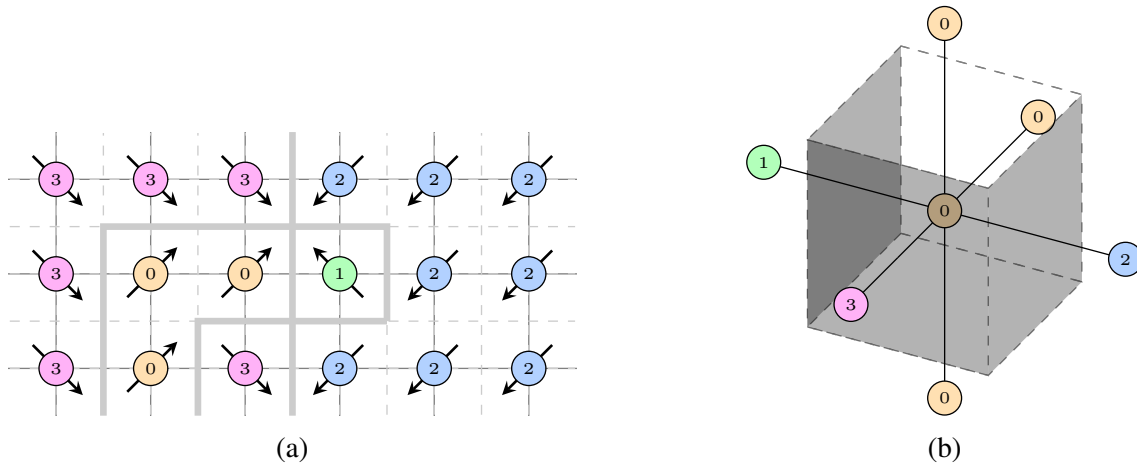


Figure 1.6: Domain walls (gray) residing on elements of the dual lattice (dashed lines) are shown for configurations of \mathbb{Z}_4 spins on (a) the square lattice, and (b) the simple cubic lattice.

1.5.2 Domain Wall Driven Phase Transitions

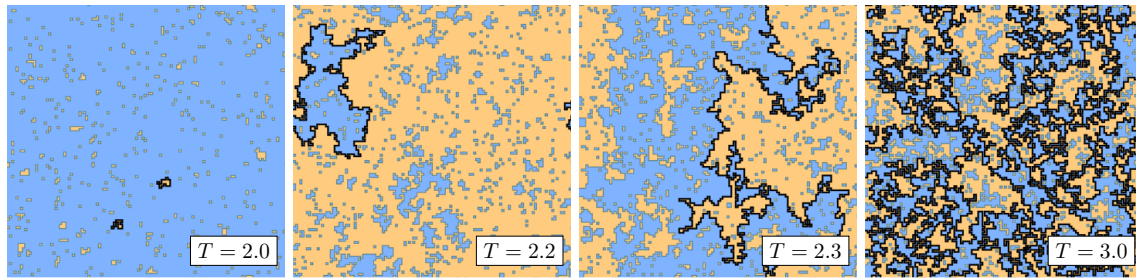
The behavior of domain walls in models with discrete symmetries, like the Ising model and the Potts models, has been studied in different representations: as the hull of geometrical spin clusters or domains, as closed graphs of high temperature expansion series, as closed loops in loop models, as Schramm-Loewner stochastic evolution curves and as kinks in quantum spin chains [96–111].

Two Dimensional Ising Ferromagnet

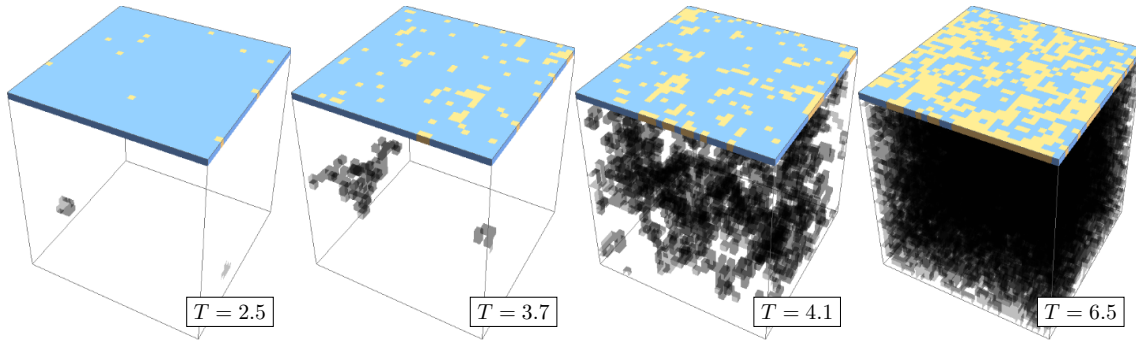
In the standard formulation of the Ising ferromagnet on a square lattice, spins σ_i , which can be in one of two states $\sigma_i \in \{-1, +1\}$, are placed at each vertex i of a square lattice Λ and the Hamiltonian with nearest neighbor interaction is given by

$$\mathcal{H} = - \sum_{\langle i, j \rangle \in \Lambda} \sigma_i \sigma_j \quad (1.2)$$

The minimum energy configuration, realized at zero temperature, is a ferromagnetic one where all the spins are in the same state. When the temperature T is increased, thermal fluctuations flip a few spins to the opposite state and the system maintains long range order



(a) Ising transition on the square lattice



(b) Ising transition on the simple cubic lattice

Figure 1.7: Proliferation of domain walls (black) across the order-disorder transition of the Ising model in (a) two dimensions, and (b) three dimensions.

(Fig. 1.7a). With further increase in temperature, flipped spins appear more frequently and tend to form domains or droplets of their own.

The domain walls correspond to the boundaries of these geometrical droplets [112]. At low temperatures, the domain walls appear as small closed loops (Fig. 1.7a). When a single spin fluctuates to the opposite state, it gets surrounded by a loop four segments long. When consecutive spins fluctuate to the opposite state, the length of the loop increases and the geometry of the loop becomes more tortuous, representing higher-order polyominoes. Above a critical temperature $T_c = 1/\ln(1 + \sqrt{2}) = 2.269\dots$, the loops become so numerous that in any given configuration, on an average, they are able to connect with each other to form a giant network which spans across the system. This effectively breaks the system down into numerous domains, results in the destruction of long range order and the onset of disorder where the spins align arbitrarily.

Three Dimensional Ising Ferromagnet

In three dimensions, the Ising model shows an order-disorder transition as well. In this case, however, the domain walls reside on the plaquettes of the dual lattice. A single spin flipped to the opposite state is surrounded by six plaquettes. Larger domains of flipped spins are separated by cuboidal bubbles of domain walls instead of loops. Even though the geometrical unit of the domain wall has changed, the thermodynamic behavior of the three dimensional system remains qualitatively similar to that of its two dimensional counterpart. At low temperatures, most spins are ordered and only a few domain wall bubbles are present in the system (Fig. 1.7b). With increasing temperature, the bubbles begin to grow in size and density. At high temperatures, the bubbles proliferate and break the system into numerous domains, allowing the spins to disorder.

1.5.3 Vortices

Vortices represent one of the simplest topological defects associated with continuous symmetric order parameters. They play a crucial role in the physics of superfluids [42, 43, 45–55, 57, 60, 65, 86], superconductors [61–64, 66–68], and Josephson junction arrays [113, 114]. Vortices are defects with codimension two and they appear as $d - 2$ dimensional elements on the dual lattice (Fig. 1.8). The winding number at a point in space, which acts as a measure of vorticity, is usually calculated in the continuum by traversing a closed circuit around that point and counting the number of signed rotations $\oint \nabla\theta/2\pi$ completed in the order parameter space by the spin orientations on the circuit [42]. On the lattice, the circuit integral is replaced by a circuit sum while the gradient is replaced by a finite difference. On an integer lattice, the circuit is usually chosen to be a square plaquette, although a smaller triangular plaquette would work as well.

*Definition.*³ Suppose the four spins at the corners of a square plaquette in Λ are oriented

³This definition will be updated in Sec. 3.3.3. Throughout this work, thereafter, the new definition will be used.

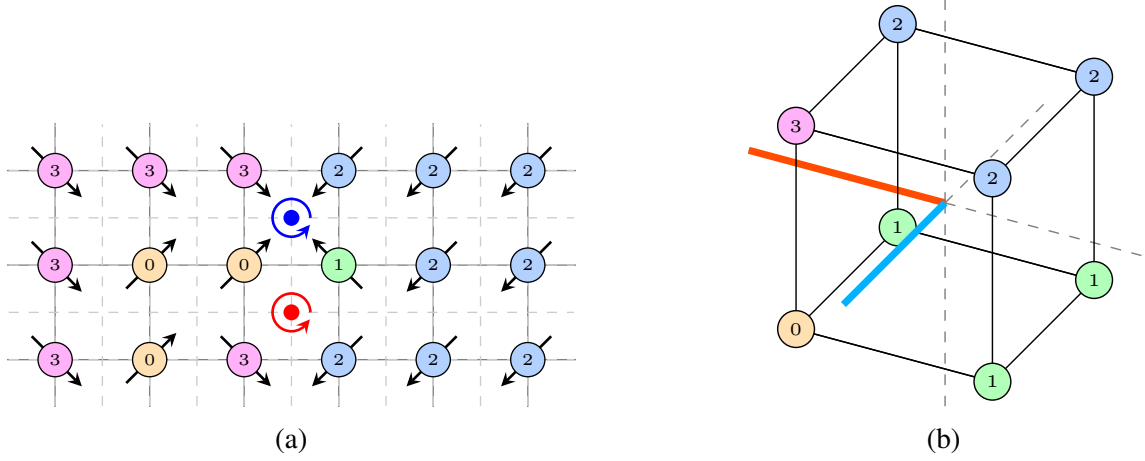


Figure 1.8: Vortices (blue) and antivortices (red) residing on elements of the dual lattice (dashed lines) are shown for configurations of \mathbb{Z}_4 spins on (a) the square lattice, and (b) the simple cubic lattice.

at angles $\theta_i, \theta_j, \theta_k$ and θ_l when read in an anticlockwise sense. The winding number $\omega_{i'}$ associated with the $d - 2$ dimensional element $i' \in \Lambda'$ which pierces the center of the square plaquette, is given by [59, 115]

$$\omega_{i'} = \frac{1}{2\pi}([\theta_j - \theta_i]_{2\pi} + [\theta_k - \theta_j]_{2\pi} + [\theta_l - \theta_k]_{2\pi} + [\theta_i - \theta_l]_{2\pi}) \quad (1.3)$$

Here $[\theta_j - \theta_i]_{2\pi} = \theta_j - \theta_i + 2\pi\alpha$, with $\alpha \in \mathbb{Z}$ chosen such that $\theta_j - \theta_i + 2\pi\alpha$ lies in $(-\pi, +\pi]$. A vortex or an antivortex appears at i' if $\omega_{i'} > 0$ or $\omega_{i'} < 0$, respectively. Unless mentioned otherwise, the term vortex will henceforth be used to refer to both vortex and antivortex defects.

1.5.4 Relationship Between Vortices and Domain Walls

The formula (1.3) for calculating winding number on the lattice brings out a remarkable connection between domain walls and vortices. Non-zero values for terms like $[\theta_j - \theta_i]_{2\pi}$ imply the presence of a domain wall between the two spins θ_j and θ_i . If the domain wall is viewed as carrying a flux $[\theta_j - \theta_i]_{2\pi}$, then the winding number represents the net imbalance of four flux lines incoming at i' . This shows that the formation of vortices is

dependent on the formation of domain walls. The system cannot sustain any vortex defect if domain walls do not form because all the terms contributing to the winding number will be zero. The dependence, however, does not hold true in reverse. The system can sustain numerous domain walls in a manner such that the contributions to the winding number cancel out at each i' and not a single vortex is formed. In this thesis, we will show that these special types of domain wall configurations are responsible for the existence of some of the intermediate phases.

1.5.5 Vortex Driven Phase Transitions

The most popular as well as one of the oldest example of a vortex driven phase transition is the Berezinskii-Kosterlitz-Thouless transition in the two dimensional XY ferromagnet [42, 47, 48].

Two Dimensional XY Ferromagnet

In the standard formulation of the XY ferromagnet on a square lattice, two dimensional unit vector spins θ_i , which can orient at any angle between 0 and 2π , are placed at each vertex i of a square lattice Λ and the Hamiltonian with nearest neighbor interaction is given by

$$\mathcal{H} = - \sum_{\langle i,j \rangle \in \Lambda} \cos(\theta_i - \theta_j) \quad (1.4)$$

The minimum energy configuration obtained at zero temperature is one where all the spins are in the same state. When the temperature becomes non-zero, the spins fluctuate gently and produce spin waves. In two dimensions, however, the spin waves destroy long-range order [116] and the system exhibits quasi-long-range order instead. The U(1) symmetry of the model, which could have been broken at low temperatures, now remains restored at all non-zero temperatures. Since the model does not exhibit symmetry breaking at any

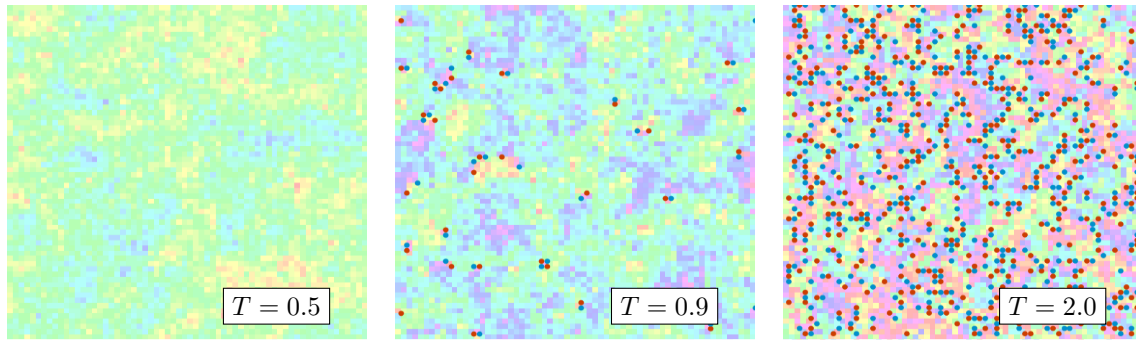


Figure 1.9: Phase transition in the XY model driven by proliferation of vortices (red) and antivortices (blue) on a square lattice.

non-zero temperature, the existence of a phase transition in the model had been a topic of debate in the past. It is now known that the unbinding and proliferation of vortices drives the transition. At low temperatures, vortices and antivortices form tightly bound dipoles with spin waves in the background (Fig. 1.9). As the temperature is increased, the density and average separation between the dipoles increases slightly [117, 118]. Across a certain temperature $T \approx 0.90$, the density increases considerably and the dipoles unbind into a plasma of free vortices and antivortices. This drives a phase transition from the quasi-long-range ordered phase to the disordered phase.

Three Dimensional XY Ferromagnet

The phase diagram of the XY model in three dimensions differs qualitatively from that of its two dimensional counterpart. Even though spin waves appear in the system at non-zero temperatures, they are not sufficient to destroy long-range order. Therefore the U(1) symmetry gets broken, the system exhibits a non-zero magnetization and sustains a massless Goldstone mode. At low temperatures, in the ordered phase, the vortex string defects form small loops (Fig. 1.5). The density and average size of these loops increase with temperature. Above a critical temperature, the strings begin to proliferate and the system undergoes a disordering transition.

1.5.6 Energy versus Entropy Balance for Defects

We now return to the \mathbb{Z}_n models, where domain walls and vortices can appear simultaneously. Given the widespread use of \mathbb{Z}_n models as effective theories for condensed matter systems, quantum phase transitions and lattice gauge theories, there is a surprising lack of direct studies regarding the interplay of the defects in these models. A few suggestions regarding the interplay has ensued from approximate energy versus entropy balance calculations, which provide an estimate of the temperature range in which formation of the defects becomes favorable [95, 115]. These estimates have focussed only on a particular form of interaction: the ferromagnetic clock potential. This potential assigns an energy cost $-\cos(\theta_i - \theta_j)$, proportional to the extent of alignment between neighboring spin angles. The corresponding Hamiltonian with nearest neighbor interaction is

$$\mathcal{H} = \sum_{\langle i,j \rangle \in \Lambda} 1 - \cos(\theta_i - \theta_j) \quad (1.5)$$

The balance calculation leading to an estimate of the proliferation temperature for the defects in this model goes as follows.

Proliferation of Domain Walls

First, we calculate the temperature at which the formation of a domain wall of length l becomes favorable. Extended loops of domain walls can be modelled by non-backtracking random walks, which provides an upper bound $4 \times 3^{l-1}$ for the number of walls of length l on a square lattice. For simplicity, we assume that spins in the system differ from their neighbors by either zero states or one state, i.e. $[\theta_i - \theta_j]_{2\pi} = 0, \pm 2\pi/n$. Therefore our system sustains domain wall defects which only separate neighboring spins which differ by one state. The free energy at temperature T for such a domain wall, of a given length

l , is obtained by subtracting the entropy term from the energy.

$$F(l) = l(1 - \cos(2\pi/n)) - T \ln 3 \quad (1.6)$$

We have neglected the terms which are independent of l . Assuming a positive value of l , $F(l)$ changes sign at $T_{dw} = (1 - \cos(2\pi/n)) \ln 3$. For $T < T_{dw}$, $F(l)$ has a minimum at $l = 0$. Above this temperature, the minimum shifts to $l \rightarrow \infty$ and the formation of large domain walls is expected to be favorable.

Proliferation of Vortices

Next, we calculate the temperature at which the formation of a single vortex becomes favorable. The existence of domain walls separating spins by only one state implies that a 2π winding of the \mathbb{Z}_n spin space is completed for a vortex when at least n domain walls, all with $[\theta_i - \theta_j]_{2\pi} = +2\pi/n$ or all with $[\theta_i - \theta_j]_{2\pi} = -2\pi/n$, meet at the vortex. For this calculation, we assume that the vortex resides on a lattice with coordination number n . A lattice with periodic boundary conditions can never sustain the formation of a single vortex as any valid configuration of spins will always generate a complimentary antivortex with such a boundary condition [95, 118]. Therefore, we impose open boundary conditions on the lattice. In doing so, the n domain walls starting from the single vortex can terminate at the boundaries without looping back into the lattice. Assuming that each of the n domain walls continue for a length l , the energy cost of the vortex is $e_{vx} \approx e_{vx}^0 + nl(1 - \cos(2\pi/n))$ where e_{vx}^0 is the core energy of the vortex. Assuming that the lattice is two dimensional, the single vortex can be placed at any of the L^2 vertices, where L is the lattice length along each axis. The free energy of the vortex at a temperature T is therefore $F = e_{vx} - 2T \ln L$. Since the length of the domain walls emanating from the vortex to the system boundaries will be of the order of L , the energy term will be linear in L while the entropy term is logarithmic in L . Therefore, in the thermodynamic limit, the free energy will be positive at all finite temperatures and formation of vortices will be unfavorable. This argument

suggests that only domain walls can proliferate in \mathbb{Z}_n models while vortices cannot.

There is, however, an interesting possibility which makes proliferation of vortices quite feasible, and it has to do with symmetry enhancement. When proliferation of domain walls becomes favorable above the temperature T_{dw} , which we estimated previously, the entire system fragments into numerous domains. Therefore, the spins are able to change their orientations arbitrarily over large distances. The net orientation of a block of spins in such a configuration is no longer restricted to the n discrete angles but takes values uniformly between 0 and 2π . The order parameter, which captures the macroscopic symmetry of the system, therefore exhibits a continuous U(1) symmetry [95]. This emergent symmetry makes the \mathbb{Z}_n clock ferromagnet indistinguishable from the XY ferromagnet at macroscopic length scales. Therefore, the standard Kosterlitz-Thouless estimate for the formation energy of a single XY vortex becomes valid [48]. According to this estimate, the linear dependence of the vortex energy on L reduces to a logarithmic one: $e_{vx} \approx e_{vx}^0 + \pi \ln L$. This can now be countered by the logarithmic L dependence of the entropy term. The free energy

$$F(L) \sim e_{vx}^0 + \pi \ln L - 2T \ln L \quad (1.7)$$

changes sign at $T_{vx} = \pi/2$, if the constant core energy term is assumed to be negligible while L is taken to be a positive integer multiple of the lattice spacing. When $T > T_{vx}$, F becomes negative and formation of vortices becomes favorable. This calculation suggests that domain wall proliferation can lead to symmetry enhancement, which in turn can lead to favorable conditions for vortex proliferation.

For $n = 3$, our calculation provides an estimate of $T_{dw} \approx 1.65$ and $T_{vx} \approx 1.57$. Therefore, vortex proliferation is expected to preempt the formation of the symmetry enhanced phase and directly lead the system to disorder from the ordered phase. For $n \geq 4$, however, T_{dw} is smaller than T_{vx} and the possibility of a symmetry enhanced intermediate phase exists. These estimates are, however, valid only for the two dimensional clock ferromagnets. For

three dimensional clock ferromagnets, on the other hand, it has been suggested that the domain walls and vortices proliferate together at the same temperature and the intermediate phase is absent for all n [95]. With this rough picture in mind, we begin a direct investigation, using Monte Carlo simulation, into the role played by the two types of defects in \mathbb{Z}_n spin models.

1.6 Outline of the Thesis

In Chapter 2, we simulate the \mathbb{Z}_3 clock ferromagnet on a square lattice and show that the vortices and domain walls proliferate simultaneously across the order-disorder transition. In order to decouple the proliferation, we suppress the formation of the vortices by increasing their core energy. For weak suppression, we find that the two types of defects continue to proliferate simultaneously, but at a higher temperature. The order-disorder transition shifts to that temperature as well. For strong suppression, the simultaneous proliferation decouples and the order-disorder transition splits into two revealing an intermediate phase in between. We find that a $U(1)$ symmetry emerges in this intermediate phase and the system exhibits quasi-long-range order (QLRO). We demonstrate that the QLRO-disorder transition is driven by the proliferation of vortices while the order-QLRO transition is driven by domain wall proliferation. More specifically, we demonstrate that the latter transition is driven by the percolation of domain walls.

In Chapter 3, we show that vortex suppression splits the order-disorder transition in the \mathbb{Z}_4 clock ferromagnet on the square lattice and opens up an intermediate symmetry enhanced QLRO phase. However, a visual inspection of defect configurations in the disordered phase reveals an anomaly. We notice that the number of vortices in this phase is much larger than the number of antivortices, even though the system has periodic boundary conditions. We trace this anomaly back to a flaw in the standard method for calculating winding number. The flaw stems from adherence of the calculation to a rule of modular

arithmetic and manifests itself in models with even number of discrete states. We propose a modification to the calculation which violates the rule and, therefore, identifies the vortex defects correctly. When we repeat our simulation using this modified calculation and suppress the vortices, a partial symmetry broken region appears instead of the QLRO phase. The QLRO phase is recovered only when $\pm\pi$ domain walls, which separate opposite spin states, are suppressed as well. We show that this combination of vortex and $\pm\pi$ domain walls drives the QLRO-disorder transition in models with higher values of even n as well. We also show how this combination plays a role in the \mathbb{Z}_3 antiferromagnet on the square lattice.

In Chapter 4, we show that the order-disorder transition in the \mathbb{Z}_3 ferromagnet on a simple cubic is accompanied by a simultaneous percolation of domain walls and vortex strings. Strong suppression of the vortex strings splits the transition and opens up an intermediate phase where the domain walls percolate but the symmetry is partially broken instead of being enhanced. Since the transition from the ordered phase to the intermediate phase in this model and that in the model on the square lattice are both driven by percolation of domain walls, it is surprising that the resultant phase has different characteristics. In order to distinguish between the percolation process in the two cases, we study the percolation properties of individual types of $(a | b)$ domain walls, for each pair of states a and b . We find that the $(0 | 1)$ domain walls percolate on their own in the partial symmetry broken phase but remain at a percolation threshold throughout the QLRO phase. We also show that the order-disorder transition in the \mathbb{Z}_4 clock ferromagnet on a simple cubic lattice is also driven by a simultaneous percolation of vortex strings and domain walls. By suppressing the vortex strings, we obtain a partially symmetry broken phase in which the $(0 | 1)$ domain walls are observed to percolate on their own.

In Chapter 5, we investigate the phase diagram of the \mathbb{Z}_6 clock ferromagnet on the simple cubic lattice for which the apparent emergence of $U(1)$ symmetry in an intermediate region has been a topic of debate. We show that the apparent emergence, which has been

attributed to fluctuations induced by the disordering transition, persists even when that transition is destroyed by complete suppression of vortex strings and $\pm\pi$ domain walls. We demonstrate that the intermediate region is generated by the proliferation of vortex strings belonging to the \mathbb{Z}_3 subgroup of \mathbb{Z}_6 and is characterized by the simultaneous percolation of two types of domain walls. When the \mathbb{Z}_3 vortex strings are suppressed, the two types of domain walls stop percolating but the \mathbb{Z}_n symmetry broken behavior continues. When we suppress the formation of domain walls separating spins which differ by two states, \mathbb{Z}_n symmetry breaking is replaced by partial symmetry breaking due to restoration of a \mathbb{Z}_2 symmetry.

In Chapter 6, we study effect of lowering the core energy of vortices on the \mathbb{Z}_n ferromagnets. We start with the \mathbb{Z}_3 ferromagnet on the square lattice and show that the order-disorder transition splits into two for strong enhancement of vortices. The intermediate phase exhibits a sublattice ordering of vortices and antivortices. This vortex-antivortex lattice phase cannot be captured using a conventional symmetry-based order parameter. Therefore, we define a sublattice order parameter using the vortices themselves and show how this order parameter is able to clearly demarcate the vortex-antivortex lattice phase - from the ordered phase at the low temperature side and the disordered phase at the high temperature side. The formation of the vortex-antivortex lattice is demonstrated using vortex enhancement for ferromagnets on the square lattice for higher n as well. In three dimensions, however, the vortex strings are observed to form a condensate instead of a vortex-antivortex lattice.

In Chapter 7, we summarize the main results arising out of this work and conclude with a list of open problems.

Chapter 2

Symmetry Enhancement via Domain

Wall Percolation

An approximate energy versus entropy balance calculation (Sec. 1.5.6) for domain walls and vortices suggests that the temperature for vortex proliferation lies below that of domain wall proliferation for the \mathbb{Z}_3 ferromagnet on the square lattice. However, the formation of a vortex necessarily requires the presence of domain walls (Sec. 1.5.4), making it impossible for the vortices to proliferate before the domain walls. Does this imply that vortices proliferate simultaneously with domain walls, if not later, in the \mathbb{Z}_3 ferromagnet? Does the proliferation temperature lie close to that of the order-disorder transition in the model? Can we identify the defect responsible for driving the transition?

2.1 \mathbb{Z}_3 Clock Ferromagnet on the Square Lattice

2.1.1 Hamiltonian

The \mathbb{Z}_3 clock ferromagnet on the square lattice Λ is defined by the Hamiltonian

$$\mathcal{H} = \sum_{\langle i,j \rangle \in \Lambda} 1 - \cos(\theta_i - \theta_j) \quad (2.1)$$

where the spin vector at vertex $i \in \Lambda$ can orient at three different angles $\theta_i \in \{0, 2\pi/3, 4\pi/3\}$. The cosine potential has been subtracted from unity in order to set the lowest energy level at zero. The model is known to undergo an order-disorder transition at $T = 3/2 \ln(1 + \sqrt{3}) = 1.49 \dots$ [119].

2.1.2 Monte Carlo Simulation Algorithm

We have performed Monte Carlo simulation of this model, on square lattices containing $N = L^2$ spins, at different temperatures T using the Metropolis algorithm [120]. In this algorithm, the sum

$$E_i = \sum_{\{j \mid \langle i,j \rangle \in \Lambda\}} 1 - \cos(\theta_i - \theta_j) \quad (2.2)$$

representing the interaction between a spin θ_i at vertex $i \in \Lambda$ and its nearest neighbors at vertices j is calculated twice: once with the current angle of the spin, and once after proposing a new candidate angle θ'_i , which is chosen arbitrarily from the $n = 3$ possible values. The difference ΔE - between E_i with θ'_i and E_i with θ_i - determines whether the candidate angle will be accepted as the new angle of the spin. Specifically, the candidate is accepted with a probability $\min[1, \exp(-\Delta E/T)]$. These stochastic updates are performed at the vertices of the lattice in an arbitrary sequence. One Monte Carlo step is said to be completed after a complete lattice sweep, i.e. L^2 attempted updates.

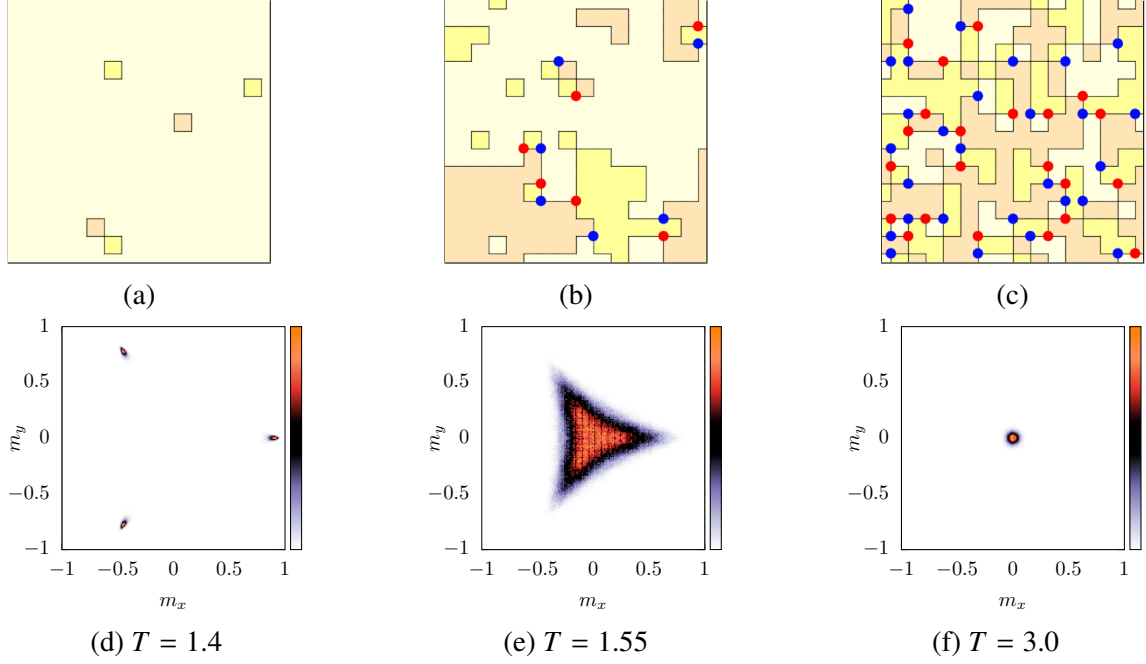


Figure 2.1: Typical spin configurations obtained on a $L = 16$ square lattice for the \mathbb{Z}_3 ferromagnet at different temperatures T overlaid with domain wall (black), vortex (blue) and antivortex (red) defects. The order parameter distribution obtained for a $L = 32$ system is also shown at the corresponding temperatures.

After each step, we have calculated the winding number (1.3) at each vertex $i' \in \Lambda'$ in order to generate the configuration of vortices corresponding to the spin configuration. We have also determined the configuration of domain walls, identified by $\theta_i \neq \theta_j$ at each edge of Λ' .

At low temperatures, the configurations show long range order wherein a majority of the spins are aligned along a common direction. The few spins which are misaligned get surrounded by domain walls. Vortices are absent at these temperatures (Fig. 2.1a). As the temperature is increased, the number of domain walls increases and a few vortices begin to appear in the form of bound vortex-antivortex dipoles (Fig. 2.1b). Beyond a certain temperature, the number of domain walls and vortices increase drastically and the system disorders. Some of the vortices separate out from their antivortices, while the others remain paired (Fig. 2.1c).

2.1.3 Order Parameter

We have also studied the symmetry manifested by the system at each of these temperatures. The order parameter for the \mathbb{Z}_3 model, in its two component vector form (m_x, m_y) , is given for a system of $N = L^2$ spins by

$$\begin{aligned} m_x &= \sum_{i \in \Lambda} \cos \theta_i / N \\ m_y &= \sum_{i \in \Lambda} \sin \theta_i / N \end{aligned} \quad (2.3)$$

At high temperatures, the symmetry is restored as evidenced by the single peak at $m_x = 0, m_y = 0$ (Fig. 2.1f). At low temperatures, the distribution $P(m_x, m_y)$ of the order parameter clearly shows a breaking of the three-fold symmetry (Fig. 2.1d).

Once in a while, over the course of a simulation, the system can muster sufficient fluctuation to jump over the transverse barriers (Fig 1.4b) and change the state in which its symmetry is broken. However, the frequency of these jumps decreases at lower temperatures. The frequency also decreases with increase in system size and in the thermodynamic limit, the system is expected to remain symmetry broken in one particular state. In such a case, the state in which the symmetry is broken will depend on the state in which the system was initialized.

In order to ascertain that the system breaks its symmetry in each of the $n = 3$ states, we have run an ensemble of twenty simulations. In each simulation of the ensemble, the system was initialized in a completely ordered configuration. The ordering spin state was chosen arbitrarily over the $n = 3$ possibilities across the ensemble. The $n = 3$ spots in Fig. 2.1d shows that the system is indeed capable of breaking symmetry in each of the n possible states. The same procedure of accumulating the order parameter distribution over an ensemble of simulations will be followed for subsequent models as well.

2.1.4 Thermodynamic Observables

In order to capture the phase transition in a quantitative manner, we have measured the magnetization $|m|$ and the magnetic susceptibility χ .

$$\begin{aligned} |m| &= \sqrt{m_x^2 + m_y^2} \\ \chi &= N(\langle |m|^2 \rangle - \langle |m| \rangle^2) / T \end{aligned} \quad (2.4)$$

In addition, we have also measured the number density of the vortex and domain wall defects. In the case of vortices, the density ρ_{vx} is given by the fraction of dual vertices $i' \in \Lambda'$ which contain a non-zero winding number. For domain walls, the density ρ_{dw} is given by the fraction of dual edges in Λ' across which $\theta_i \neq \theta_j$. In order to calculate the thermodynamic averages of these observables at each temperature, we have discarded the first 10^4 uncorrelated configurations for equilibration and performed measurements over the next 10^5 uncorrelated configurations.

2.1.5 Phase Diagram

The order-disorder transition is clearly captured by a decay of the magnetization across $T \sim 1.5$ (Fig. 2.2a). The susceptibility peaks at the same temperature and the peak grows with L (Fig. 2.2c). The density of both types of defects is found to increase simultaneously across the transition (Fig. 2.2b). Since there is no ascertainable gap between the proliferation of the two defects, an intermediate phase with emergent U(1) behavior can be ruled out. However, this same observation raises an interesting possibility. If the intermediate phase does not appear because the vortex proliferation preempts its formation, can we uncover the phase by delaying the proliferation of vortices?

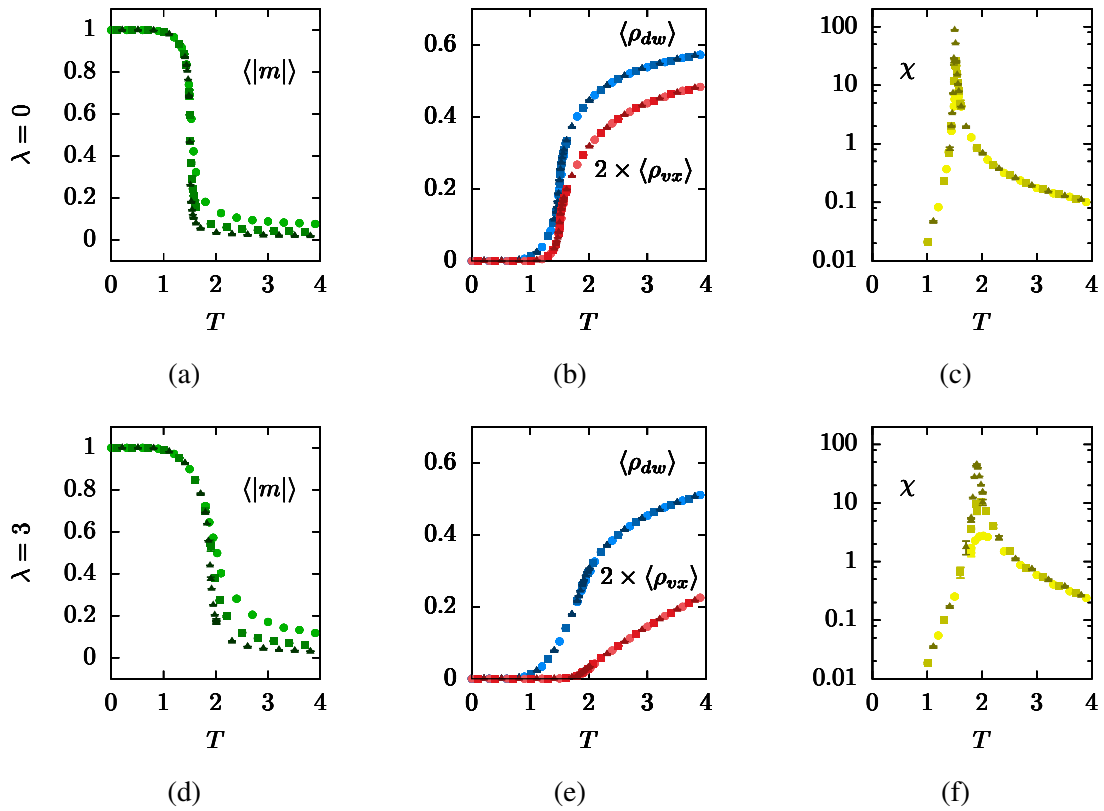


Figure 2.2: Top Panel: The density of domain walls and vortices increases simultaneously across the order-disorder transition captured by the decay in magnetization and the peak in magnetic susceptibility. Bottom Panel: Upon slightly raising the core energy of the vortices by an amount λ , proliferation of the two types of defects as well as the transition shift to a higher temperature. System sizes correspond to $L = 16$ (circle), $L = 32$ (square) and $L = 64$ (triangle).

2.2 Vortex Suppression

The standard method for delaying the proliferation of vortices is to raise their core energy e_{vx}^0 (1.7) by an amount λ [50, 53, 59, 60]. For $\lambda > 0$, the proliferation temperature of vortices shifts to a higher value. When this increment is applied to every vortex in a given configuration, the modified Hamiltonian becomes

$$\mathcal{H} = \sum_{\langle i,j \rangle \in \Lambda} 1 - \cos(\theta_i - \theta_j) + \lambda \sum_{i' \in \Lambda'} |\omega_{i'}| \quad (2.5)$$

In the \mathbb{Z}_3 model, all spin configurations that are possible on a square plaquette are found to generate winding numbers 0, +1 or -1. This allows us to take the absolute value of the winding number as an indication of whether a vortex defect is present at the dual vertex.

The introduction of the second term requires a modification in the energy calculation step of the Metropolis algorithm. In addition to the nearest-neighbor interaction energy, we have to calculate the number of vortices present in the four plaquettes neighboring a vertex $i \in \Lambda$. The candidate spin will be accepted with a probability depending on the difference between the initial and final energies, now calculated including the λ term.

2.2.1 Increased Cost of Computation

The calculation of winding numbers for the four plaquettes surrounding each vertex $i \in \Lambda$ increases the computational cost of the algorithm drastically. In addition, the Metropolis algorithm is known to suffer from large autocorrelation times near critical points [120]. In general, cluster algorithms are used as a way out of this problem [121, 122]. However, we are not aware of any cluster algorithm which can tackle the plaquette interactions that are effectively introduced into this model by the calculation of the winding number. The use of the Metropolis algorithm, coupled with the computational cost of the numerous winding number calculations, have severely limited our ability to investigate the behavior

of the model at large system sizes, specially near the transitions. As a consequence, we have not been able to obtain reliable values of the critical exponents which would allow us to determine the nature and order of the transitions in this and subsequent models. Instead, we have focussed on the nature of the phases themselves.

2.2.2 Weak Suppression of Vortices

For a slight suppression of the vortices using $\lambda = 3$, we find that the rise of vortex density shifts to a higher temperature $T \approx 2$ (Fig. 2.2e). However, the rise in domain wall density shifts to this temperature as well. The slight increase in λ is, therefore, unable to decouple the simultaneous proliferation of the defects. Interestingly, the temperature, at which the magnetization decays and the susceptibility peaks, also shifts to a higher value (Fig. 2.2d). This suggests that the order-disorder transition is driven by the simultaneous proliferation of the two types of defects.

We also note that with $\lambda > 0$, the decay of the magnetization and the increase in defect densities become more gradual. Usually, first-order transitions are accompanied by a strong jump in the order-parameter. Across second-order transitions, in comparison, the order-parameter gradually decays to zero. If the decay becomes even more gradual, does it indicate that the transition is changing its order to a higher one like that of the infinite order BKT transition? Since we have not measured the critical exponents for the transition, we are unable to address this question at the moment. However, we have found that the trend of the transition shifting to higher temperature with increasing λ continues till $\lambda \approx 8$. This trend is accompanied by the increase in defect density and decay of magnetization becoming even more gradual with increasing λ .

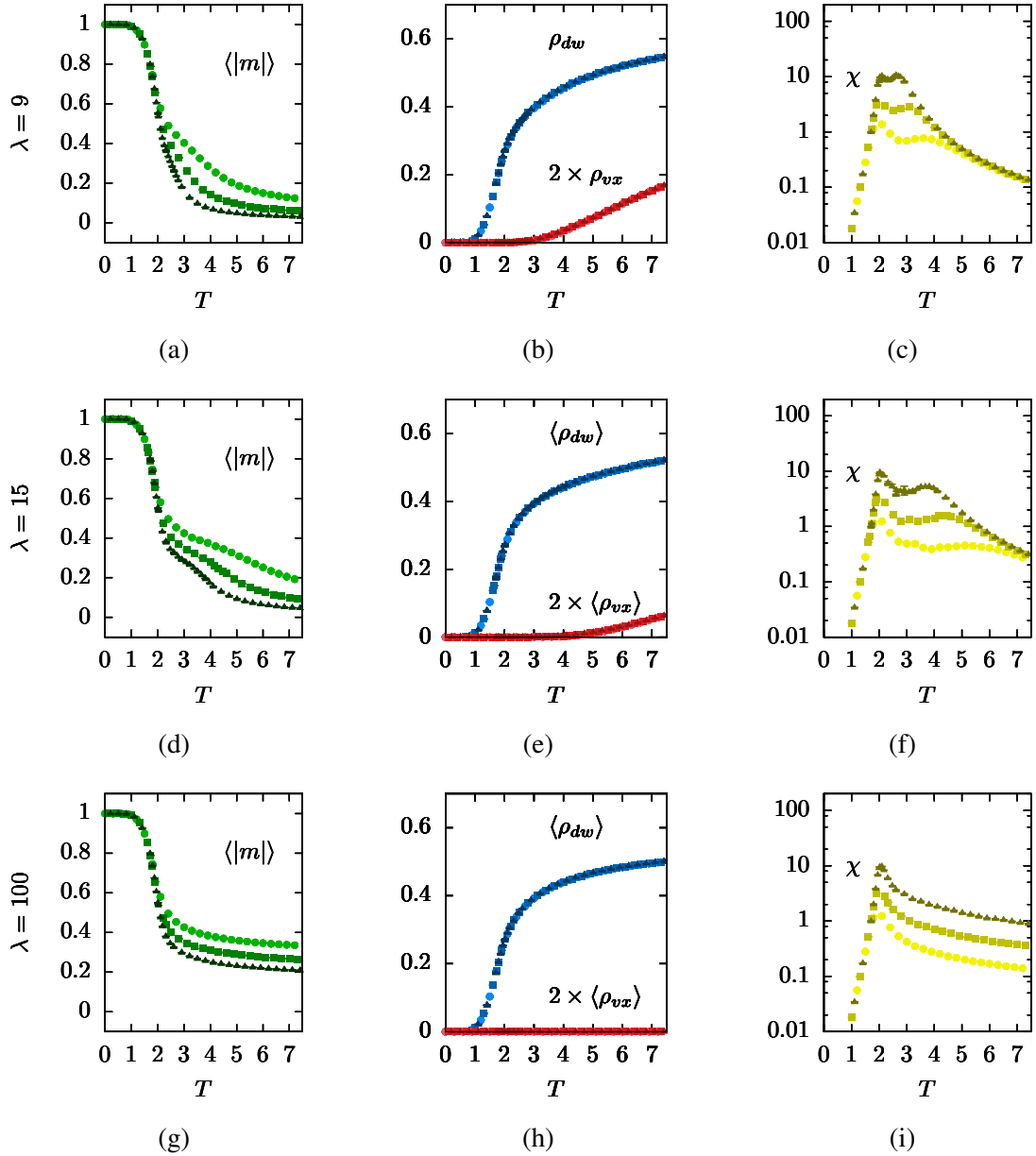


Figure 2.3: With strong suppression of vortices, the vortices proliferate at a temperature higher than that of domain wall proliferation. This decoupling of defect proliferation forces the order-disorder transition to split and admit an intermediate phase. The split is evidenced by a two-step decay in the magnetization $|m|$ and double peaks in the susceptibility χ . The transition from the intermediate phase to the disordered phase shifts to higher temperatures with increasing λ . System sizes correspond to $L = 16$ (circle), $L = 32$ (square) and $L = 64$ (triangle).

2.2.3 Strong Suppression of Vortices

For $\lambda = 9$, the vortices begin to proliferate at a temperature $T \approx 3.5$ which is clearly higher than the temperature $T \approx 2.2$ of domain wall proliferation (Fig. 2.3b). However, the maximum value attained by the vortex density ($\langle \rho_{vx} \rangle = 0.015$ at $T = 4.0$) for this λ is much smaller than that attained at lower values of λ , e.g. $\langle \rho_{vx} \rangle = 0.24$ at $T = 4.0$ for $\lambda = 0$. This confirms that the formation of vortices is being suppressed by increasing λ . With further increase in suppression, using $\lambda = 15$ (Fig. 2.3e), the proliferation of vortices shifts further in temperature and finally recedes to very high temperatures for $\lambda = 100$ (Fig. 2.3h). Since the vortex proliferation has decoupled from domain wall proliferation, the manner in which the domain wall density increases around $T \approx 2.2$ remains constant, independent of the change in λ .

The decoupling of defect proliferation has a drastic influence on the thermodynamic observables. The order-disorder transition appears to split and the magnetization exhibits a two-step decay for $\lambda = 9$ (Fig. 2.3a). The gap between the two decay steps increases with λ . The first decay from the ordered phase to the intermediate region, which occurs at $T \approx 2.2$, is close to the temperature where the domain walls start proliferating. The second decay, from the intermediate region to the disordered phase, continues to shift to higher temperatures closely following the shift in vortex proliferation. For extreme suppression of vortices with $\lambda = 100$, the second decay recedes to very high temperatures (Fig. 2.3g). This behavior is also reflected in the data for susceptibility. At $\lambda = 9$, we observe the formation of two peaks (Fig. 2.3c). With increasing λ , the second peak shifts to higher temperatures while the first peak remains at $T \approx 2.2$. This set of observations establishes that the transition from the ordered phase to the intermediate phase is driven by the proliferation of domain walls while the transition from the intermediate phase to the disordered phase is driven by the proliferation of vortices.

We have also measured the specific heat of the system $c_v = (\langle H^2 \rangle - \langle H \rangle^2)N/T^2$ at different temperatures for each value of λ . For $\lambda = 0$, c_v peaks at $T \approx 1.5$ (Fig. 2.4a). The peak

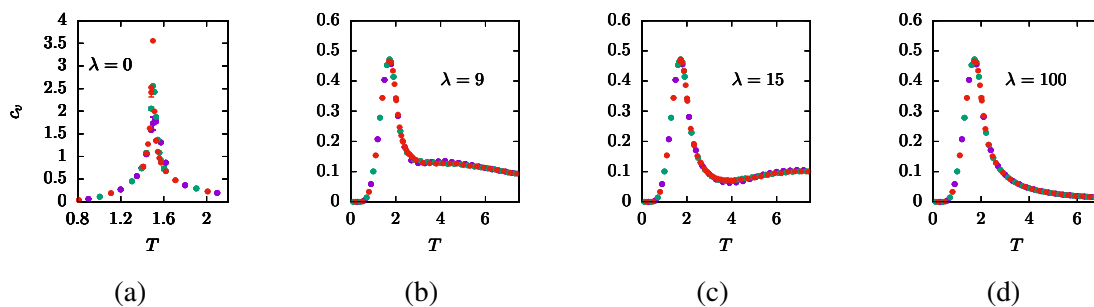


Figure 2.4: Variation of specific heat in the 2D \mathbb{Z}_3 ferromagnet at different values of λ . System sizes correspond to $L = 16$ (purple), $L = 32$ (green) and $L = 64$ (red).

is observed to grow with increasing system size. This reflects the second-order nature of the order-disorder transition. With $\lambda = 9$, we find that the peak splits into a sharp peak at $T \approx 1.7$ and a shallow bump around $T \approx 4.2$ (Fig. 2.4b). Neither of these two features show a system size dependence. With increasing λ , the shallow bump keeps shifting to higher temperatures while the sharp peak remains at $T \approx 1.8$. The observation that this peak does not scale with system size suggests that the order of transition has increased from second order to, possibly, one with an essential singularity. In fact, it is known that the transition from order to intermediate phase in two dimensional \mathbb{Z}_5 and higher models is a BKT transition with an essential singularity and that the specific heat which accompanies the transition does not show any system size dependence [15, 16].

Before exploring the nature of the intermediate phase, we note that the manner in which the thermodynamic observables change with system size, makes it difficult to accurately ascertain the extent of the intermediate phase for the range of λ values considered here. We find that for $\lambda = 9$, the second peak in the susceptibility moves closer towards the first peak with increasing system size (Fig. 2.3c). Therefore, it is possible that the two peaks will merge above a certain system size. Even for $\lambda = 15$, the second peak starts to move towards the first with increasing system size (Fig. 2.3f). On the other hand, we find that the location of the second peak shifts to higher temperatures with increasing values of λ , for a given system size. The competing effect of system size and λ , therefore, gives rise to two alternate scenarios:

1. There exists a threshold λ_+ , above which the intermediate phase has a non-zero extent in the thermodynamic limit.
2. The intermediate region shrinks to a point in the thermodynamic limit for all finite λ and the model exhibits an extended intermediate phase only in the $\lambda \rightarrow \infty$ limit.

A systematic characterization of the rate at which the intermediate region shrinks with system size and the rate at which the region expands with λ is required in order to answer this question.

2.3 Symmetry Enhanced Intermediate Phase

The data for $\lambda = 100$, provides a large range of temperatures in which the properties of the intermediate phase can be studied clearly. A measurement of the order parameter distribution, accumulated over an ensemble of simulations, inside this phase shows an annular structure which indicates the emergence of U(1) symmetry (Fig. 2.5a). Typical spin configurations obtained in this phase show a gradual change of the states across large distances. In addition, the configurations show absence of vortices but proliferation of domain walls (Fig. 2.5b). The manner in which the domain walls span across the entire system suggests that their proliferation can be captured in a quantitative manner using the framework of percolation theory.

2.3.1 Domain Wall Percolation

Percolation theory deals with the statistics of clustering processes [123]. A variety of clustering processes exhibit two types of phases: one in which a constituent cluster is large enough to span across the entire system, and another in which none of the clusters are large enough to do so. Suitably defined clusters of spins in a variety of spin models like the Ising, Potts and XY models exhibit a percolation transition which can

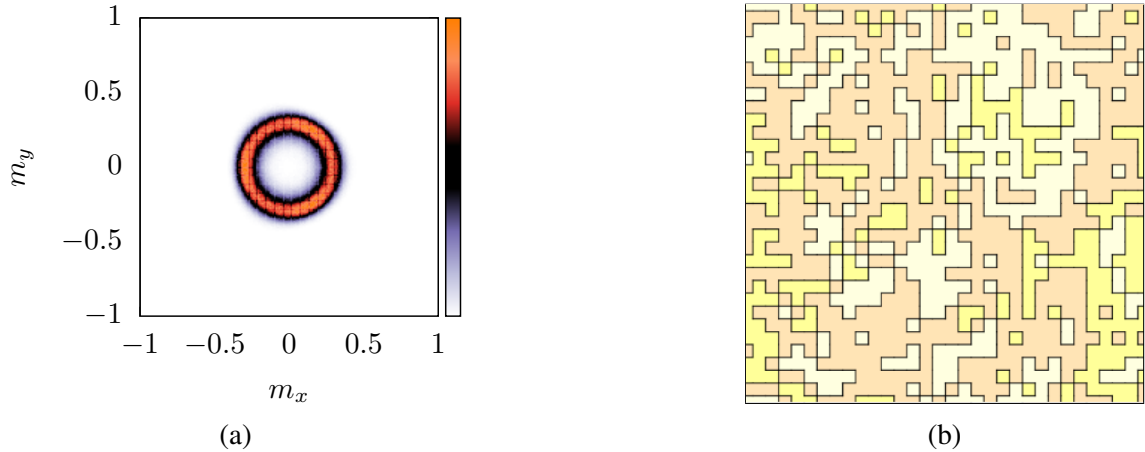


Figure 2.5: The intermediate phase uncovered using strong suppression of vortices ($\lambda = 100$) reveals (a) an emergent U(1) symmetry in the order parameter distribution obtained at $T = 5$ for a $L = 32$ system, and (b) proliferation of domain walls but absence of vortices in typical spin configurations obtained at the same temperature.

be mapped exactly onto the thermodynamic transition [96–98, 104, 122, 124, 125]. The key to this mapping lies in joining two neighboring spins into the same cluster using a particular stochastic scheme. The perimeter of these stochastically generated clusters can be viewed as a stochastic version of the domain walls. While a study of the percolation properties exhibited by such domain walls are an interesting topic in its own right, we will restrict ourselves to the percolation properties of geometric domain walls in this thesis. The percolation transition of these geometric domain walls need not coincide with the thermodynamic transition.

For each configuration, geometric domain walls are constructed by joining two domain wall segments which reside on adjacent edges of Λ' , i.e. which share a common vertex $i' \in \Lambda'$. We have labelled isolated domain wall clusters using the Hoshen-Kopelman algorithm [123] and identified the largest cluster. The fraction P_{dw} of dual edges in this largest cluster measures the strength of percolation and serves as an order parameter for the percolation transition. Setting aside the largest cluster for each configuration, we have binned the sizes of all the other clusters into a distribution $n(s)$. By accumulating data for this distribution over 10^5 uncorrelated configurations, we have measured the average size

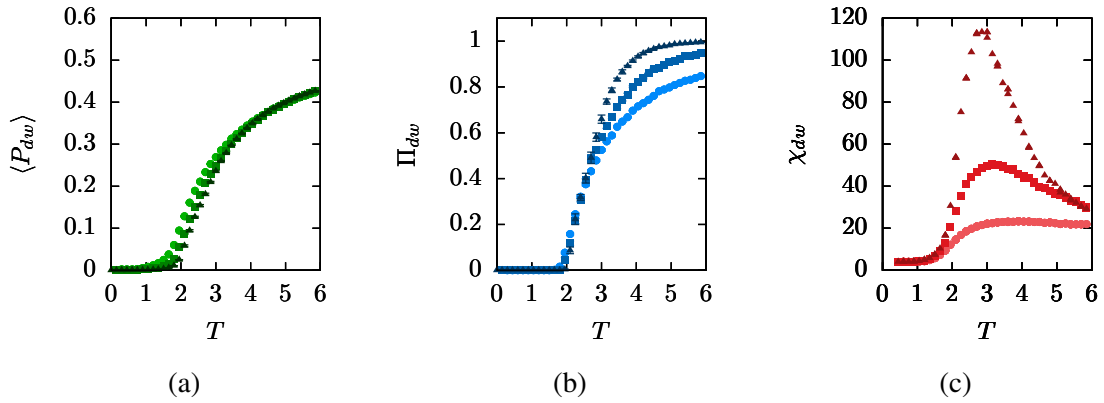


Figure 2.6: Measurement of standard percolation observables for geometric domain walls show that (a) the percolation strength P_{dw} increases in the intermediate phase $T > 2.2$, (b) the spanning probability Π_{dw} saturates to unity in that phase and (c) the average size of domain walls χ_{dw} peaks near the transition from the ordered phase to the intermediate phase. System sizes correspond to $L = 16$ (circle), $L = 32$ (square) and $L = 64$ (triangle).

of clusters according to the formula

$$\chi_{dw} = \frac{\sum_s s^2 n(s)}{\sum_s s n(s)} \quad (2.6)$$

This observable is similar to magnetic susceptibility and diverges at a continuous percolation transition [123]. In addition, for each configuration, we have checked if any cluster, formed using open boundary conditions, spans from one face of the system to the opposite face. The average of this Boolean measurement over the configurations gives the spanning probability Π_{dw} . In the thermodynamic limit, the value of this observable is one in the percolated phase, and zero otherwise.

Our measurements show that the size of the largest cluster rises across the transition from the ordered to the intermediate symmetry enhanced phase (Fig. 2.6a). The spanning probability saturates to unity in the intermediate phase and the curves for different L cross near $T \approx 2.2$, which is very close to our estimate for the temperature of the thermodynamic transition from the ordered phase to the intermediate phase (Fig. 2.6b). A high precision estimate of the thermodynamic transition and percolation temperatures is required to ascertain if the two transitions actually coincide without the need for a stochastic scheme.

This result shows that the symmetry enhancing transition from the ordered phase is driven not just by the proliferation, but more specifically, by the percolation of domain walls. We have checked that the domain walls continue to percolate in the symmetry enhanced phase and also in the disordered phase. Therefore, domain wall percolation does not distinguish between these two phases. It is the proliferation of vortex defects which brings about the distinction between the symmetry enhanced phase and the disordered phase.

2.3.2 Two-Point Correlations

While the result obtained for domain wall percolation vindicates the picture of symmetry enhancement due to domain wall proliferation, it does not provide any answer regarding the nature of ordering in the symmetry enhanced phase. The magnetization, at each temperature in this phase, is found to gradually decay with increasing system size (Fig. 2.3g) in a manner characteristic of critical behavior. Such a slow decay at each temperature has also been reported for the quasi-long-range ordered (QLRO) phase in the two dimensional XY ferromagnet [126]. In the XY model, the phase exhibits QLRO because a system with a continuous symmetry cannot exhibit long-range order in two dimensions [116]. Does the continuous U(1) symmetry, even though emergent, bring about QLRO in the intermediate phase of the present model? This type of order can be characterized using two-point spin-spin correlations $C(r) = \langle \cos(\theta_0 - \theta_r) \rangle$, where θ_0 and θ_r are spins located an Euclidian distance r apart on the lattice and the average is over all such pairs. In the QLRO phase, the correlation is expected to decay as a power-law $C(r) \propto r^{-\eta}$, where the exponent η changes with temperature [115]. Since a power-law decay of $C(r)$ is typically obtained at a critical point, the entire QLRO phase can be viewed as a line of critical points.

We have measured $C(r)$ at different temperatures in the intermediate phase and for different system sizes. In order to capture the expected power-law behavior over a range of r , we have simulated the systems with upto $L = 256$, despite the computational difficulties (2.2.1). Our results clearly show that $C(r)$ decays as a power-law with an exponent

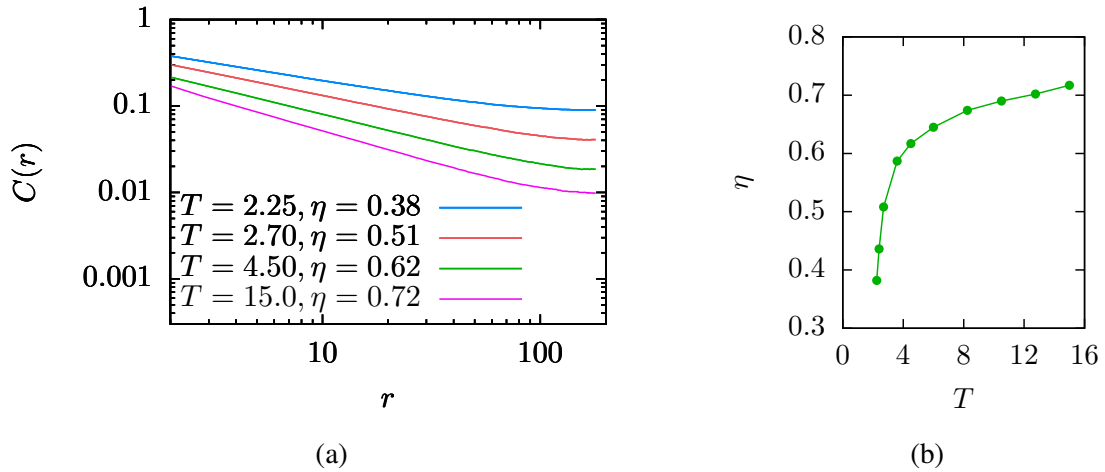


Figure 2.7: Measurement of two-point correlation for a $L = 256$ system shows a power-law decay whose exponent η changes with temperature, thus confirming the QLRO nature of the phase.

which changes with temperature (Fig. 2.7a). The small tapering effect at the end of $C(r)$ is due to the finite size of the system. In the thermodynamic limit, this effect is expected to vanish and $C(r)$ is expected to exhibit a full power-law decay. We have also measured the exponent η at different temperatures (Fig. 2.7b) and find that it increases from a value $\eta \approx 0.35$, obtained right after the order-QLRO transition, and saturates at $\eta \approx 0.75$ for higher temperatures. This result is quite surprising because η in the QLRO phase of \mathbb{Z}_n clock models with $n > 4$, increases from $\eta = 4/n^2$ at the order-QLRO transition to $\eta = 1/4$ at the QLRO-disorder transition [16]. Our results show that η in the QLRO phase of the \mathbb{Z}_3 model starts from $\eta > 1/4$ at the order-QLRO transition itself. It would be interesting to adapt the Kosterlitz renormalization group equations for the XY model [127] to the present model and analyze the behavior of η in this QLRO phase.

\mathbb{Z}_3 is the smallest \mathbb{Z}_n group which is cyclic in nature. By demonstrating that this symmetry can get enhanced to $U(1)$, we have made a strong case for the possibility that every discrete and cyclic symmetry can show enhancement to $U(1)$. This demonstration has been possible because we have correctly identified the mechanism which drives symmetry enhancement: percolation of domain walls in the absence of vortex proliferation. Does the same mechanism enhance \mathbb{Z}_n symmetries to $U(1)$ for higher n as well?

Chapter 3

Vortex Winding Number and Role of $\pm\pi$ Domain Walls

The energy versus entropy balance calculation (Sec. 1.5.6) suggests that the temperature for vortex proliferation in \mathbb{Z}_n clock models is higher than that for domain wall proliferation when $n \geq 4$. Therefore, an intermediate symmetry enhanced phase, in which the domain walls proliferate but vortices do not, is expected to occur naturally for $n \geq 4$. However, \mathbb{Z}_n clock models are known to exhibit such an intermediate phase only for $n \geq 5$ [10, 12, 16]. The \mathbb{Z}_4 clock model exhibits a single order-disorder transition. Is this single transition driven by a simultaneous proliferation of domain walls and vortices, in a manner similar to the \mathbb{Z}_3 case?

The \mathbb{Z}_4 ferromagnet supports a family of interaction potentials, of which the clock potential is only a special case [128]. Another member of this family is the Potts potential which prefers neighboring spins to be in the same state and penalizes any dissimilarity with an energy cost, i.e it has a Kronecker delta form $-\delta(\theta_i, \theta_j)$. These two potentials can be smoothly changed into one another by varying a single parameter [128]. For all the potentials characterized by the variation of this parameter, the \mathbb{Z}_4 ferromagnet exhibits a single order-disorder transition which is continuous in nature. Surprisingly, however, the

critical exponents of these transitions vary continuously with the parameter in an apparent violation of the universality paradigm. This continuously varying critical behavior is generated by an interplay between n -fold symmetry breaking perturbations (which has the effect of generating domain walls) and vortices at the transition [37]. It implies that a simultaneous proliferation of domain walls and vortices is responsible for driving the order-disorder transition. However, there has been no direct demonstration of this simultaneous proliferation. Furthermore, the behavior of the system under suppression of vortices has not been studied. Can the suppression split the order-disorder transition and open up an intermediate symmetry enhanced phase in the \mathbb{Z}_4 clock ferromagnet, as it did in the \mathbb{Z}_3 case?

3.1 \mathbb{Z}_4 Clock Ferromagnet on the Square Lattice

3.1.1 Hamiltonian

The \mathbb{Z}_4 clock ferromagnet with a λ increment of the vortex core energy is described by the Hamiltonian

$$\mathcal{H} = \sum_{\langle i,j \rangle \in \Lambda} 1 - \cos(\theta_i - \theta_j) + \lambda \sum_{i' \in \Lambda'} |\omega_{i'}| \quad (3.1)$$

where the spin vector at vertex $i \in \Lambda$ can orient at four different angles $\theta_i \in \{0, \pi/2, \pi, 3\pi/2\}$.

3.2 Phase Diagram

We have simulated the \mathbb{Z}_4 model using the Metropolis algorithm and measured the $n = 4$ version of the vector order parameter (m_x, m_y) (), the density of domain walls ρ_{dw} and the density of vortices ρ_{vx} for different system sizes.

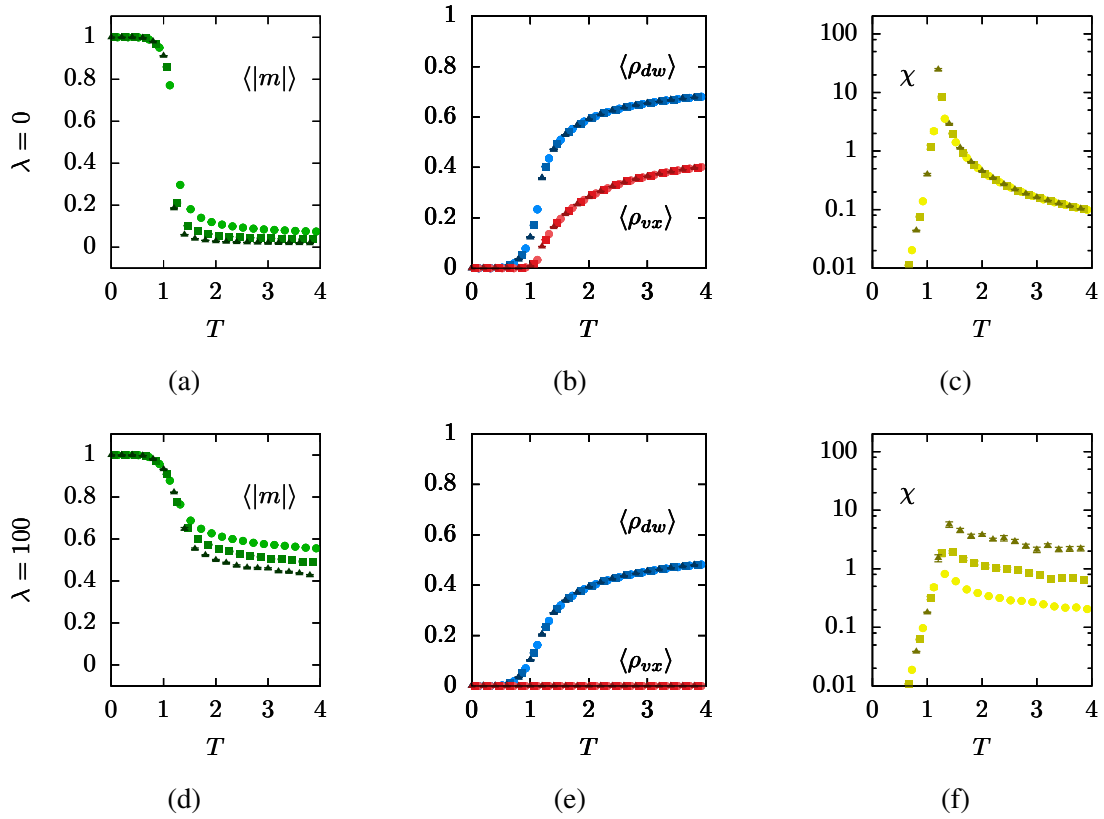


Figure 3.1: Top panel: The magnetization $|m|$ decays across the order-disorder transition in the \mathbb{Z}_4 clock ferromagnet on a square lattice, accompanied by a simultaneous increase in the densities of domain walls ρ_{dw} and vortices ρ_{vx} . Bottom panel: With extreme suppression of vortices, the order-disorder transition splits and the disordering transition recedes to very high temperatures. The system shows a single transition order-QLRO transition accompanied by the proliferation of domain walls. Data has been obtained for system sizes $L = 16$ (circle), $L = 32$ (square) and $L = 64$ (triangle).

The order-disorder transition, in the model without vortex suppression ($\lambda = 0$), is captured by a decay in magnetization at $T \approx 1.1$ (Fig. 3.1a). The magnetic susceptibility χ shows a peak at this temperature as well (Fig. 3.1c). We find that the density of domain walls and vortices both increase simultaneously across the transition temperature (Fig. 3.1b). This explains why the \mathbb{Z}_4 clock ferromagnet does not exhibit an intermediate phase.

With increase in vortex suppression strength λ , the simultaneous proliferation of the two types of defects and the accompanying transition shift to higher temperatures and then split into two in a manner similar to that observed in the case of the \mathbb{Z}_3 ferromagnet. An intermediate phase appears between the split transitions. The transition from the interme-

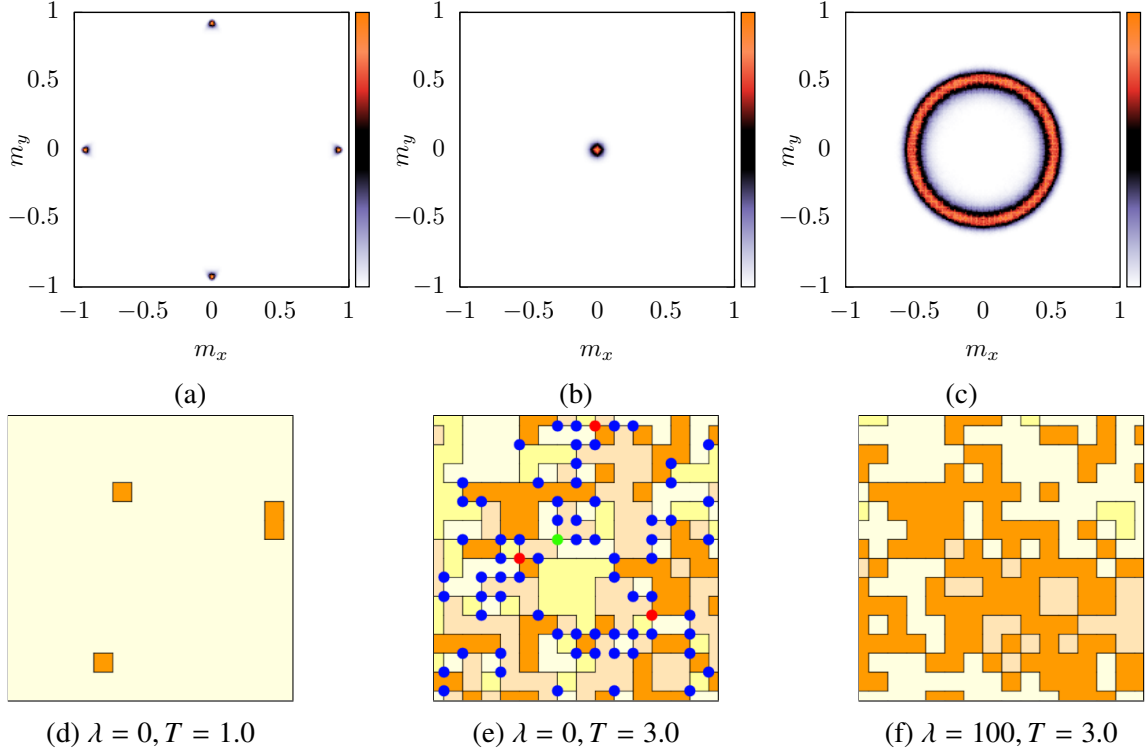


Figure 3.2: Typical spin and defect configurations obtained for the \mathbb{Z}_4 clock ferromagnet on a $L = 16$ lattice and the order parameter distribution obtained for a $L = 32$ system obtained in the ordered phase (a),(d); in the disordered phase (b),(e); in the intermediate symmetry enhanced phase (c),(f). Note the unusual dominance of vortices (blue) over antivortices (red) in the disordered phase. A vortex with winding number $+2$ (green) is also present in the configuration for that phase.

intermediate phase to the disordered phase, which is associated with vortex proliferation, recedes to very high temperatures with extreme suppression of vortices using $\lambda = 100$ (Fig. 3.1d). On the other hand, the transition from the ordered phase to the intermediate phase, which is associated with domain wall proliferation, remains at $T \approx 1.5$.

Our measurement of the order parameter distribution $P(m_x, m_y)$ for $\lambda = 0$, reveals that the ordered phase breaks a four-fold symmetry (Fig. 3.2a), which gets restored in the disordered phase (Fig. 3.2b). In the intermediate phase obtained for $\lambda = 100$, the distribution clearly shows an enhancement of the symmetry to $U(1)$ (Fig. 3.2c). So far the behavior of the system is similar to that obtained for the \mathbb{Z}_3 model. This might suggest that domain wall driven symmetry enhancement and vortex driven symmetry restoration is a generic feature of \mathbb{Z}_n ferromagnets on the square lattice.

An inspection of the spin and defect configurations shows that a few domain walls appear in the ordered phase (Fig. 3.2d) and begin to proliferate in the symmetry enhanced phase (Fig. 3.2f). However, we come across a glaring anomaly, when we inspect the defect configurations obtained in the disordered phase. While vortices are expected to proliferate in the disordered phase, we also expect an equal number of vortices and antivortices to appear in any given configuration because we are simulating a system with periodic boundary conditions (Sec. 1.5.6). However, our simulation shows an outright dominance of vortices over antivortices in the disordered phase (Fig. 3.2e). In addition, we find vortices with winding number +2 but no antivortices with winding number -2. This unphysical behavior suggests that we should verify the correctness of our method for identifying the vortex defects. Our attempt at this verification has revealed a flaw in the standard method for calculating winding number.

3.3 Winding Number Calculation

Consider a small region (Fig. 3.3) of the spin configuration (Fig. 3.2e) which appears to sustain more vortices than antivortices, and even a vortex with winding number +2. Let us evaluate the winding number for each plaquette explicitly using the standard method (Eq. 1.3).

3.3.1 Standard Method

On the bottom-left plaquette, the angles when read in an anticlockwise sense are: $0, 3\pi/2, \pi$ and $\pi/2$. Their contribution to the winding number is calculated as $([3\pi/2 - 0]_{2\pi} + [\pi - 3\pi/2]_{2\pi} + [\pi/2 - \pi]_{2\pi} + [0 - \pi/2]_{2\pi})/2\pi$. Upon evaluating the modular difference for each term, the winding number becomes $(-\pi/2 - \pi/2 - \pi/2 - \pi/2)/2\pi = -1$. Therefore, we obtain an antivortex in this region. The negative sign obtained in this case arises from our convention of going anticlockwise around the plaquette. If we go clockwise, the sign should flip. We can verify this by computing the winding number in the reverse

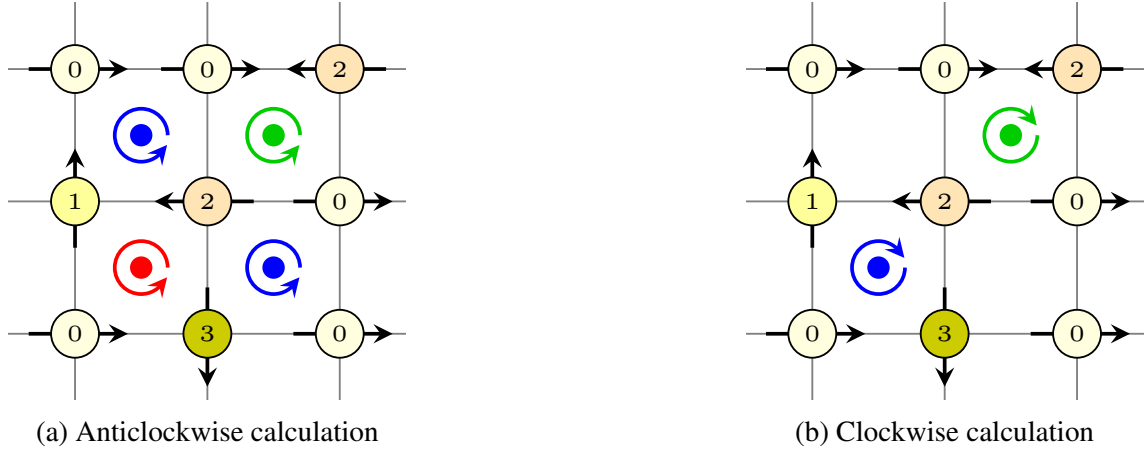


Figure 3.3: Vortex defects identified using the standard method in (a) the anticlockwise sense and (b) the clockwise sense for a configuration of \mathbb{Z}_4 spin states. Red, blue and green denote defects with winding number -1, +1 and +2, respectively.

sense, which gives us $([\pi/2 - 0]_{2\pi} + [\pi - \pi/2]_{2\pi} + [3\pi/2 - \pi]_{2\pi} + [0 - 3\pi/2]_{2\pi})/2\pi = (+\pi/2 + \pi/2 + \pi/2 + \pi/2)/2\pi = +1$. Indeed, we obtain a vortex with winding number +1 on the bottom-left plaquette (Fig. 3.3b).

On the top-left plaquette, the angles when read in an anticlockwise sense are $\{\pi/2, \pi, 0, 0\}$ (Fig. 3.3a). Their contribution is evaluated as $([\pi - \pi/2]_{2\pi} + [0 - \pi]_{2\pi} + [0 - 0]_{2\pi} + [\pi/2 - 0]_{2\pi})/2\pi = (+\pi/2 + \pi + 0 + \pi/2)/2\pi = +1$, indicating the presence of a vortex. The calculation when carried out in the clockwise sense, should give an antivortex. When we actually carry out this calculation: $([0 - \pi/2]_{2\pi} + [0 - 0]_{2\pi} + [\pi - 0]_{2\pi} + [\pi/2 - \pi]_{2\pi})/2\pi = (-\pi/2 + 0 + \pi - \pi/2)/2\pi = 0$, we find absence of a vortex, which should not be the case (Fig. 3.3b). The calculation on this plaquette clearly results in unphysical behavior. We will show that this behavior arises from a rule of modular arithmetic.

3.3.2 Violation of Modular Arithmetic

We note that every contributing term in the anticlockwise calculation has flipped sign during the clockwise computation, except for one: that representing the modular difference between angles 0 and π on the right edge of the top-left plaquette. In the anticlockwise calculation, this term appears as $[0 - \pi]_{2\pi} = [-\pi]_{2\pi}$. According to the rule of modular arith-

metic, the value should be adjusted to lie in $(-\pi, +\pi]$. Therefore we obtain the adjusted value $[-\pi]_{2\pi} = +\pi$. In the clockwise calculation, this term appears as $[\pi - 0]_{2\pi} = [+ \pi]_{2\pi}$. Since the argument already lies in the interval $(-\pi, +\pi]$, we obtain $[+\pi]_{2\pi} = +\pi$. Due to this half-closed nature of the interval, we obtain $+\pi$ as the answer for the modular difference of the term, in both anticlockwise and clockwise calculation. However, for identifying a physical vortex, we need the answer to flip sign when the sense is reversed. Clearly, this cannot be achieved if we continue to adjust the answer to lie within the half-closed interval as dictated by modular arithmetic. The interval should be symmetric, i.e. it should either be closed on both ends or be open on both ends. If it is open on both ends, the calculation of $[+\pi]_{2\pi}$ as well as $[-\pi]_{2\pi}$ becomes undefined. If, on the other hand, we use an interval $[-\pi, +\pi]$, which is closed at both ends, we obtain $[+\pi]_{2\pi} = +\pi$ and $[-\pi]_{2\pi} = -\pi$, which is precisely what we require. We conclude that in order to obtain a physical winding number, we must violate the interval criterion of modular arithmetic.

3.3.3 Modified Method

Using our new criterion for choosing the interval, we propose a modification to the winding number calculation which remedies the flaw in the standard method (Eq. 1.3). Our new definition of winding number, to be used hereafter, is as follows.

Definition. The winding number $\omega_{i'}$ associated with the $d-2$ dimensional element $i' \in \Lambda'$ which pierces the center of the square plaquette, is given by

$$\omega_{i'} = \frac{1}{2\pi}([\theta_j - \theta_i]_{2\pi} + [\theta_k - \theta_j]_{2\pi} + [\theta_l - \theta_k]_{2\pi} + [\theta_i - \theta_l]_{2\pi}) \quad (3.2)$$

Here $[\theta_j - \theta_i]_{2\pi} = \theta_j - \theta_i + 2\pi\alpha$, with $\alpha \in \mathbb{Z}$ chosen such that $\theta_j - \theta_i + 2\pi\alpha$ lies in $[-\pi, +\pi]$.

This modification, although subtle, can imply a drastic change in the physics of vortex defects. In particular, the numerical results in statistical models, quantum condensed matter systems and gauge theories, which have identified vortices using the standard method,

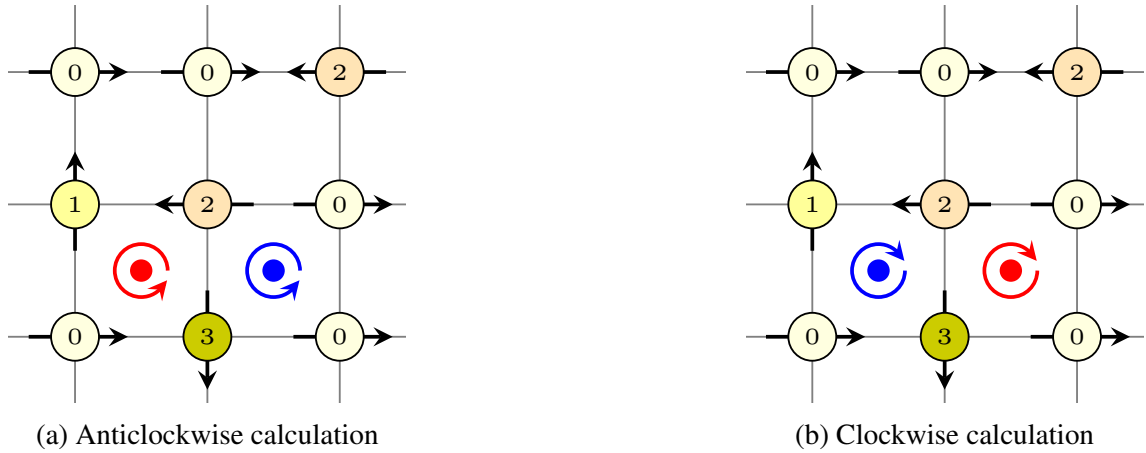


Figure 3.4: Vortex defects identified using the modified method in (a) the anticlockwise sense and (b) the clockwise sense for a configuration of \mathbb{Z}_4 spin states. Red, blue and green denote defects with winding number -1 , $+1$ and $+2$, respectively.

are now suspect. However, we note that the need for the modified method arises only when angle differences of $\pm\pi$ are present in the system. Such differences do not appear in models with odd number of states. Therefore, our results for the \mathbb{Z}_3 ferromagnet, obtained in Chapter 2, do not need revision. However, we need to revise the simulation results obtained for the \mathbb{Z}_4 ferromagnet. Before proceeding to revise the results, let us complete the evaluation of winding number for the other plaquettes (Fig. 3.3a) using the standard method and compare them to the new winding numbers obtained for the same spin configurations using our modified calculation.

Using the standard method, we obtain a vortex with winding number $+1$ in the anticlockwise sense on the bottom-right plaquette (Fig. 3.3a) and find that the vortex disappears when the sense is reversed (Fig. 3.3b). This unphysical behavior occurs due to the presence of angles 0 and π on the top edge of the plaquette. The vortex with winding number $+2$ appears on the top-right plaquette (Fig. 3.3a) due to the presence of $\pm\pi$ angle differences on all the four edges. Upon reversal of sense, the winding number does not flip sign but remains as $+2$ (Fig. 3.3b). This explains the absence of antivortices with winding number -2 in the disordered phase (Fig. 3.2e). The only legitimate vortex identified among all the four plaquettes seems to be the one belonging to the bottom-left plaquette (Fig. 3.3).

We now evaluate the winding number for the same spin configuration using our modified method (Eq. 3.2). As expected, we find the legitimate vortex on the bottom-left plaquette even using our modified method (Fig. 3.4a). Upon reversal to a clockwise sense, the vortex turns into an antivortex (Fig. 3.4b). Surprisingly, we do not find any vortex on the top-left and top-right plaquettes using our method. The vortices identified on these plaquettes using the standard method were, therefore, false vortices. If the standard method identifies such false vortices in large numbers, we should be careful in interpreting the data reported in the literature for models with even states. On the bottom-right plaquette we find a vortex in the anticlockwise sense, which turns into an antivortex in the clockwise sense (Fig. 3.4b). Of particular interest is the identification of vortices with +2 winding number using the standard method. We have evaluated the winding number for all possible spin configurations on a square plaquette for models with different values of n using our modified method. In none of the configurations did we find vortices with winding number ± 2 . Therefore, none of the models with finite n on a square lattice should exhibit winding numbers other than 0, -1 or +1. Hereafter, we discard the use of the standard method and resort to the use of our modified method for calculating winding number.

3.4 \mathbb{Z}_4 Clock Ferromagnet on the Square Lattice Revisited

As we begin our revision of the simulation results obtained for the \mathbb{Z}_4 clock ferromagnet, we find that the behavior of magnetization, susceptibility and domain wall density remains the same as that obtained in the previous case (Fig. 3.5a). This is expected because the winding number calculation has no relation to these quantities if we are not suppressing the vortices ($\lambda = 0$). However, the vortex density is found to be halved from a saturation value of $\rho_{vx} \approx 0.4$ at $T = 4$ in the previous simulation (Fig. 3.1b) to a value of $\rho_{vx} \approx 0.2$ at the same temperature in the modified simulation (Fig. 3.5b).

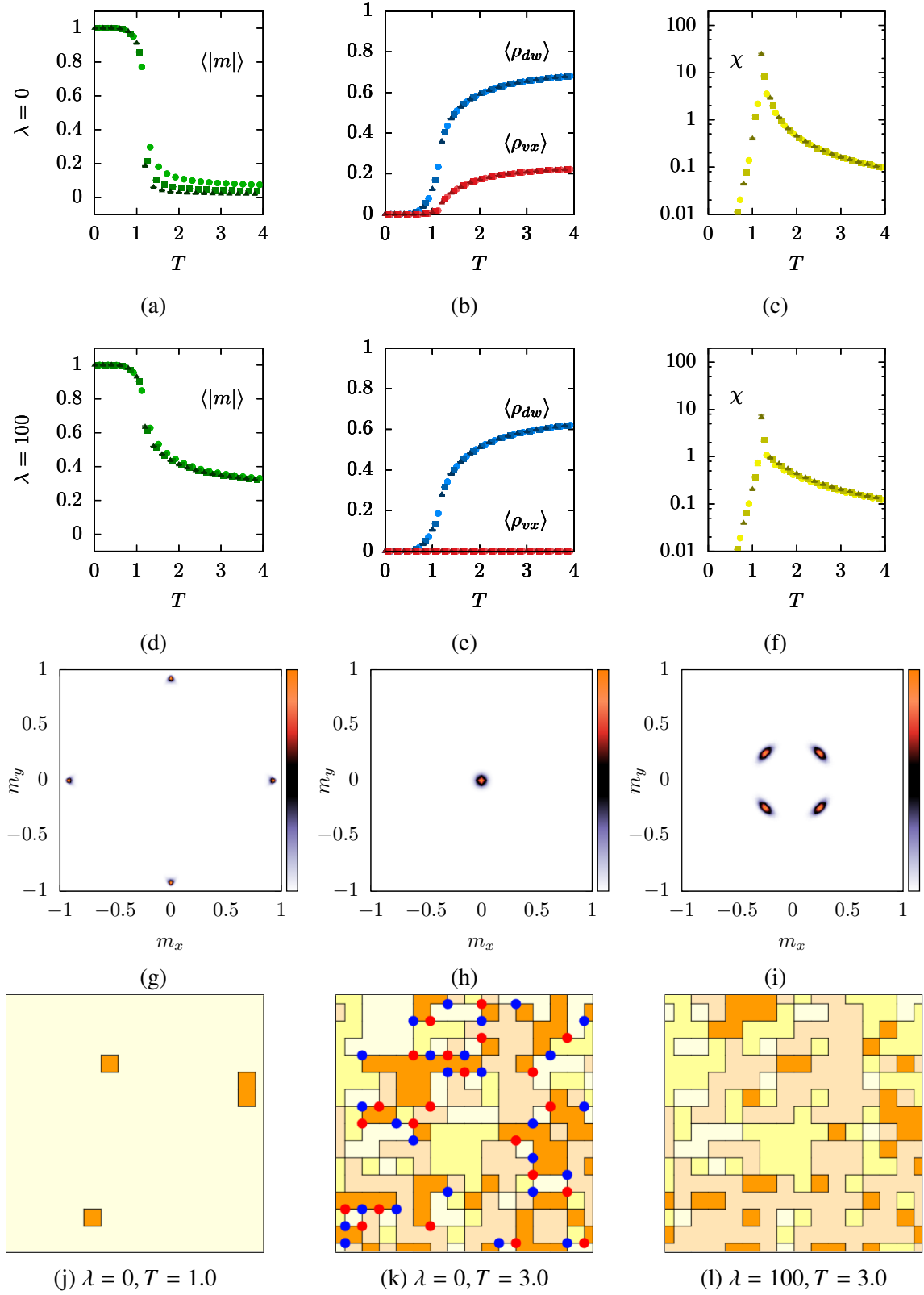


Figure 3.5: Revision of the data displayed in Fig. 3.1 and Fig. 3.2, arising due to the simulation being reperformed using our modified method for calculating winding number.

With extreme suppression of the vortices ($\lambda = 100$), all the thermodynamic observables (Fig. 3.5b) show a change in behavior compared to the previous results (Fig. 3.1). The domain wall density now touches a higher value $\rho_{dw} \approx 0.6$ at $T = 4$ (Fig. 3.5e) compared to a value of $\rho_{dw} \approx 0.5$ at the same temperature in the previous simulation (Fig. 3.1e). The magnetization, which showed a gradual decrease with system size at each point in the symmetry enhanced phase due to the onset of QLRO, now remains nearly constant with system size at each temperature (Fig. 3.5d). A similar change in behavior is observed in the portion of the susceptibility curve to the right of the peak (Fig. 3.5f). These results suggest that the QLRO of the symmetry enhanced phase, obtained in the previous simulation, has been replaced by a different type of order. The order parameter distribution at a temperature in this new phase shows a breaking of the four-fold symmetry but at angles offset from the spin angles by $\pi/4$ (Fig. 3.5i). This is precisely the pattern we had obtained for a partial symmetry broken phase from the renormalization picture of the continuum theory (Fig. 1.4c). This result suggests that the ordered phase undergoes a partial symmetry breaking transition driven by the proliferation of domain walls when the vortices are suppressed. Is this behavior particular to the \mathbb{Z}_4 ferromagnet? Does it occur for all \mathbb{Z}_n ferromagnets with $n > 3$? Or does it occur only for ferromagnets with even n ? In order to answer this question, we study the effect of vortex suppression on the next ferromagnet in the series, the \mathbb{Z}_5 ferromagnet.

3.5 \mathbb{Z}_5 Clock Ferromagnet on the Square Lattice

The \mathbb{Z}_5 clock ferromagnet with vortex suppression on the square lattice is described by the same Hamiltonian (3.1), except that each spin vector at vertex $i \in \Lambda$ can now orient at five different angles $\theta_i \in \{0, 2\pi/5, 4\pi/5, 6\pi/5, 8\pi/5\}$. This is the first model in the series of \mathbb{Z}_n clock ferromagnets which naturally exhibits an intermediate symmetry enhanced QLRO phase between a low temperature ordered phase and a high temperature disordered phase without the need for vortex suppression [15, 16]. While the decay in magnetization can

be used to locate the disordering transition, the order-QLRO transition can be located by noting the temperature at which the n -fold symmetry breaking perturbation (1.1) becomes irrelevant and gives way to the U(1) symmetric phase. In other words, we can search for the temperature across which $m_{5\phi}$ decays to zero [14], where

$$\begin{aligned} m_{n\phi} &= \langle \cos n\phi \rangle \\ \phi &= \arctan(m_y/m_x) \end{aligned} \quad (3.3)$$

We have simulated the ferromagnet and measured the thermodynamic observables, once without vortex suppression ($\lambda = 0$) and once with extreme vortex suppression ($\lambda = 100$).

For $\lambda = 0$, we find that the vortex density increases at a temperature $T \approx 1$, which is slightly higher than the temperature $T \approx 0.9$ across which the domain wall density increases (Fig. 3.6b). This is reflected in the behavior of the order parameter as well. The measure of symmetry breaking $m_{5\phi}$ decays from a unity to zero across $T \approx 0.9$ (Fig. 3.6a) while the magnetization decays at a slightly higher temperature $T \approx 1$. Therefore, the \mathbb{Z}_5 symmetry, which is broken in the ordered phase $T < 0.9$, gets enhanced to U(1) in the intermediate phase and restored at higher temperatures.

For $\lambda = 100$, the proliferation of vortices recedes to very high temperatures (Fig. 3.6e) along with the disordering transition. The narrow extent of symmetry enhanced phase obtained in the $\lambda = 0$ case, gets extended across a large range of temperatures above $T \sim 0.9$. The QLRO nature of the phase is reflected in the gradual decay of the magnetization with increasing system size at each temperature (Fig. 3.6d). The decay of $m_{5\phi}$, which marks the order-QLRO transition, and the proliferation of domain walls occurs around $T \approx 0.9$ (Fig. 3.6e). This result suggests that domain wall proliferation leads to symmetry enhancement and vortex proliferation leads to symmetry restoration in the \mathbb{Z}_5 ferromagnet.

The intermediate symmetry enhanced region occurs naturally, without the need for vortex suppression, in ferromagnets with higher $n \geq 5$ as well. [12, 15–18]. We have shown that

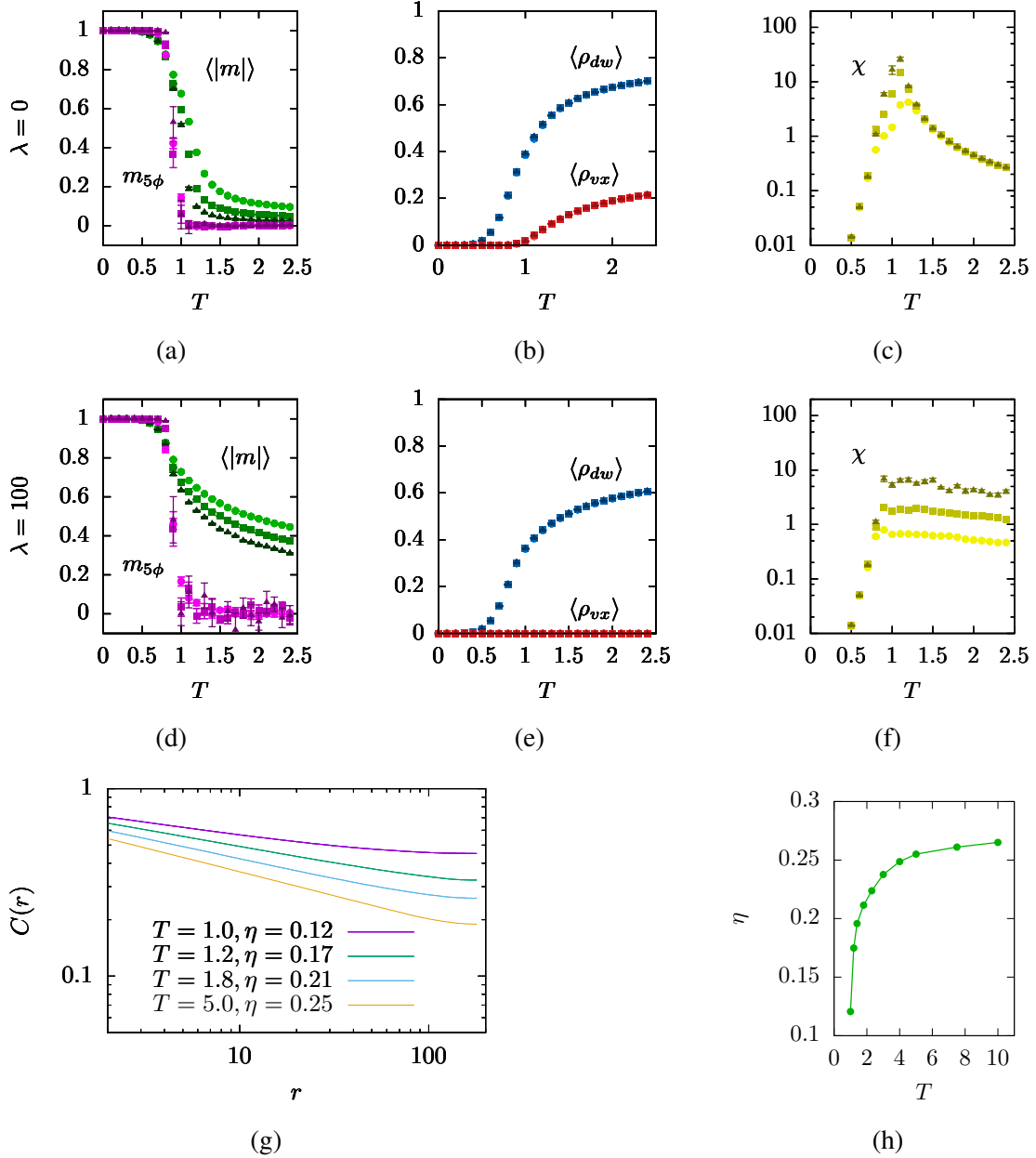


Figure 3.6: Top panel: The decay of $m_{5\phi}$ marks the onset of symmetry enhancement and the decay of magnetization marks the disordering transition in the \mathbb{Z}_5 clock ferromagnet on a square lattice. The former is accompanied by an increase in the density of domain walls ρ_{dw} while the latter is accompanied by increase in vortex density ρ_{vx} . Middle panel: With extreme suppression of vortices, the disordering transition recedes to very high temperatures. The system shows a single transition order-QLRO transition accompanied by the proliferation of domain walls. System sizes are the same as those in (Fig. 3.1). Bottom panel: Two-point correlations at different temperatures in the QLRO phase for a $L = 256$ system with $\lambda = 100$.

the \mathbb{Z}_3 ferromagnet also exhibits symmetry enhancement, albeit with the suppression of vortices. This raises an important question. Does the \mathbb{Z}_4 ferromagnet exhibit only partial symmetry breaking and never symmetry enhancement? This would be rather odd because there is no apparent reason for the \mathbb{Z}_4 ferromagnet to display a special behavior. On the other hand, we remind ourselves that we did obtain a symmetry enhanced phase in the \mathbb{Z}_4 ferromagnet when we suppressed the formation of vortices using the standard method for calculating winding number (Fig. 3.2c). It implies that, while using the standard method, some feature of the model got suppressed along with the vortices and opened up a symmetry enhanced phase but is no longer getting suppressed when the modified method is being used. In order to identify this feature, we need to revisit the sample spin configurations for which we calculated the winding numbers explicitly (Fig. 3.3a).

3.6 Role of $\pm\pi$ Domain Walls

We observe that the standard method always places a non-zero winding number on plaquettes which contain at least one angle difference of $\pm\pi$, whereas the modified method does not necessarily identify a vortex in such cases. This implies that with a non-zero vortex suppression λ , every instance of a $\pm\pi$ angle difference gets suppressed when using the standard method. Every instance of a $\pm\pi$ angle difference represents a $\pm\pi$ domain wall segment. For example, the four edges containing $\pm\pi$ angle differences in the top-right plaquette (Fig. 3.3a) represent four $\pm\pi$ domain wall segments. When using the standard method in the anticlockwise sense, a vortex is identified on this plaquette and λ suppresses this vortex, thus effectively suppressing the formation of the $\pm\pi$ domain walls. However, the modified method does not identify a vortex on that plaquette (Fig. 3.4a) and, therefore, does not suppress any of those $\pm\pi$ domain walls. Is suppression of $\pm\pi$ domain walls the feature which holds the key to obtaining a symmetry enhanced phase in the \mathbb{Z}_4 ferromagnet?

In order to answer this question, we have simulated the \mathbb{Z}_4 clock ferromagnet with extreme suppression of vortices as well as $\pm\pi$ domain walls. The Hamiltonian which includes energy costs for suppressing the two types of defects is given by

$$\mathcal{H} = \sum_{\langle i,j \rangle \in \Lambda} 1 - \cos(\theta_i - \theta_j) + \lambda \sum_{i' \in \Lambda'} |\omega_{i'}| + \delta\epsilon_{\pm\pi} \sum_{\langle i,j \rangle} \delta([\theta_i - \theta_j]_{2\pi}, \pm\pi) \quad (3.4)$$

where the last term increases the energy cost of a domain wall separating $\pm\pi$ angle differences by an amount $\delta\epsilon_{\pm\pi}$.

For $\lambda = 100$ and $\delta\epsilon_{\pm\pi} = 100$, we find that the behavior of the thermodynamic variables (Fig. 3.7) precisely match the behavior of the variables obtained when suppressing the vortices identified by the standard method (Fig. 3.1). The magnetization shows a decay from the ordered phase to an intermediate phase throughout which its value decays gradually with system size at each temperature, indicating the onset of QLRO (Fig. 3.7a). The order parameter distribution clearly shows an emergence of U(1) symmetry (Fig. 3.7d).

In summary, if we start with the order-disorder transition in the $\lambda = 0$ \mathbb{Z}_4 clock ferromagnet and suppress the formation of vortices alone, then the transition splits and the intermediate phase shows partial symmetry breaking. The transition from the ordered phase to the intermediate phase is driven by the proliferation of domain walls, including $\pm\pi$ domain walls while the transition from the intermediate phase to the disordered phase is driven by vortices. If instead, we start with the order-disorder transition and suppress the formation of vortices as well as $\pm\pi$ domain walls, the transition splits and the intermediate phase exhibits symmetry enhancement with QLRO. The order-QLRO transition is driven by all domain walls, except for the $\pm\pi$ type, while the QLRO-disorder transition is driven by a simultaneous proliferation of vortices and $\pm\pi$ domain walls.

The $\pm\pi$ domain walls do not appear in ferromagnets with odd n . However, they do appear in ferromagnets with higher values of even n . This naturally raises the question: Is the QLRO-disorder transition in those models driven by the combined proliferation of

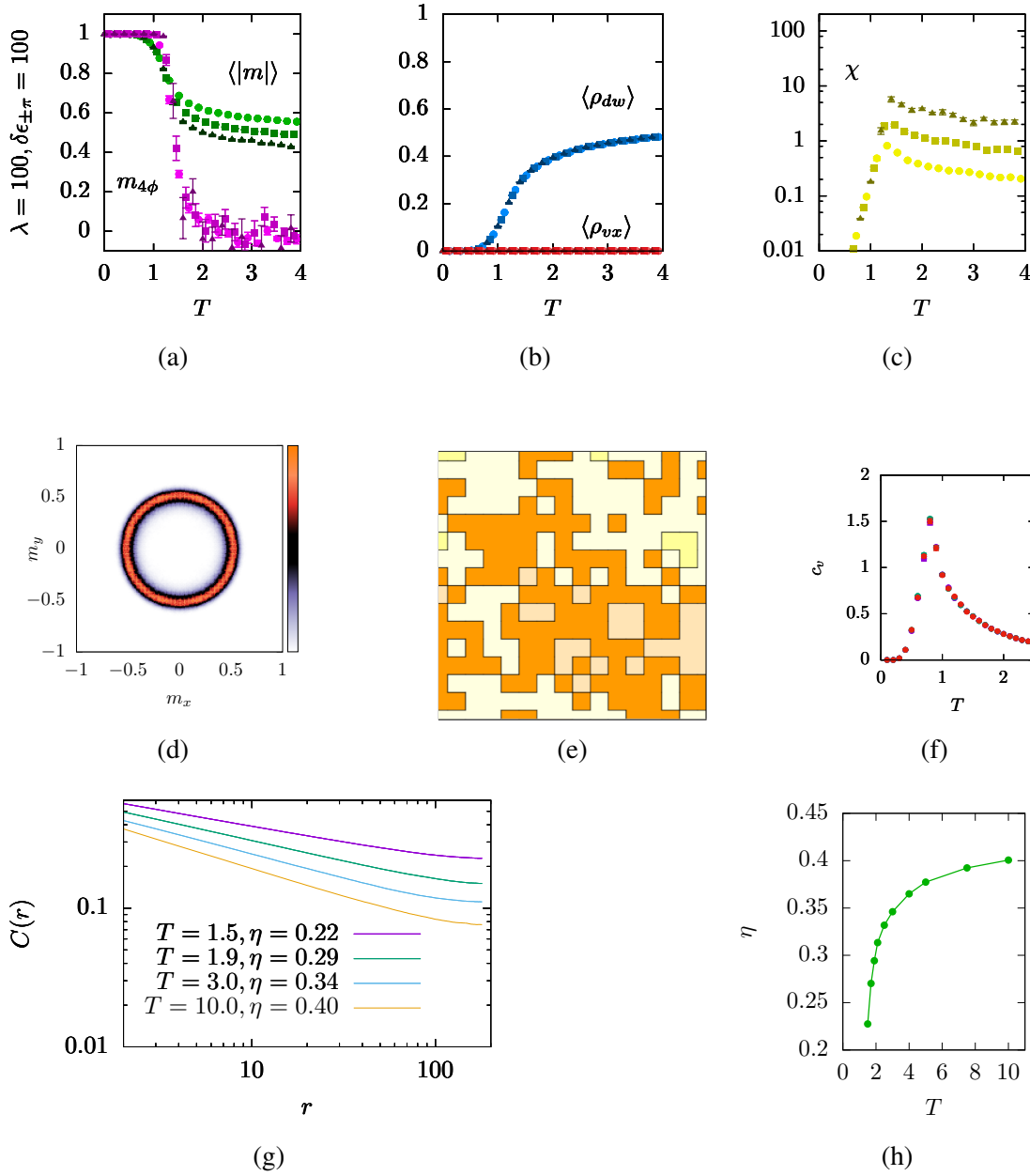


Figure 3.7: Extreme suppression of vortices and $\pm\pi$ domain walls in the \mathbb{Z}_4 clock ferromagnet on the square lattice removes the disordered phase and leaves the model with a single order-QLRO transition, which is accompanied by the rise in the density of the remaining domain walls. In the QLRO phase at $T = 3.0$, (d) the order parameter distribution obtained for a $L = 32$ system shows emergence of U(1) symmetry and (e) typical spin configurations show the proliferation of domain walls. System sizes are the same as those in (Fig. 3.1). (f) The specific heat peak accompanying the order-QLRO transition does not show any system size dependence, the sizes reported here being $L = 16$ (purple), $L = 32$ (green) and $L = 64$ (red). The QLRO nature of the phase is established by the power-law decay of two-point correlations obtained at different temperatures for a $L = 256$ system with $\lambda = 100$ and $\delta\epsilon_{\pm\pi} = 100$.

vortices and $\pm\pi$ domain walls as well?

3.7 \mathbb{Z}_6 Clock Ferromagnet on the Square Lattice

We have simulated the \mathbb{Z}_6 clock ferromagnet on the square lattice, which is described by the same Hamiltonian (3.4) but with spin vectors at each vertex $i' \in \Lambda'$ pointing along one of six angles $\theta_i \in \{2\pi s_i/6 \mid s_i \in \{0, 1, \dots, 5\}\}$.

For $\lambda = 0$, we find that the vortices proliferate at $T \approx 1.0$ while the domain walls proliferate at $T \approx 0.5$ (Fig. 3.8b). However, the density of $\pm\pi$ domain walls, labelled as $\rho_{dw, \pm\pi}$, increases across $T \approx 1.0$, close to the temperature of vortex proliferation (Fig. 3.8c). $m_{6\phi}$ decays at $T \sim 0.4$, indicating the existence of an intermediate symmetry enhanced phase from that temperature to $T \sim 1.0$ (Fig. 3.8a). Above this temperature, the magnetization shows a decay and signals the onset of disorder. When we suppress the formation of vortices alone, the disordered phase recedes to very high temperatures and leaves behind a partially symmetry broken phase as indicated clearly by the value of $m_{6\phi}$ flipping sign and going negative (Fig. 3.8d). The $\pm\pi$ domain walls continue to proliferate in this phase while vortices are absent. When the $\pm\pi$ domain walls are suppressed as well using $\delta_{\epsilon_{\pm\pi}} = 100$, we find that the partially symmetry broken phase is replaced by a symmetry enhanced QLRO phase (Fig. 3.8g).

This result suggests that the combined proliferation of vortices and $\pm\pi$ domain walls drives the QLRO-disorder transition in ferromagnets with higher values of even n as well. With increasing n , however, the number of angle differences that are possible in the \mathbb{Z}_n ferromagnet increases and a specific angle difference, particularly an angle difference of precisely $\pm\pi$, appears in relatively smaller proportions. Since the contribution of $\pm\pi$ domain walls starts diminishing with increasing n , we expect that the partially symmetry broken phase will not appear under vortex suppression in the $n \rightarrow \infty$ XY model. For small n , however, the effect of $\pm\pi$ domain walls is clearly significant.

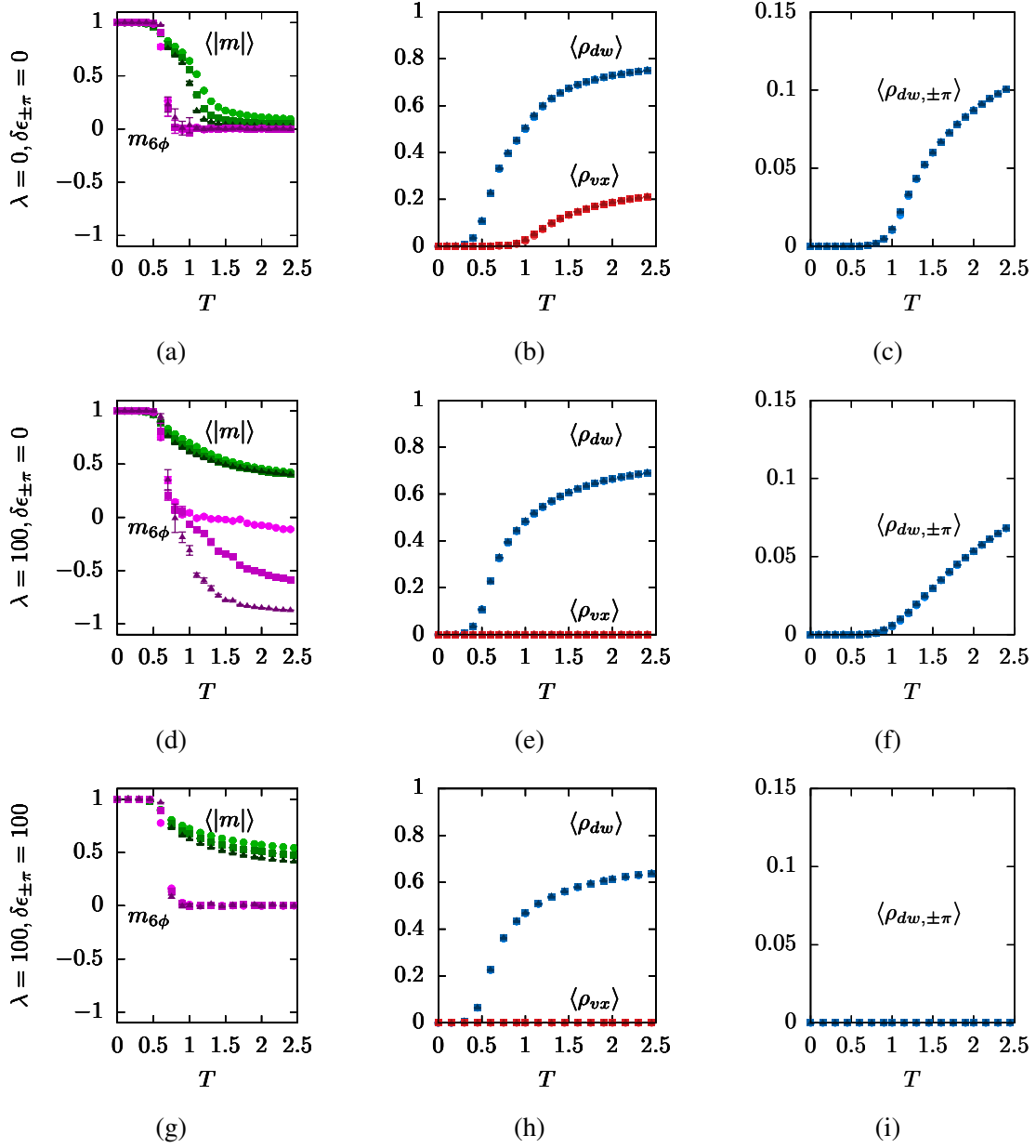


Figure 3.8: The \mathbb{Z}_6 clock ferromagnet on a square lattice shows an order-QLRO transition accompanied by increase of domain wall density and a QLRO-disorder transition accompanied by increase in the densities of vortices and $\pm\pi$ domain walls. Upon extreme suppression of domain walls, the system shows a single transition from the ordered phase to a partially symmetry broken phase. When $\pm\pi$ domain walls are also suppressed, the system exhibits a single order-QLRO transition driven by the proliferation of the remaining vortices. System sizes are the same as those in (Fig. 3.1).

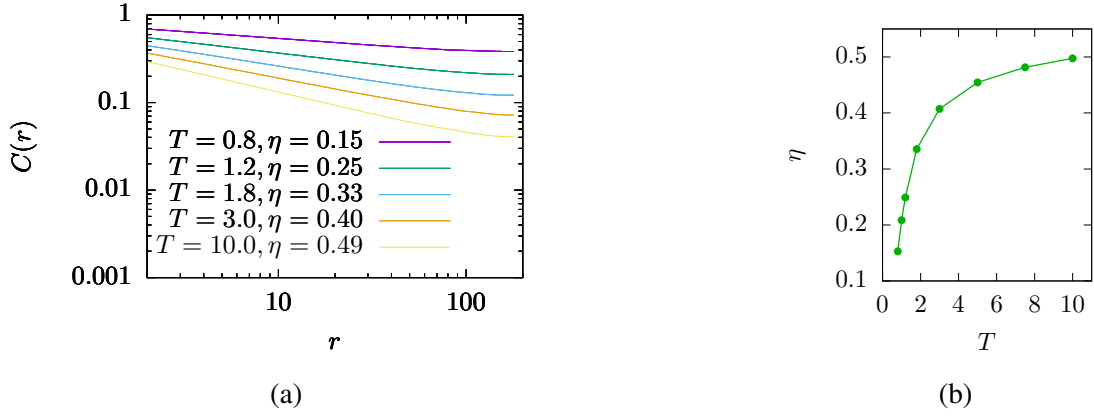


Figure 3.9: The QLRO nature of the intermediate phase obtained by suppression of vortices and $\pm\pi$ domain walls in the 2D \mathbb{Z}_6 ferromagnet is established by observing the power-law decay of the two-point correlation function (a) for a $L = 256$ system at different temperatures in that phase. (b) The exponent η of the power-law continues to increase with temperature and saturates around $\eta \approx 0.52$ at large temperatures.

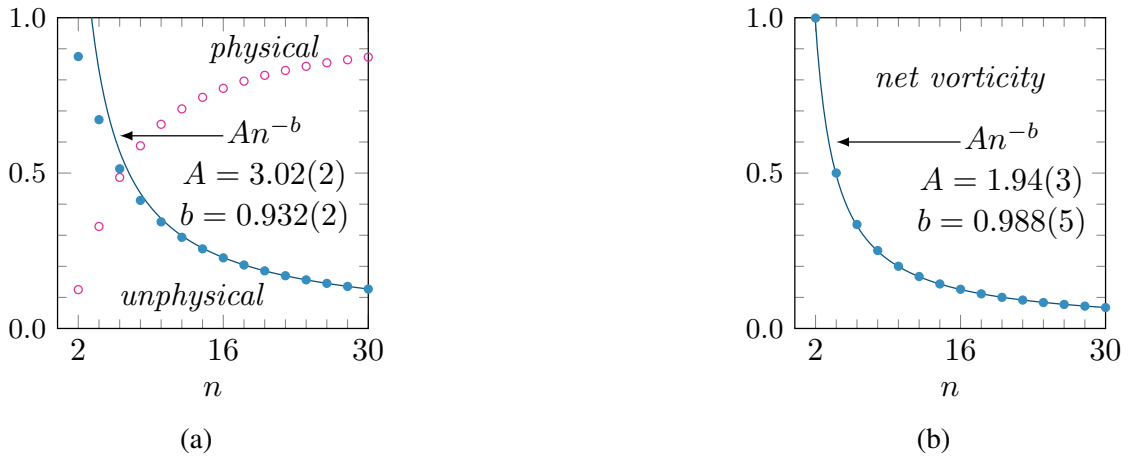


Figure 3.10: For even values of n , the fraction of spin configurations on a plaquette for which the standard method identifies unphysical vortices is shown in (a), while the net vorticity for a $L = 32$ square lattice with periodic boundary conditions, averaged over 10^4 random configurations, is shown in (b).

We would like to provide a rough estimate of how severe the effect of the false vortices, identified by the standard winding number calculation, might be for larger values of even n . For each n , we have generated all the n^4 possible configurations of spins on a square plaquette and calculated the fraction of configurations which contain a false or unphysical vortex (for which the winding number does not flip sign upon reversal of sense). Our results show that the effect is quite severe for $n = 4$ and $n = 6$ (Fig. 3.10a). For these cases, the number of plaquette configurations with unphysical vortices is higher than those with physical vortices. Although the relative proportion of false vortices decreases with increasing n , we still find a significant fraction of such vortices for $n = 30$. The false identification of will have severe effects in the phase where vortices proliferate, i.e. the disordered phase. For example, we found that the disordered phase obtained in the simulation of the \mathbb{Z}_4 ferromagnet contains a larger number of vortices than antivortices, resulting in a net positive winding number for the spin configuration, even though a system with periodic boundary conditions is expected to show net zero winding number. We have measured the net winding number of configurations containing \mathbb{Z}_n spins, averaged over 10^4 random (disordered) configurations. The standard method leads to a net positive winding number for all even n . Surprisingly, the $n = 2$ Ising case also shows a net winding number even though vortices should not be present in that model at all (Fig. 3.10b). On the other hand, we have verified that our modified method does not identify any unphysical vortices. It always identifies an equal number of vortices and antivortices on lattices with periodic boundary conditions.

3.8 \mathbb{Z}_3 Antiferromagnet on the Square Lattice

The role played by topological defects is not restricted to ferromagnets alone. Antiferromagnets with discrete symmetries on a bipartite lattice can be mapped onto equivalent ferromagnetic models [129]. Therefore, the defects present in the ferromagnetic model might govern the physics of antiferromagnets as well. One of the simplest examples which



Figure 3.11: Schematic spin configuration showing \mathbb{Z}_3 spin states for the antiferromagnetic model which get mapped onto effective spins states of a \mathbb{Z}_6 ferromagnetic model. Vortices and domain walls are identified using the \mathbb{Z}_6 representation.

demonstrates this feature is provided by the \mathbb{Z}_3 antiferromagnet [130–134]. On the square lattice, this antiferromagnet is shown to be disordered at all non-zero temperatures. It has been suggested that effective \mathbb{Z}_6 vortices, which proliferate at zero temperature, are responsible for the disorder [134]. If the vortices indeed drive the system to disorder, then suppression of the vortices should uncover an ordered phase at low temperatures.

We have simulated the \mathbb{Z}_3 antiferromagnet on the square lattice which is described by the Hamiltonian

$$\mathcal{H} = \sum_{\langle i,j \rangle \in \Lambda} 1 + \cos(\theta_i, \theta_j) \quad (3.5)$$

where each spin at vertex $i \in \Lambda$ can orient along one of three angles $s_i \in \{0, 2\pi/3, 4\pi/3\}$. An effective six-fold order parameter can be defined for this model by moving to a \mathbb{Z}_6 staggered representation of the \mathbb{Z}_3 spins, which is given by [129, 135]

$$\theta_i \rightarrow \theta'_i = (2\theta_i + 3\delta_{p_i,0}) \bmod 2\pi \quad (3.6)$$

Here $p_i = 0$ if i is on one sublattice and $p_i = 1$ if i is on the other. Under this transformation, each configuration of the antiferromagnetic \mathbb{Z}_3 spins can be equivalently represented as a configuration of ferromagnetic \mathbb{Z}_6 spins (Fig. 3.11). We can formulate an effective \mathbb{Z}_6 ferromagnetic model for the \mathbb{Z}_3 antiferromagnet using this transformation.

Consider a spin configuration of the antiferromagnet with angle 0 at a vertex on the sublattice with $p_i = 1$ and angle π on the neighboring vertex which belongs to the sublattice with $p_i = 0$. The energy cost between these spins is 2. In the \mathbb{Z}_6 representation, the effective angles are 0 and π . Therefore angle differences of $\pm\pi$ in the effective \mathbb{Z}_6 model are assigned an energy cost of 2. Similarly, keeping an angle 0 on the $p_i = 1$ sublattice, if we place an angle $4\pi/3$ on the vertex of the $p_i = 0$ sublattice, then the energy cost $1 + \cos(4\pi/3) = 1/2$ is assigned to the effective angle differences $\pm\pi/3$ in the \mathbb{Z}_6 representation. By definition, two effective spins oriented in the same direction cannot appear as neighbors. So the ± 0 angle difference is assigned an infinite energy cost. By the same argument, an infinite energy cost is assigned to angle differences $\pm 3\pi/2$.

We have simulated this effective \mathbb{Z}_6 ferromagnetic model on the square lattice and measured the standard thermodynamic observables in the \mathbb{Z}_6 representation at different temperatures. We find that the order parameter decays at a low temperature $T \approx 0.5$ (Fig. 3.12a). The decay is accompanied by a rise in the density of \mathbb{Z}_6 vortices (Fig. 3.12b). The order parameter distribution obtained at $T = 4$ shows symmetry restoration. This indicates that the system is disordered for $T > 0.5$ (Fig. 3.12c). Since similarly aligned spins can never appear as neighbors in this \mathbb{Z}_6 model, the density of domain walls remains as unity at all temperatures and is, therefore, not shown in the plots.

Upon suppressing the formation of the \mathbb{Z}_6 vortices, the order parameter distribution shows that the disordered phase, previously obtained for $T > 0$, has turned into a partially symmetry broken phase (Fig. 3.12f). This is expected as the $\pm\pi$ domain walls, which were found to be responsible for the partial symmetry breaking behavior in the \mathbb{Z}_6 ferromagnet (Fig. 3.8d), are still allowed to proliferate (Fig. 3.12e). When we suppress their formation as well, the order parameter distribution exhibits an emergent U(1) symmetry (Fig. 3.12i) and the magnetization exhibits a slow decay with system size at each temperature, characteristic of a QLRO phase (Fig. 3.12g). These results show that by suppressing the formation of effective \mathbb{Z}_6 vortices and $\pm\pi$ domain walls, we have been able

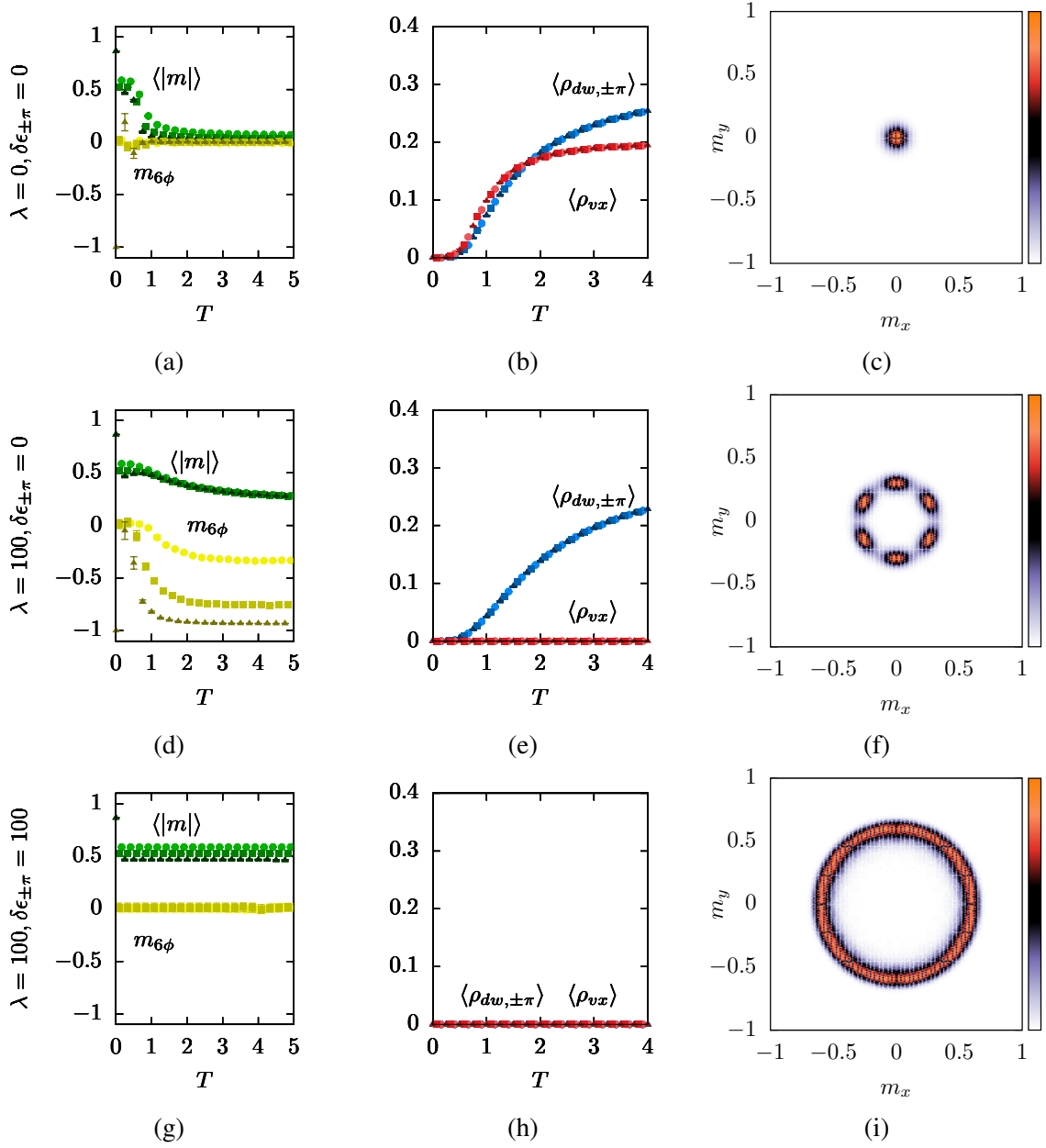


Figure 3.12: The \mathbb{Z}_3 antiferromagnet on the square lattice displays disorder at all non-zero temperatures due to proliferation of \mathbb{Z}_6 vortices. When the vortices are suppressed, the model shows a partial symmetry broken phase in which $\pm\pi$ domain walls of the \mathbb{Z}_6 representation proliferate. When the formation of these types of domain walls is suppressed as well, the model shows enhancement to $U(1)$ symmetry in the effective \mathbb{Z}_6 order parameter space. System sizes are the same as those in (Fig. 3.1). The \mathbb{Z}_6 order parameter distribution is shown for the different cases of suppression at $T = 4$ for a $L = 16$ system.

to change the disordered phase diagram of the \mathbb{Z}_3 antiferromagnet to that with a QLRO phase.

The same technique can be extended to antiferromagnets with higher values of n . On a bipartite lattice, antiferromagnets with even n get mapped onto \mathbb{Z}_n ferromagnets while those with odd n get mapped onto \mathbb{Z}_{2n} ferromagnets [129]. Therefore, the \mathbb{Z}_4 antiferromagnet would map onto a \mathbb{Z}_4 ferromagnet [128], for which we have already discussed the phase diagram and the role played by defects.

Chapter 4

Partial Symmetry Breaking via $(0 | 1)$

Domain Wall Percolation

Our investigation into the role of defects in two dimensional \mathbb{Z}_n ferromagnets was motivated by an approximate energy versus entropy calculation (Sec.1.5.6). The calculation suggested the possibility of obtaining an intermediate symmetry enhanced phase by decoupling the proliferation of defects. A key ingredient in this calculation was an estimate for the temperature at which the domain walls, modelled by random walks, begin to proliferate. In three dimensions, the domain walls appear as two dimensional sheets. Since it is difficult to obtain an analytical expression for the free energy of a two dimensional sheet which crinkles randomly, we cannot estimate the proliferation temperature of domain walls in three dimensions in a manner similar to that done in two dimensions. This, in turn, restricts us from carrying out an approximate calculation which describes the interplay between domain walls and vortex strings in three dimensions.

Monte Carlo simulations carried out for \mathbb{Z}_3 [4, 136–138] and \mathbb{Z}_6 [9] models on the simple cubic lattice have shown that vortex strings proliferate across the order-disorder transition in these systems. However, the interplay between domain walls and vortex strings at this transition has remained unexplored. Instead, it has been conjectured that the two types of

defects proliferate simultaneously for all n , which forces the ferromagnets to undergo a single order-disorder transition without realizing an intermediate phase [95]. We would like to verify whether this conjecture holds true for different values of n . If the order-disorder transition is indeed driven by the simultaneous proliferation of the defects, can we suppress the formation of vortex strings and open up an intermediate phase? Does the intermediate phase exhibit symmetry enhancement? The existence of a symmetry enhanced intermediate phase in three dimensions is a topic of debate [20–27]. A direct demonstration revealing the existence of such a phase would help settle the debate.

4.1 \mathbb{Z}_3 Ferromagnet on the Simple Cubic Lattice

4.1.1 Hamiltonian

As a first step, we consider the \mathbb{Z}_3 clock ferromagnet on a simple cubic lattice, which is described by the Hamiltonian

$$\mathcal{H} = \frac{2}{3} \sum_{\langle i,j \rangle \in \Lambda} 1 - \cos(\theta_i - \theta_j) \quad (4.1)$$

where the spin vector at vertex $i \in \Lambda$ can orient at three different angles $\theta_i \in \{0, 2\pi/3, 4\pi/3\}$. A prefactor of $2/3$ is used here to scale the gap between the low and high energy levels down to unity. This makes (Eq. 4.1) identical to the three state Potts Hamiltonian, which is the standard form used for studying three-fold symmetry breaking in the context of quantum chromodynamics and formation of cosmic strings in the early universe. This model is known to undergo a single order-disorder transition at a temperature $T \approx 1.81$ [139].

4.1.2 Order Parameter Distribution

We have simulated the model using the Metropolis algorithm at different temperatures. We find that most of the spins align along a common direction in the ordered phase at low temperatures and align arbitrarily in the disordered phase at high temperatures (Fig. 4.1). The order parameter distribution $P(m_x, m_y)$ shows that the three-fold symmetry, which is broken in the ordered phase, gets restored in the disordered phase. Our first task is to verify if this order-disorder transition is driven by a simultaneous proliferation of domain walls and vortex strings.

We have identified the defects corresponding to spin configurations obtained at different temperatures in our simulation. We observe that small bubbles of domain walls form in the ordered phase along with very small loops of vortex strings (Fig. 4.1e). With increasing temperature, both types of defects grow in size and density. When the system transitions to the disordered phase, the domain walls span across the entire system, as do the vortex strings (Fig. 4.1f). This suggests that the proliferation of both types of defects can be characterized using percolation observables.

4.2 Percolation of Domain Walls and Vortex Strings

In order to form the extended vortex strings from their individual segments, we have joined the edges of Λ' which carry a non-zero winding number and are adjacent to each other, i.e. share a vertex of Λ' in common. In particular, we have not discriminated between vortex and antivortex strings in this joining procedure. The domain walls, on the other hand, reside on the plaquettes of Λ' . To form extended domain walls, we have joined adjacent domain wall plaquettes, i.e. those which share an edge of Λ' in common. We have labelled the clusters of vortex strings and domain walls formed in this manner using the Hoshen-Kopelman algorithm [123]. For each configuration, we have measured the standard percolation observables that we had defined previously for the domain walls

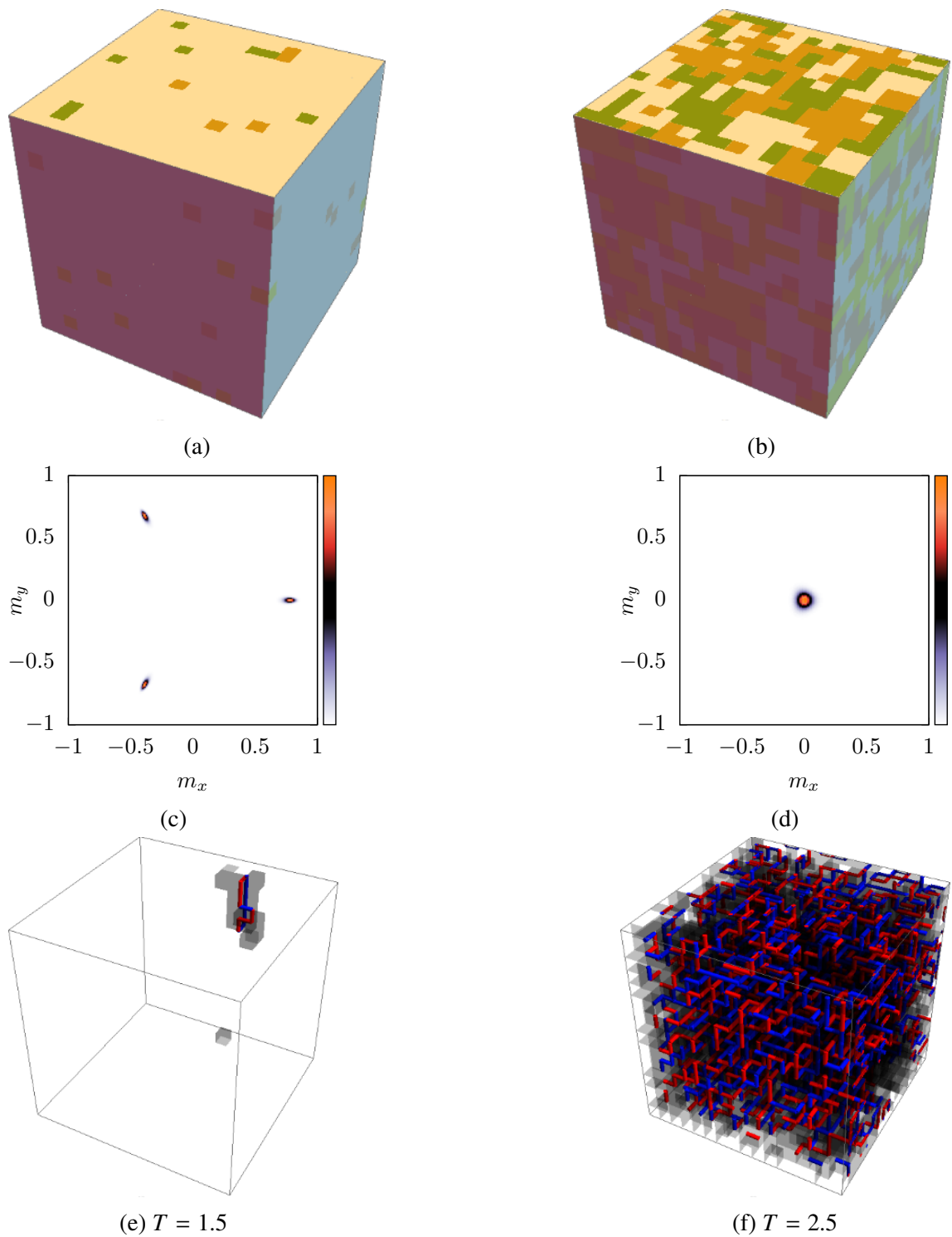


Figure 4.1: Typical spin configurations obtained on a $L = 16$ simple cubic lattice for the \mathbb{Z}_3 ferromagnet in (a) the ordered phase at $T = 1.5$ and (b) the disordered phase at $T = 2.5$. The results have been obtained using $\lambda = 0$, i.e. without suppressing the formation of vortices. The order parameter distribution obtained at the corresponding temperatures are shown in (c) and (d). The largest vortex strings and domain walls obtained for each of the spin configurations are shown in (e) and (f).

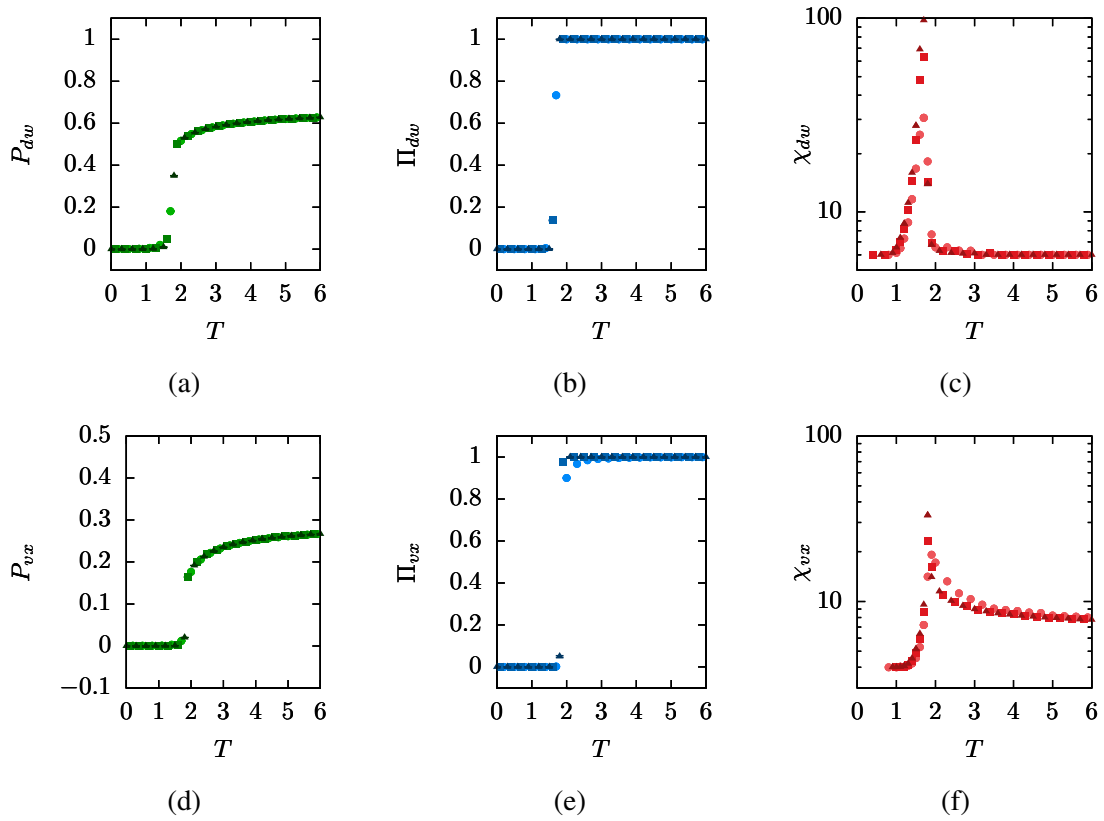


Figure 4.2: Measurement of standard percolation observables show that the percolation strength P and the spanning probability Π of the defects rise rapidly at $T \approx 1.8$. The average defect size for both types show a peak at that temperature as well. The data has been obtained for system sizes $L = 8$ (circle), $L = 12$ (square) and $L = 16$ (triangle).

in two dimensions (Sec. 2.3.1). Namely, we have measured the fraction P_{vx} of dual edges in the largest cluster of vortex strings and the fraction P_{dw} of dual plaquettes in the largest cluster of domain walls. We have also measured the respective spanning probabilities Π_{vx} and Π_{dw} . By binning the sizes of all clusters apart from the largest one in each configuration, we have formed the distribution $n(s)$ and calculated the average cluster size using $n(s)$ for each of the two types of defects.

Our simulation results show that the sizes of the largest domain walls and vortex strings increase sharply across $T \approx 1.8$ (Fig. 4.2). The spanning probabilities jump to unity above that temperature. The average size of the two types of defects peak near that temperature as well. These results demonstrate that both types of defects begin to percolate simultaneously across the order-disorder transition.

4.2.1 Phase Diagram

We have also measured the thermodynamic observables like magnetization, the measure of symmetry breaking $m_{3\phi}$ and the magnetic susceptibility. The magnetization shows a sharp decay across $T \approx 1.8$, and so does $m_{3\phi}$ (Fig. 4.3).

In addition we have also measured the density of domain walls ρ_{dw} and the density of vortex strings ρ_{vx} . The latter observable is defined as the fraction of edges in the dual lattice Λ' which are associated with a non-zero winding number. The former is defined as the fraction of plaquettes in Λ' which separate a pair of dissimilar spin states residing on Λ . The densities of both types of defects are found to increase sharply and simultaneously across $T \sim 1.8$ (Fig. 4.3). Since the defects proliferate simultaneously, it is understandable that the model does not exhibit an intermediate phase.

4.3 Suppression of Vortex Strings

In order to uncover the possibility of an intermediate phase, we increase the core energy of each vortex string segment by an amount λ . The Hamiltonian with this suppression term becomes

$$\mathcal{H} = \frac{2}{3} \sum_{\langle i,j \rangle \in \Lambda} 1 - \cos(\theta_i - \theta_j) + \lambda \sum_{e' \in \Lambda'} |\omega_{e'}| \quad (4.2)$$

where $\omega_{e'}$ represents the winding number associated with the dual edge $e' \in \Lambda'$.

4.3.1 Weak Suppression

For weak suppression with $\lambda = 0.4$, we find that vortex strings begin to proliferate at a higher temperature $T \approx 2.2$ and the domain wall proliferation shifts to that temperature as well (Fig. 4.3e). The decay of the magnetization and $m_{3\phi}$ also shifts to $T \approx 2.2$ (Fig. 4.3d).

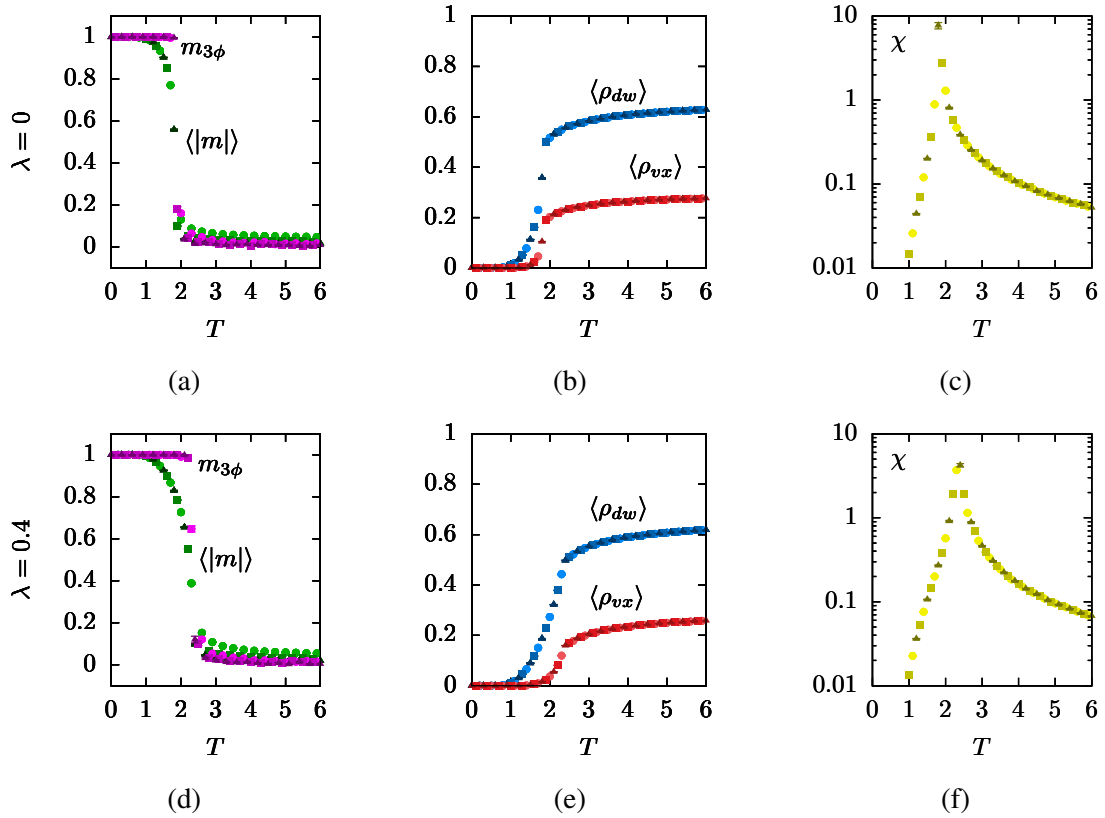


Figure 4.3: Top panel: The simultaneous decay of magnetization and $m_{3\phi}$ across $T \approx 1.8$ in the \mathbb{Z}_3 ferromagnet on the simple cubic lattice is accompanied by a peak in the magnetic susceptibility and a simultaneous increase of defect densities. Bottom panel: Weak suppression of vortex strings shifts the simultaneous proliferation of defects and the decay of magnetization as well as $m_{3\phi}$ to a higher temperature $T \approx 2.2$. System sizes correspond to those in Fig. 4.2.

With increasing λ , the shift in the transition temperature and the proliferation temperatures of the defects continue until $\lambda \approx 1.2$. The manner in which a weak suppression is unable to decouple the simultaneous proliferation is reminiscent of the behavior obtained for the \mathbb{Z}_3 ferromagnet in two dimensions. We also note that the decay of the magnetization and the increase in defect densities become more gradual with increasing λ . If this is a signature of the transition weakening with increased suppression of vortex strings, there exists a possibility that the weakly first-order transition in the model without any suppression can turn into a second order transition at some λ . Discovery of a second-order transition in a three dimensional model with \mathbb{Z}_3 symmetry has direct implications for the order of the deconfinement transition in quantum chromodynamics [3, 140]. However, since we are unable to perform reliable finite size scaling in our simulation, we keep this exciting possibility only as a conjecture.

4.3.2 Strong Suppression

For strong suppression of vortex strings with $\lambda = 1.5$, the behavior of the model changes qualitatively. The simultaneous proliferation of the defects decouple and the vortex string density increases at a temperature $T \approx 3.5$, which is higher than the temperature $T \approx 1.5$ where the domain wall density increases (Fig. 4.4b). With further increase in λ , the rise in vortex density continues to shift to higher temperatures and for extreme suppression, recedes to a very high temperature (Fig. 4.4h). On the other hand, the temperature across which the domain wall density rises, remains fixed at $T \approx 3$ with increasing λ .

The first signs of an intermediate phase is observed in the system with $\lambda = 1.5$. $m_{3\phi}$ shows a positive value in the ordered phase but becomes negative across an intermediate range of temperatures (Fig. 4.4a). In addition, the magnetization begins to exhibit a two-step decay. The first decay marks a transition from the ordered phase to the intermediate phase and occurs near the temperature $T \approx 3$, where the domain walls proliferate. The second decay, marking a transition from the intermediate phase to the disordered phase, occurs

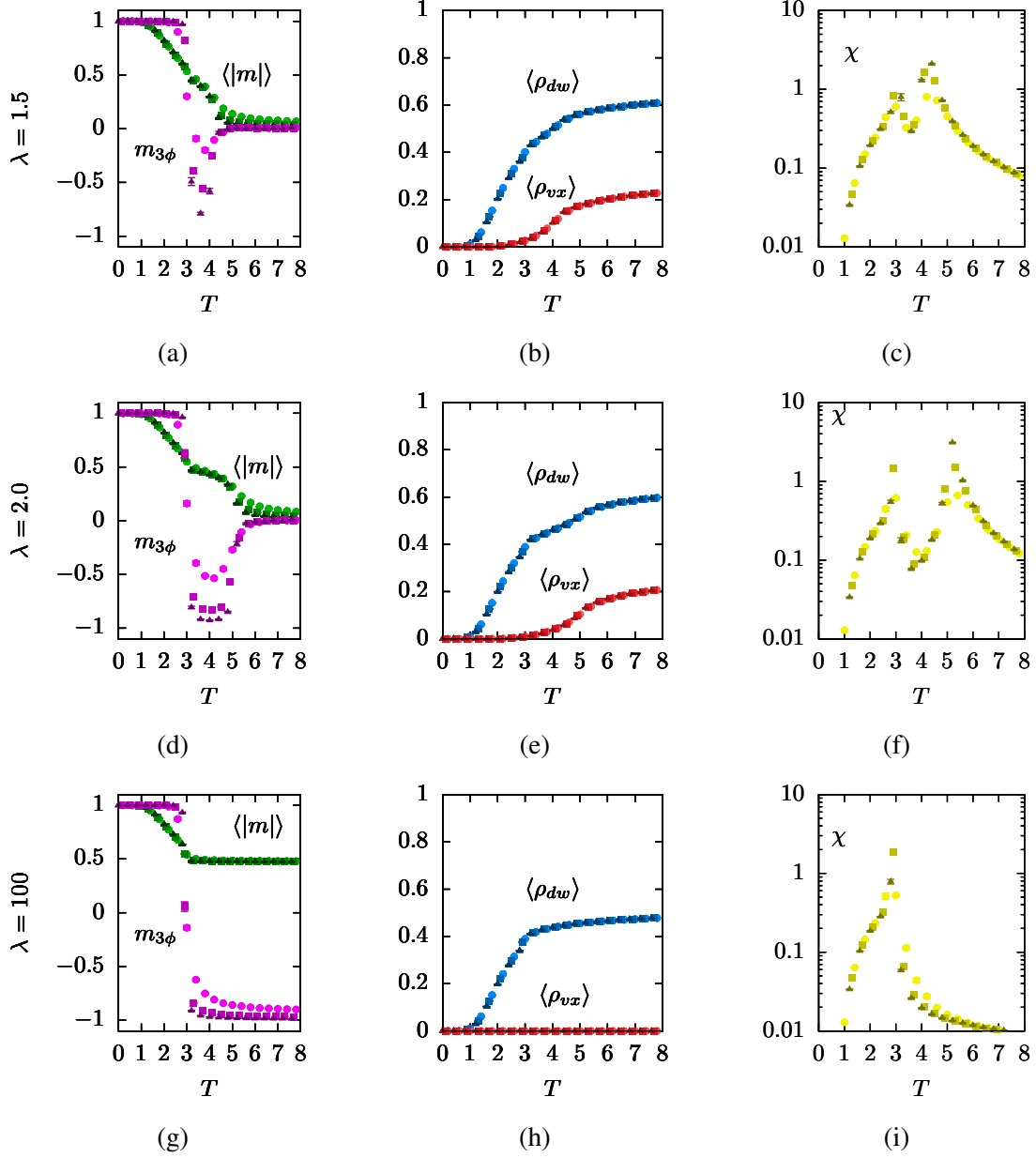


Figure 4.4: With strong suppression, the simultaneous proliferation of the defects decouples and the rise in vortex string density shifts to higher temperature along with the decay in magnetization and the second peak of susceptibility. The decay of $m_{3\phi}$ and the rise of domain wall density continues to occur at $T \approx 3.0$. For extreme suppression, the model shows a single transition from the ordered phase to the intermediate phase. System sizes correspond to those in Fig. 4.2.

at $T \approx 4.2$ where the vortex strings proliferate. The two decays are also accompanied by corresponding peaks in the magnetic susceptibility. With increasing λ , this intermediate phase grows in extent as the second decay of the magnetization shifts to higher temperatures (Fig. 4.4d). The peaks in the magnetic susceptibility shift as well (Fig. 4.4f). For extreme suppression ($\lambda = 100$), the intermediate phase extends across a large range of temperatures starting from $T \approx 3$ and the disordering transition recedes to a very high temperature (Fig. 4.4g). This set of results establish that the first transition, from the ordered phase to the intermediate phase is driven by the proliferation of domain walls. The transition from the intermediate phase to the disordered phase, which shifts with increasing λ , is driven by the proliferation of vortex strings. While these results closely match those obtained for the two dimensional model, the intermediate phase appears to be of a different kind.

4.4 Partial Symmetry Broken Intermediate Phase

4.4.1 Order Parameter

In order to investigate the nature of the intermediate phase, we focus on the case with $\lambda = 100$. The order parameter distribution at different temperatures in this phase show that the three-fold symmetry is broken with a $\pi/3$ offset in the angles (Fig. 4.5a) compared to the symmetry breaking pattern obtained in the ordered phase (Fig. 4.1c). This establishes the partial symmetry broken nature of the intermediate phase. The decay of the magnetization from near unity in the ordered phase to an intermediate value of $\langle |m| \rangle \sim 0.5$ (Fig. 4.4g) in this phase also suggests that the system is partially ordered.

Typical defect configurations show absence of vortex strings but reveal that domain walls span across the entire system (Fig. 4.5c). This suggests that the domain walls percolate in the partially symmetry broken phase. Indeed, a measurement of the percola-

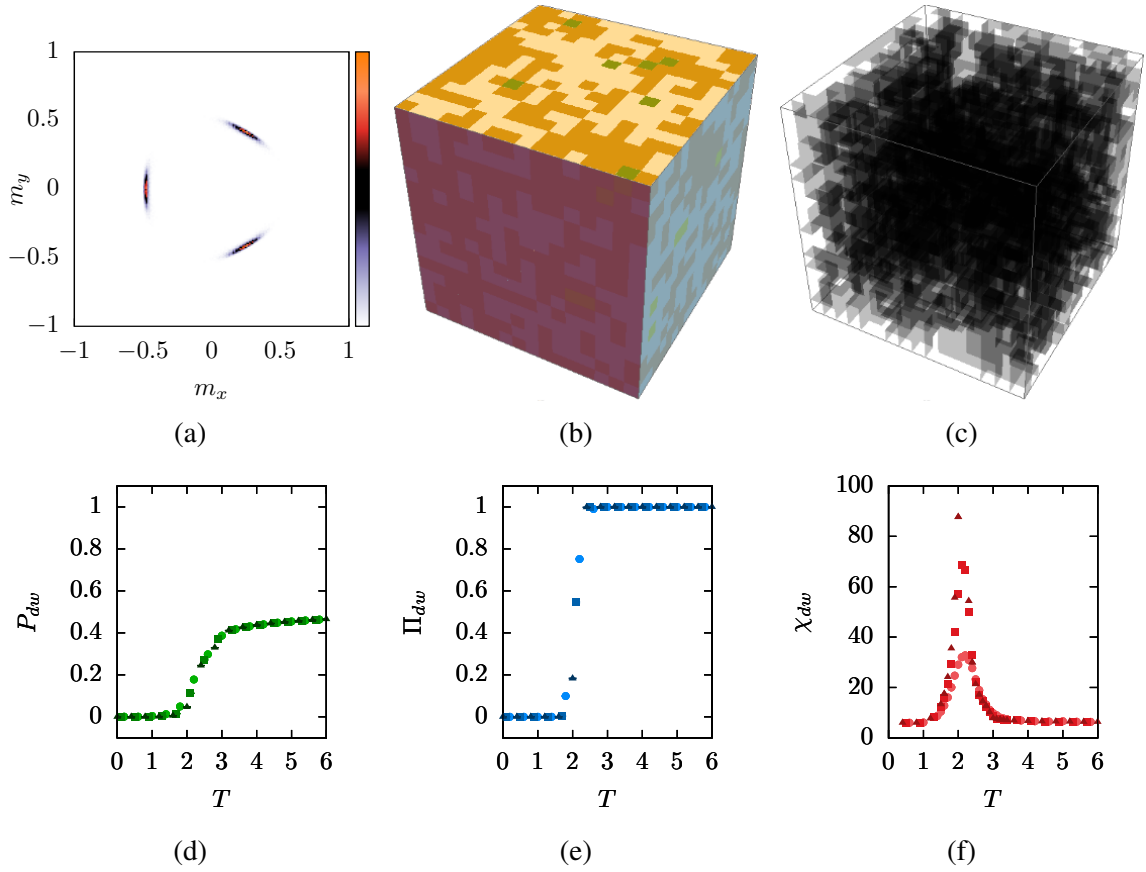


Figure 4.5: The order parameter distribution for a $L = 8$ system at $T = 6$, in the intermediate phase obtained via extreme suppression of vortex strings with $\lambda = 100$, shows a three-fold symmetry breaking, offset from the spin angles by $\pi/3$ while defect configurations obtained at the same temperature show that domain walls proliferate in the absence of vortex strings. This behavior is captured by the percolation properties of the domain walls as well. System sizes correspond to those in Fig. 4.2.

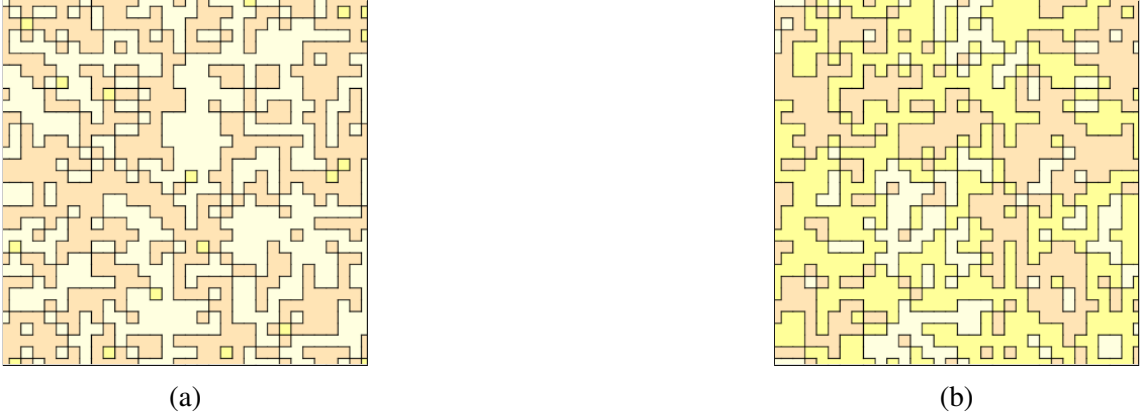


Figure 4.6: Spin and domain wall configurations obtained in (a) the partially symmetry broken phase of the three-dimensional model at $T = 6$ (a two-dimensional slice is shown here), and (b) the symmetry enhanced QLRO phase of the two-dimensional model at $T = 4$. Both configurations have been obtained from the models with extreme suppression of vortices with $\lambda = 100$.

tion observables in this phase reveals that the largest domain wall size increases across $T \approx 2$, close to the temperature of the transition from the ordered phase to the intermediate phase (Fig. 4.5d). The spanning probability saturates to unity in the latter phase (Fig. 4.5e). In addition, the average cluster size shows a peak near the transition (Fig. 4.5f). These percolation characteristics are very similar to those obtained for the domain walls in the intermediate phase of the two dimensional model (Fig. 2.6). And this is a source of concern.

The intermediate phase in the two dimensional model, which forms via the percolation of domain walls, shows symmetry enhancement and QLRO. The intermediate phase in the three-dimensional model also forms via the percolation of domain walls but shows partial symmetry breaking and partial order. How is it possible that the same defect proliferation mechanism results in the formation of two different types of phases?

4.4.2 Proliferation Pattern of Domain Walls

We have established (Fig. 2.6 and Fig. 4.5) that both intermediate phases form due to percolation of domain walls. The distinguishing feature which results in the different

properties for the two phases must, therefore, lie in the percolation pattern of the domain walls themselves. In order to identify this difference, we visually inspect typical configurations of domain walls obtained in the intermediate phase of the two-dimensional and three-dimensional models (Fig. 4.6).

In the sliced configuration of the three-dimensional model (Fig. 4.6a), we find that the percolating domain walls mostly separate two particular spin states. We now specifically consider domain walls by their individual types $(a | b)$, where a and b are the pair of spin states they separate (Sec. 1.5.1). The two dominant states in the configuration (Fig. 4.6a) are states 0 and 1. We observe that domain walls percolate across the configuration solely because domain walls of a particular type, say $(0 | 1)$, percolate on their own. This, however, is not the case for the configuration in the two-dimensional model (Fig. 4.6b). In that configuration, all the three spin states are present and the domain walls appear to percolate because we have joined the different types of $(a | b)$ domain walls into the same cluster. There is a possibility that if we do not join the different types of domain walls into the same cluster and, instead, study their percolation properties individually, none of the particular domain wall types might percolate on their own in this configuration, and more generally, the QLRO phase.

In order to investigate this possibility, we have formed clusters belonging to each type of $(a | b)$ domain walls and measured their percolation properties for the models in two and three dimensions, in the limit of extreme suppression with $\lambda = 100$.

4.4.3 Relative Relabelling of Spin States

Before presenting the results, we mention a feature of Monte Carlo simulations that needs to be accounted for this particular type of $(a | b)$ measurement. All the observables which we measured previously were invariant under the symmetry operations of the \mathbb{Z}_3 group. For example, if all the spins in a given configuration are rotated by $2\pi/3$, the values of

magnetization, susceptibility and even the density of the defects would remain invariant. On the other hand, state or angle specific observables, like the largest cluster size of domain wall type $(0 | 1)$ which we will measure next, would change under such a global rotation. This becomes a problem in finite size simulations because the system keeps migrating from one symmetry broken state to the other over the course of the simulation [22]. We have mitigated this problem by rotating all the spins by an angle such that the angle of the symmetry broken minima gets relabelled to 0 (state 0). Since discrete rotations are constituent members of the \mathbb{Z}_n symmetry group, this procedure of relabelling keeps the Hamiltonian (4.2) invariant. However, this relabelling is not sufficient. Even if we fix the symmetry broken state, the system can show fluctuations between the angles on the left and right hand side of angle 0 (state 0). In order to counter such fluctuations, we reflect all the spins in the configuration across angle 0, in a manner such that the most populous of the two angles adjacent to 0 gets relabelled to angle $2\pi/n$ or state 1. Consequently, the angle on the other side gets relabelled to $2\pi(n-1)/n$ or state $n-1$. Again, this reflection operation is a constituent member of the \mathbb{Z}_n symmetry group and, therefore, keeps the Hamiltonian (4.2) invariant.

4.4.4 Percolation Properties of $(a | b)$ Domain Walls

We have applied the relabelling scheme to every configuration generated in our simulation before measuring the percolation observables. Under this relabelling, we find that $(0 | 1)$ domain walls begin to percolate on their own at $T \approx 3$, across the transition from the ordered phase to the partial symmetry broken phase in three dimensions (Fig. 4.7a). The spanning probability of this particular type saturates to unity in the latter phase and the average $(0 | 1)$ domain wall size peaks at the transition (Fig. 4.7b). As expected from the visual inspection, none of the other types of domain walls are found to percolate on their own across the transition.

In the intermediate QLRO phase of the two dimensional model, however, we find that the

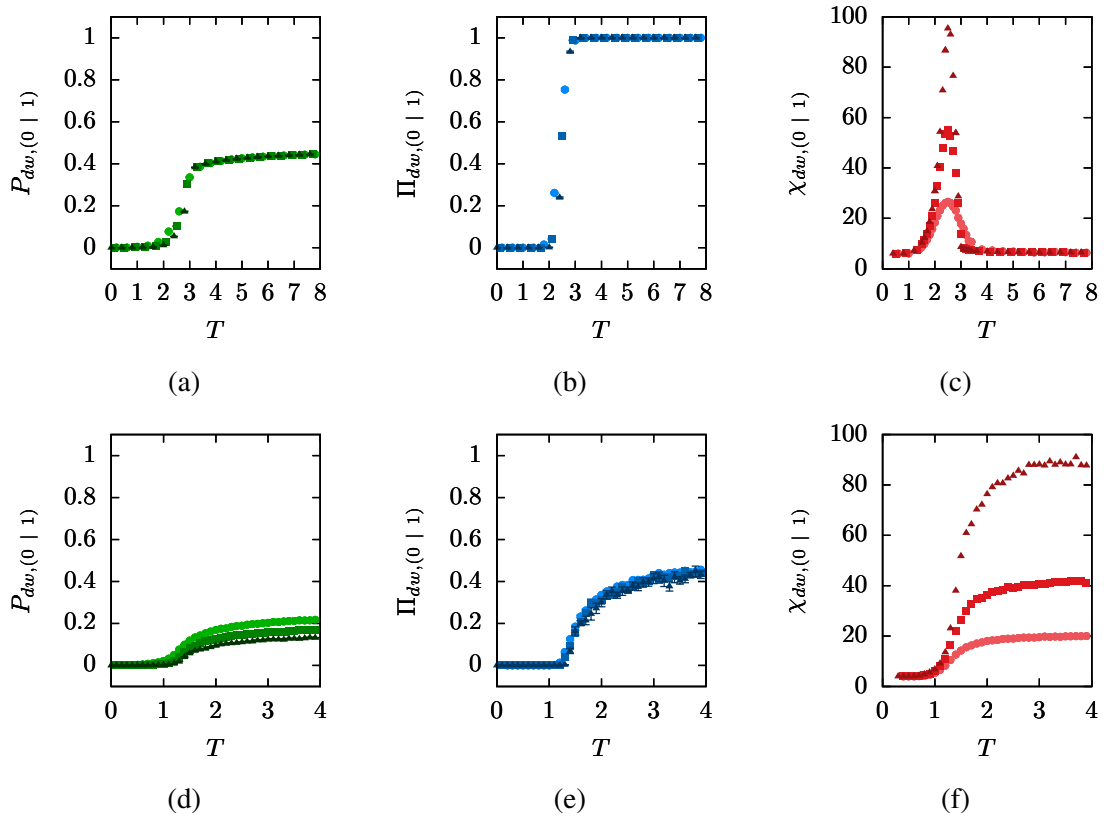


Figure 4.7: Percolation properties of $(0 | 1)$ domain walls. Top panel (a,b,c) shows the behavior for the three-dimensional model. The spanning probability saturates to unity and the average size peaks at the percolation transition at $T \approx 2.5$. Bottom panel (d,e,f) shows the behavior for the two-dimensional model. The spanning probability saturates to a value around 0.42. The percolation strength decays and the average size increases with system size throughout the QLRO phase, representative of behavior at a percolation threshold. System sizes correspond to those in Fig. 4.2.

(0 | 1) domain walls show a different behavior. The spanning probability does not saturate to unity but remains at $\Pi_{dw(0 | 1)} \sim 0.5$ (Fig. 4.7e). The largest size of (0 | 1) domain walls gradually decreases with increasing system size at each temperature in the QLRO phase (Fig. 4.7d). In addition, the average size of (0 | 1) domain walls not only peaks at the transition but continues to grow with system size at each temperature in the QLRO phase (Fig. 4.7f). This kind of behavior is found among the percolation observables at the percolation threshold. In this case, however, the entire QLRO phase appears to be a line of percolation thresholds. None of the other types of domain walls appear to percolate on their own in this case as well.

In order to elaborate on the percolation threshold behavior of the (0 | 1) domain walls, we have studying the system size dependence of the percolation observables at different temperatures in the QLRO phase (Fig. 4.8). We find that the cluster size distribution $n(s)$ follows a power-law with a cut-off which grows with increasing system size. In the thermodynamic limit, we expect an asymptotic behavior of the form $n(s) \sim s^{-\tau}$, where we have estimated the Fisher exponent $\tau = 2.10(1)$ (Fig. 4.8a). Using a hyperscaling relation, we can estimate the fractal dimension of the domain walls as $d_f = d/(\tau - 1) = 1.81$, which suggests that the walls are quite tortuous in this phase. We also note that τ does not change with temperature in this phase.

We also find a power-law system size dependence $P_{dw(0 | 1)} \sim L^{-\beta/\nu}$, where β/ν is found to decrease with temperature from $\beta/\nu = 0.45$ at $T = 1.70$ to $\beta/\nu = 0.36$ at $T = 9.0$ (Fig. 4.8c). On the other hand, the power-law size dependence of the mean domain wall size $\chi_{dw(0 | 1)} \sim L^{\gamma/\nu}$ does not appear to change significantly with temperature and falls within the range $1.06 < \gamma/\nu < 1.18$ (Fig. 4.8d).

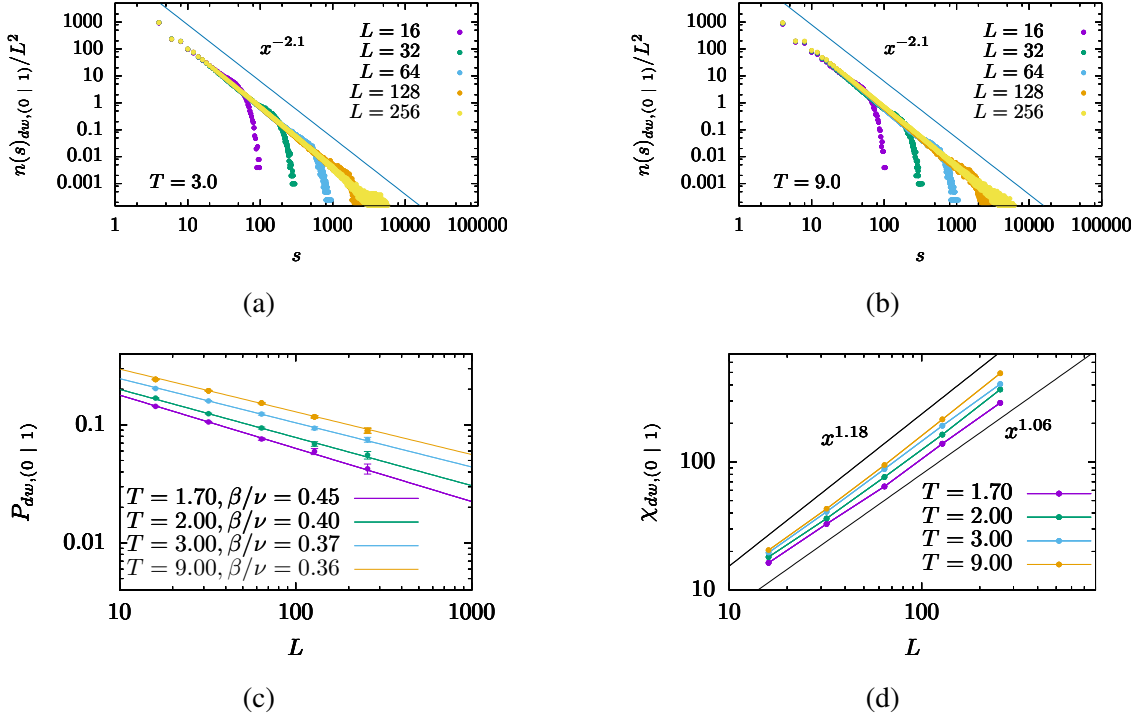


Figure 4.8: System size dependence of percolation observables at different temperatures in the QLRO phase of the 2D \mathbb{Z}_3 ferromagnet obtained by suppressing vortex formation with $\lambda = 100$.

4.4.5 Percolation of (0 | 1) Domain Walls

The percolation of the (0 | 1) domain walls is, therefore, the salient feature which distinguishes between the intermediate phases in the two models. This feature also explains why the intermediate phase breaks a partial symmetry in the three-dimensional model but not in the two-dimensional one. The percolation of (0 | 1) domain walls implies a percolation of state 0 clusters and state 1 clusters as well. This implies that the spin texture is dominated by angles 0 and $2\pi/3$. Consequently, the average orientation of the system becomes $\pi/3$. Such an intermediate value of the order parameter orientation is a signature of partial symmetry breaking (Fig. 4.5a). For an ensemble of simulations initialized in an ordered configuration arbitrarily from one of the three states, the symmetry will be partially broken along the π and $5\pi/3$ directions as well. The order parameter distribution accumulated from across these ensembles will show the $\pi/3$ offset pattern of three-fold partial symmetry breaking (Fig. 4.5a).

Another viewpoint towards the same result is obtained by mapping the states 0 and 1 of the \mathbb{Z}_3 model onto the two states of the \mathbb{Z}_2 Ising model. This effectively highlights an implicit \mathbb{Z}_2 symmetry hidden in the \mathbb{Z}_3 ferromagnet. In the ordered phase of the ferromagnet, most of the spins are in state 0. This implies that most of the spins are in one state of the mapped Ising model, i.e. the \mathbb{Z}_2 symmetry is broken. In the intermediate phase, most of the spins in the \mathbb{Z}_3 ferromagnet arbitrarily pick up either state 0 or state 1. In terms of the Ising model, the \mathbb{Z}_2 symmetry gets restored. We infer that restoration of the implicit \mathbb{Z}_2 symmetry forces the system to show a partial order instead of complete order [29].

The crucial difference between the two-dimensional and three-dimensional behavior lies in the fact that simultaneous percolation of multiple clusters (also known as polychromatic percolation) can be sustained by the simple cubic lattice due to its higher connectivity, but not by the square lattice [141]. Since the two-dimensional system cannot accommodate the simultaneous percolation of state 0 and state 1 clusters, and yet the temperature is ripe for domain wall proliferation, the (0 | 1) domain walls are unable to percolate and remain only at a percolation threshold.

The natural question which arises next is: do ferromagnets with higher n exhibit a partial symmetry breaking on the simple cubic lattice as well? For the next ferromagnet in the series, the \mathbb{Z}_4 clock ferromagnet, we have obtained a QLRO phase on the square lattice (Sec. 3.6). Does the QLRO phase transform into a partial symmetry broken phase when the model is placed on the simple cubic lattice?

4.5 \mathbb{Z}_4 Clock Ferromagnet on the Simple Cubic Lattice

We have simulated the \mathbb{Z}_4 clock ferromagnet, described by the Hamiltonian (3.4), on the simple cubic lattice. Without suppression of either vortex strings or $\pm\pi$ domain walls ($\lambda = 0$ and $\delta\epsilon_{\pm\pi} = 0$), the model exhibits a single order-disorder transition at $T \approx 2.2$ accompanied by a simultaneous proliferation of vortex strings and domain walls (Fig. 4.9b).

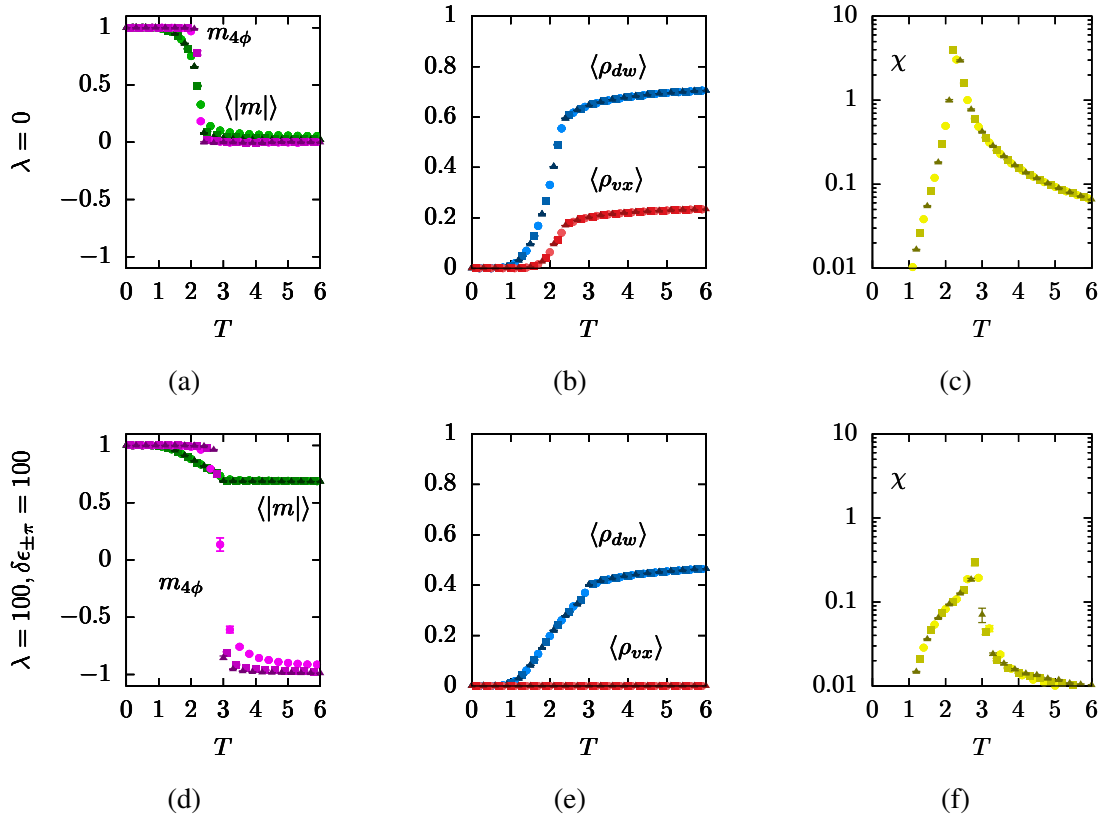


Figure 4.9: The order-disorder transition in the \mathbb{Z}_4 clock ferromagnet on a simple cubic lattice, captured by the decay in magnetization at $T \approx 2.2$, is accompanied by a simultaneous proliferation of domain walls and vortex strings (a,b,c). Upon extreme suppression of the vortex strings and $\pm\pi$ domain walls, the system shows a transition from the ordered phase to a partially symmetry broken phase (d,e,f).

This is reflected in the decay of the magnetization at the temperature where the densities of both types of defects show an increase. On the square lattice, a single order-QLRO transition was obtained for the model by suppressing both vortex strings and $\pm\pi$ domain walls. With $\lambda = 100$ and $\delta\epsilon_{\pm\pi} = 100$ on the simple cubic lattice, the model again shows a single transition but from the ordered phase to a phase where $m_{4\phi}$ becomes negative (Fig. 4.7d). This order parameter shows a four-fold symmetry breaking pattern offset from the angles of symmetry breaking in the ordered phase by $\pi/4$ (Fig. 4.10b). Upon measuring the percolation properties of individual types of domain walls, we find that none of the types apart from $(0 | 1)$ domain walls percolate on their own in this phase (Fig. 4.10c). This result suggests that the partial order in the partially symmetry broken phase of this model is generated because the spins align arbitrarily along one of the two angles: 0 and $\pi/2$.

In the $\mathbb{Z}_2 \times \mathbb{Z}_2$ Ashkin-Teller representation of the \mathbb{Z}_4 ferromagnet [128], the four states of the \mathbb{Z}_4 spin space can be mapped on to a combination of two Ising states (σ, τ) as: $\{0, 1, 2, 3\} \rightarrow \{(+, +), (+, -), (-, -), (-, +)\}$. Using this representation, it is easy to see that a phase in which states 0 and 1 appear in equal proportion translates to a phase where one of the Ising models (the τ Ising model in this case) gets disordered but the other (σ Ising model) remains ordered. Such a phase is known as the $\langle \sigma \rangle$ phase in the Ashkin-Teller literature [31, 32]. And this is precisely the phase which we have uncovered by suppressing the formation of the $\pm\pi$ domain walls. The decomposition of the model into the two Ising models also provides an explanation for the percolation behavior. We have discussed (Sec. 1.5.2) that the order-disorder phase transition in the three dimensional Ising model is driven by the percolation of domain walls. Since one of the Ising models get disordered in the partially symmetry broken phase, the domain walls corresponding to that \mathbb{Z}_2 symmetry, which we have labelled as $(0 | 1)$ domain walls, percolate on their own in that phase. Incidentally, we have suppressed the domain walls belonging to the other \mathbb{Z}_2 symmetry group in the guise of $\pm\pi$ domain walls.

This result demonstrates that the phase diagram of the model is dictated by the interplay between the defects of the symmetry group (\mathbb{Z}_4 vortices) as well as its subgroups (two types of \mathbb{Z}_2 domain walls). It is, therefore, natural to expect rich phase diagrams in systems possessing symmetries which decompose into multiple subgroups. For example, if we consider a $\mathbb{Z}_6 \rightarrow \mathbb{Z}_2 \times \mathbb{Z}_3$ decomposition, we should be able to uncover a rich phase diagram governed by the interplay of \mathbb{Z}_2 domain walls, \mathbb{Z}_3 domain walls, \mathbb{Z}_3 vortices and \mathbb{Z}_6 vortices. And this example is precisely what we explore next.

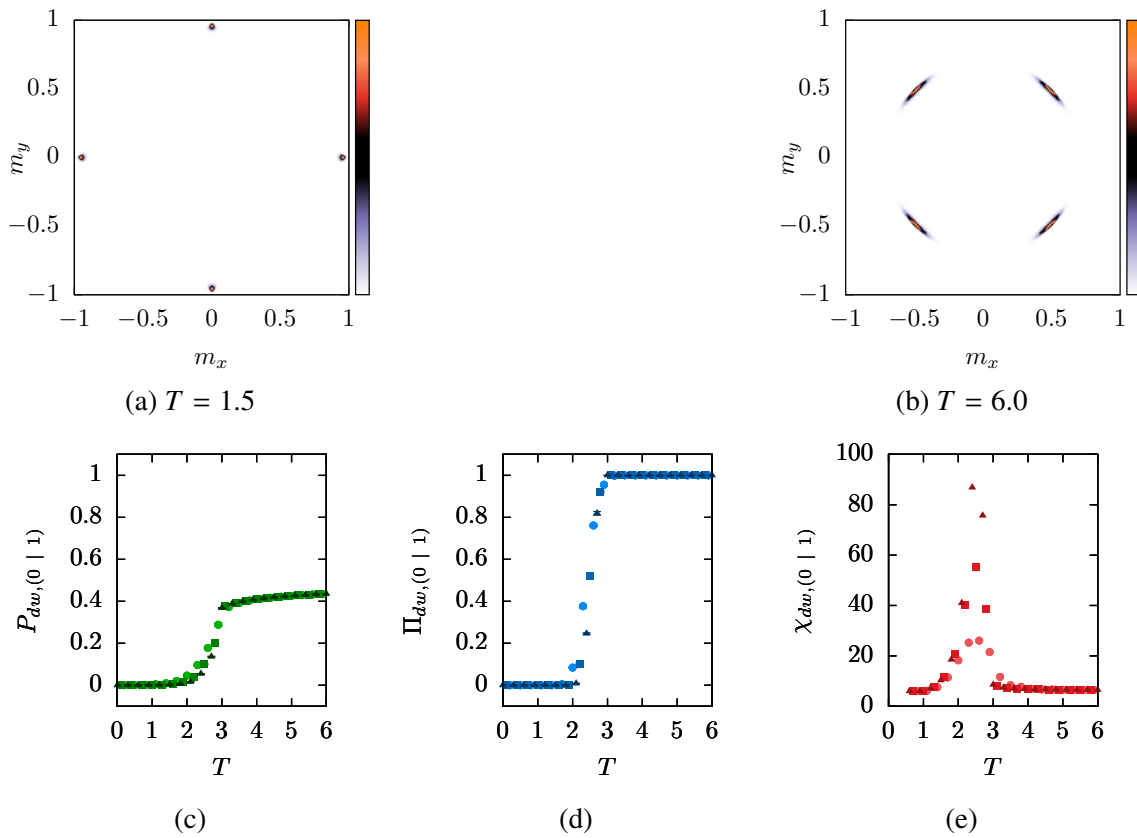


Figure 4.10: The order parameter distribution shows how the four-fold symmetry which is broken in (a) the ordered phase is offset by $\pi/4$ in (b) the partially symmetry broken phase. The latter phase also shows percolation of $(0 | 1)$ domain walls (c,d,e).

Chapter 5

Role of Subgroup Defects

The \mathbb{Z}_6 clock ferromagnet on the simple cubic lattice has been studied extensively because, apart from being a statistical model in its own right, the ferromagnet serves as an effective theory for the three-state Potts antiferromagnet on the simple cubic lattice and the stacked triangular Ising antiferromagnet [20–24, 34]. It also models the breaking of a six-fold symmetry which characterizes ferroelectric domains in hexagonal manganite multiferroics [9]. The phase diagram of the \mathbb{Z}_6 model, however, has been a topic of debate. In two dimensions, the model clearly exhibits an emergent U(1) phase, which lies intermediate between the low temperature ordered phase and the high temperature disordered phase. In three dimensions, on the other hand, there is no clear indication for the existence of such a phase. Monte Carlo simulations show an intermediate region where the order parameter distribution shows an emergence of U(1) symmetry [27]. However, the extent of the region continues to shrink with increasing system size. There has been no direct demonstration of whether the intermediate region stops shrinking above a certain system size and becomes a stable phase or if it continues to shrink and vanishes in the thermodynamic limit. While suggestions have been made for a stable intermediate phase [25, 26], renormalization group calculations suggest that the apparent emergence of U(1) symmetry is a finite size effect [23, 24]. In contrast, the U(1) symmetry is known to

emerge, and remain thermodynamically stable, at the disordering transition point as the transverse length scale of the system diverges at that point. In particular, this length scale begins to grow rapidly below the disordering transition temperature. Therefore, systems with small sizes, i.e. with sizes falling below the growing length scale, exhibit an apparent U(1) emergence below the disordering transition. For sufficiently large systems, the apparent emergent behavior is likely to give way to a \mathbb{Z}_6 symmetry broken phase and the model is expected to exhibit a single order-disorder transition [23, 24]. There has also been a suggestion that vortex strings and domain walls proliferate at the same temperature in this model, due to which an intermediate phase is not realized [95].

5.1 \mathbb{Z}_6 Clock Ferromagnet on the Simple Cubic Lattice

We have simulated the \mathbb{Z}_6 clock ferromagnet, described by the Hamiltonian

$$\mathcal{H} = \sum_{\langle i, j \rangle \in \Lambda} 1 - \cos(\theta_i - \theta_j) \quad (5.1)$$

on a simple cubic lattice. The spin vectors at each vertex $i \in \Lambda$ can orient at six different angles $\theta_i \in \{2\pi s/6 \mid s \in \{0, 1, \dots, 5\}\}$.

We have measured the vector order parameter at different temperatures. The magnetization decays across $T \approx 2.2$ (Fig. 5.1a). However, $m_{6\phi}$ decays at a lower temperature at $T \approx 1.5$. The distribution of the order parameter shows that the six-fold symmetry is broken in the ordered phase $T < 1.5$, enhances to U(1) in the intermediate region $1.5 < T < 2.2$ and gets restored in the disordered phase $T > 2.2$. Monte Carlo simulation using cluster algorithms for larger system sizes show that the extent of the intermediate region shrinks with increasing system size, and hence the controversy regarding the existence of the intermediate phase [27]. We will, however, adopt a different approach. Instead of performing simulations on larger system sizes and tracking the rate at which the region shrinks, we will attempt to infer the nature of the intermediate region by studying

the behavior of the topological defects in the model.

We have measured the density of vortex strings ρ_{vx} and the density of domain walls ρ_{dw} at different temperatures (Fig. 5.1b). Our results show that, contrary to previous suggestions [95], the defects do not proliferate simultaneously. The vortex strings proliferate at a higher temperature $T \approx 2.2$ while the domain walls proliferate at a lower temperature $T \approx 1.5$. However, a decoupled proliferation of the defects does not guarantee that the intermediate phase exhibits symmetry enhancement. In fact, for the \mathbb{Z}_3 and \mathbb{Z}_4 clock ferromagnets we have obtained a partially symmetry broken phase at intermediate temperatures. Is the apparent symmetry enhancement a result of large transverse fluctuations induced by the disordering transition? If it so, the fluctuations should vanish when the disordering transition is shifted to very high temperatures. We have demonstrated that the transition from the symmetry enhanced phase to the disordered phase in the two dimensional \mathbb{Z}_6 clock ferromagnet shifts to very high temperatures when the formation of vortices and $\pm\pi$ domain walls are suppressed.

5.1.1 Suppression of \mathbb{Z}_6 Vortex Strings and $\pm\pi$ Domain Walls

We have simulated the clock model with the suppression terms, given by the Hamiltonian

$$\mathcal{H}' = \sum_{\langle i,j \rangle \in \Lambda} 1 - \cos(\theta_i - \theta_j) + \lambda \sum_{e' \in \Lambda'} |\omega_{e'}| + \delta\epsilon_\pi \sum_{\langle i,j \rangle} \delta([\theta_i - \theta_j]_{2\pi}, \pm\pi) \quad (5.2)$$

For extreme suppression of the vortex strings and $\pm\pi$ domain walls using $\lambda = 100$ and $\delta\epsilon_\pi = 100$, we find that the disordering transition shifts to very high temperatures (Fig. 5.1f). However, the apparent U(1) emergence continues in a manner identical to the model without suppression. In fact, the shift of the disordering transition only serves to extend the apparent U(1) region. This result suggests that the emergent behavior might not be caused by fluctuations induced by the disordering transition but, instead, is a feature of the region itself.

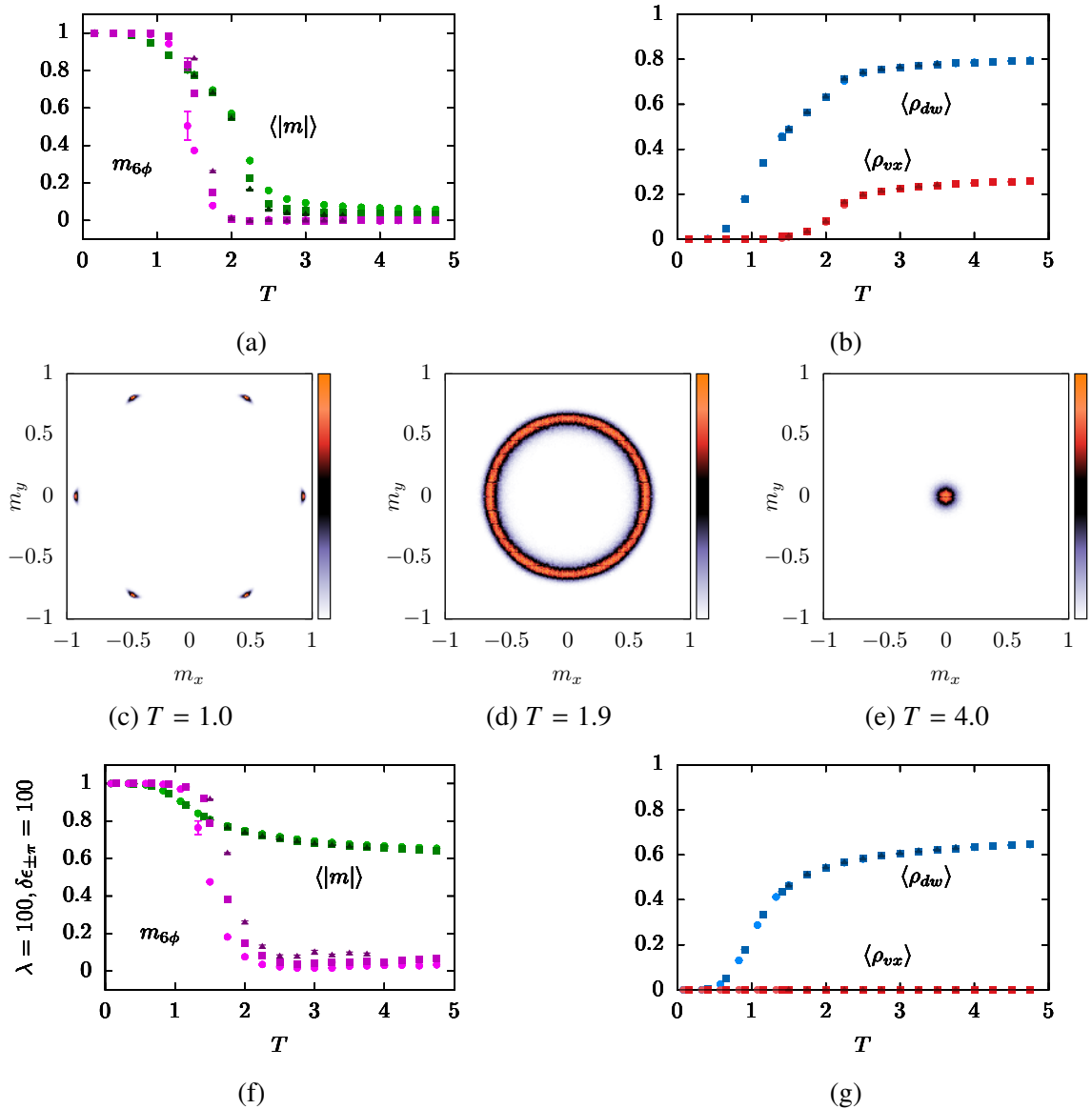


Figure 5.1: The \mathbb{Z}_6 clock ferromagnet on the simple cubic lattice shows an intermediate region below the order-disorder transition where the order parameter distribution obtained for a $L = 8$ system exhibits apparent emergence of U(1) symmetry and $m_{6\phi}$ become zero. The density of vortex strings rises near the disordering transition whereas the density of domain walls rises near the decay of $m_{6\phi}$. Upon suppression of the vortex strings and $\pm\pi$ domain walls, $m_{6\phi}$ continues to decay at the temperature where domain walls begin to proliferate. The data has been obtained for system sizes $L = 8$ (circle), $L = 12$ (square) and $L = 16$ (triangle).

With the vortex strings and $\pm\pi$ domain walls suppressed, the domain walls are left in charge of dictating the nature of the intermediate region. We note that $m_{6\phi}$ decays close to the temperature where the remaining domain walls begin to proliferate. When we suppress the formation of these remaining domain walls, the system shows complete ordering and the apparent emergent behavior gets destroyed. While this trivially establishes the necessity of domain walls for the existence of the emergent behavior, it does not provide much information. We, therefore, turn to a visual inspection of the spin configurations obtained in the ordered phase and in the intermediate region.

In the ordered phase, most of the spins align along a common direction with a few spins fluctuating to the adjacent angles to the left and right of the common angle (Fig. 5.2a). This is expected because the cosine potential of the model gradually increases the energy cost for larger differences between angles. In the intermediate region, however, we find that the common angle and its two adjacent angles are present in a nearly equal proportion (Fig. 5.2b). Effectively, the change from the ordered phase to the intermediate region mimics that of a three state model. Does the change actually represent a transition belonging to the \mathbb{Z}_3 subgroup of the \mathbb{Z}_6 model?

In order to verify this conjecture, we need to choose an effective \mathbb{Z}_3 order parameter.

5.1.2 Restoration of \mathbb{Z}_3 Symmetry

A simple scheme to transform \mathbb{Z}_6 spin states into effective \mathbb{Z}_3 spin states is given by $s \rightarrow s_3 = s \bmod 3$. While the \mathbb{Z}_6 angles are $\theta = 2\pi s/6$, the effective \mathbb{Z}_3 angles are $\theta_3 = 2\pi s_3/3$. Under this scheme, if any three consecutive angles in the \mathbb{Z}_6 spin space are present in equal proportion in a system, all the three angles of the \mathbb{Z}_3 order parameter space get represented in equal proportion. In such a case, the effective \mathbb{Z}_3 vector order

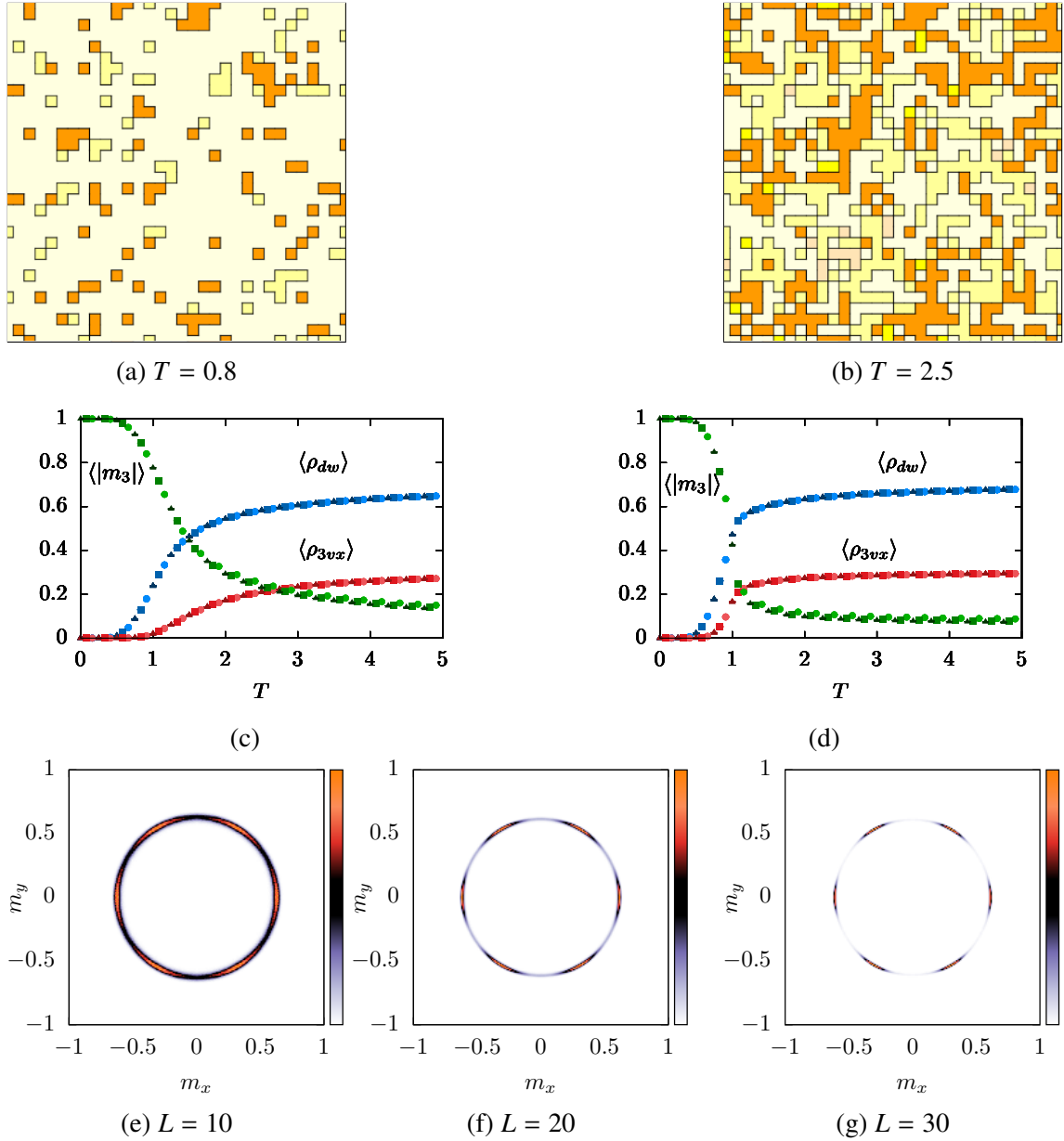


Figure 5.2: Suppression of vortex strings and $\pm\pi$ domain walls leaves the model with an ordered phase (a) and a high temperature region (b) where three consecutive spin states appear in equal proportion. The \mathbb{Z}_3 magnetization decays in this region (c) and the decay grows sharper (d) when the energy cost between the three states is made degenerate to mimic a Potts potential. The order parameter distribution obtained at $T = 2.0$ for the degenerate Hamiltonian shows \mathbb{Z}_6 symmetry breaking with increasing system size.

parameter (m_{3x}, m_{3y}) shows zero magnetization $|m_3| = 0$.

$$\begin{aligned} m_{3x} &= \sum_{i \in \Lambda} \cos \theta_{3i} / N \\ m_{3y} &= \sum_{i \in \Lambda} \sin \theta_{3i} / N \end{aligned} \quad (5.3)$$

where N is the number of spins and the magnetization is given by $|m_3| = \sqrt{m_{3x}^2 + m_{3y}^2}$.

Since we know that the disordering transition in the \mathbb{Z}_3 ferromagnet is driven by a simultaneous proliferation of domain walls and \mathbb{Z}_3 vortex defects, it would be useful to check if conjectured effective \mathbb{Z}_3 transition in the present case is also driven by the simultaneous proliferation of the domain walls and vortices associated with the \mathbb{Z}_3 subgroup. In order to identify these subgroup vortices, we calculated the winding number $\omega_{3e'}$ at each dual edge $e' \in \Lambda'$ using our proposed method (3.2), but with the θ values replaced by their corresponding θ_3 values. We have measured the density ρ_{3vx} of these \mathbb{Z}_3 vortices.

We find that the density of the \mathbb{Z}_3 vortices increases simultaneously with the density of domain walls across $T \approx 1.5$ (Fig. 5.2c). This is accompanied by a decay in the effective \mathbb{Z}_3 magnetization from the ordered phase into the intermediate region. However, the magnetization does not decay fully to zero but saturates at a small positive value. The change, therefore, appears to be a crossover rather than a transition. One reason behind this crossover behavior might be that the effective \mathbb{Z}_3 model, which the mapping $\theta \rightarrow \theta_3$ tries to generate, is not really a \mathbb{Z}_3 model. Consider three consecutive angles in the \mathbb{Z}_6 spin space: $0, \pi/3$ and $2\pi/3$. The energy cost between angles 0 and $\pi/3$ is $1 - \cos(\pi/3) = 1/2$. The cost between angles $\pi/3$ and $2\pi/3$ is also $1 - \cos(-\pi/3) = 1/2$. However, the cost between angles 0 and $2\pi/3$ is $1 - \cos(2\pi/3) = 3/2$. In a \mathbb{Z}_3 ferromagnet, the energy cost between all pairs of dissimilar angles is expected to be the same. Can we transform the crossover behavior into a transition by bringing down the interaction energy of angles differing by $2\pi/3$, thus making the interaction energy between three consecutive states

degenerate? For this purpose, we introduce a new term into the previous Hamiltonian

$$\mathcal{H} = \mathcal{H}' - \sum_{\langle i,j \rangle} \delta([\theta_i - \theta_j]_{2\pi}, \pm 2\pi/3) \quad (5.4)$$

Upon simulating the model described by this Hamiltonian, we find that densities of both domain wall and \mathbb{Z}_3 vortex string defects begin to increase at a lower temperature $T \approx 1$ (Fig. 5.2d). In addition, this increase is found to be sharper than that obtained in Fig. 5.2c. This change in the behavior of defect densities, in turn, has an effect on the magnetization which now decays in a sharper manner at $T \sim 1$. However, even by making the $\pm 2\pi/3$ domain wall cost degenerate with that of the $\pm\pi/3$ domain walls, the magnetization does not decay to zero but saturates at a small positive value $\langle |m_3| \rangle \sim 0.07$. This suggests that the intermediate region, while closely resembling the characteristics of a \mathbb{Z}_3 disordered phase, might not be truly \mathbb{Z}_3 disordered. Before investigating the nature of the phase further, we note that the order parameter distribution in this region shows apparent U(1) emergence for small systems but shows a clear breaking of the \mathbb{Z}_6 symmetry for larger systems (Fig. 5.2f).

The residual \mathbb{Z}_3 magnetization in the intermediate region is reminiscent of the intermediate values for magnetization obtained in partially ordered phases. We have shown that a characteristic signature of partial symmetry breaking in three dimensions is the percolation of a single type of domain wall. Clearly, the order parameter distribution in the intermediate region does not display the $\pi/6$ offset pattern expected of a partially symmetry broken phase. However, a measurement of the percolation properties characterizing the particular types of domain walls might provide a clue regarding the nature of this region.

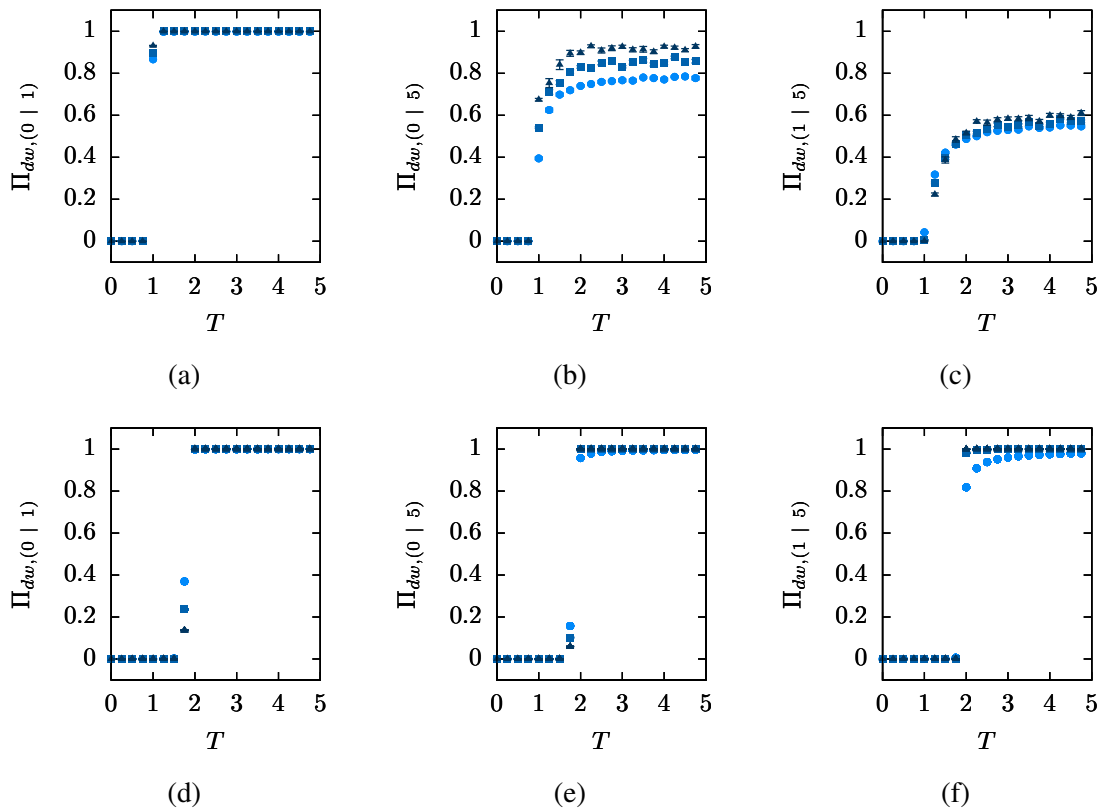


Figure 5.3: Top panel: Measurement of spanning probability show that two types of domain walls (0 | 1) and (0 | 5) percolate in the intermediate region, while a third type (1 | 5) appears to remain on a percolation threshold. Bottom panel: In the disordered phase of the \mathbb{Z}_3 ferromagnet on the simple cubic lattice, all the three types of domain walls percolate.

5.1.3 Percolation of $(a | b)$ Domain Walls

Our measurements show that, in the intermediate region, not one but two particular types of domain walls percolate on their own. The particular types are: $(0 | 1)$ and $(0 | 5)$. The spanning probability saturates to unity for $(0 | 1)$ domain walls in the intermediate region (Fig. 5.3a). In addition, the increase in spanning probability with system size for $(0 | 5)$ suggests that the probability will reach unity in the thermodynamic limit (Fig. 5.3b). Although a third type $(1 | 5)$ shows a non-zero spanning probability, the system size dependence suggests that it will not percolate in the thermodynamic limit (Fig. 5.3c). This result provides a fresh impetus to the proposal that the intermediate region is indeed \mathbb{Z}_3 disordered. We have measured the percolation properties of the three particular types of domain walls in the \mathbb{Z}_3 clock ferromagnet on the simple cubic lattice. We find that all the three types begin to percolate on their own at the order-disorder transition in the model (Fig. 5.3d). This result suggests two alternate scenarios:

1. the change from the ordered phase to the intermediate region of the \mathbb{Z}_6 ferromagnet with the degenerate Hamiltonian is truly a phase transition, or
2. the change does not appear as a thermodynamic transition but as a percolation transition in terms of the particular types of domain walls. In the latter case, the percolation transition would be reminiscent of that obtained across a Kertesz line [123].

5.1.4 Suppression of \mathbb{Z}_3 Vortex Strings

The natural question which comes up next is: does an intermediate phase appear if we decouple the simultaneous proliferation of the domain walls and \mathbb{Z}_3 vortex strings by suppressing the latter? In order to suppress the formation of the \mathbb{Z}_3 vortices, we raise their core energy by an amount λ_3 . The Hamiltonian with the addition of this new term

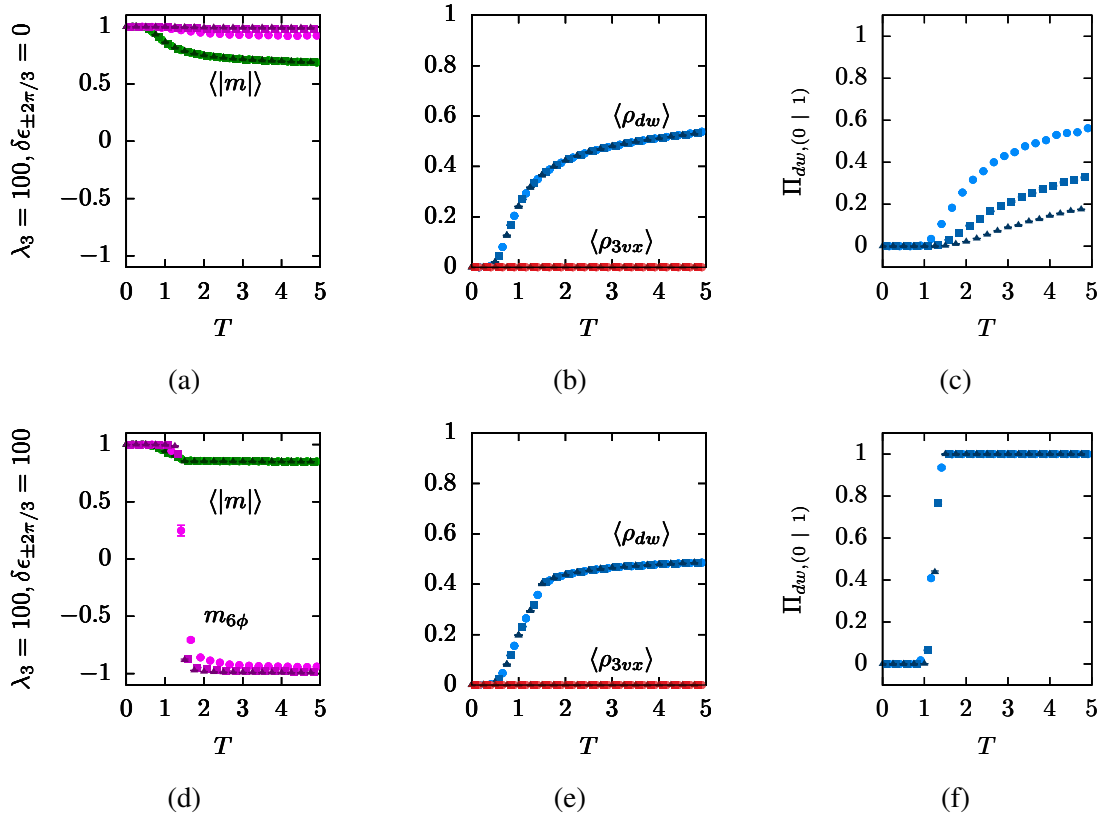


Figure 5.4: Top panel: When \mathbb{Z}_3 vortex strings are suppressed, $m_{6\phi}$ saturates at unity along with the magnetization. None of the individual types of domain walls percolate in this region. Bottom panel: When $\pm 2\pi/3$ domain walls are also suppressed, the system exhibits a transition from the ordered phase to a partially symmetry broken phase in which only the $(0|1)$ domain walls begin to percolate again.

becomes:

$$\mathcal{H} = \mathcal{H}' - \sum_{\langle i,j \rangle} \delta([\theta_i - \theta_j]_{2\pi}, \pm 2\pi/3) + \lambda_3 \sum_{e' \in \Lambda'} |\omega_{3e'}| \quad (5.5)$$

With extreme suppression of the \mathbb{Z}_3 vortex strings, using $\lambda_3 = 100$, we find that the simultaneous proliferation of the domain walls and \mathbb{Z}_3 vortex strings decouples (Fig. 5.4b). The proliferation of the latter defects recedes to higher temperatures and leaves behind a new region where the domain walls proliferate alone. Interestingly, we find that the magnetization, of both the \mathbb{Z}_6 (Fig. 5.4a) and \mathbb{Z}_3 order parameters jump to a value close to unity in this region. The most interesting change, however, appears in the behavior of $m_{\cos 6\phi}$. The value of this observable shifts from a near zero value in the previous intermediate region (Fig. 5.1f) to a value close to unity in this new region (Fig. 5.4a). Therefore, in terms of the order parameter, this new region is very similar to the ordered phase. However, we find a crucial difference between the ordered phase and the new region. Domain walls do not proliferate in the ordered phase while they do so in the new region (Fig. 5.4b). In addition, we find that none of the individual types of domain walls percolate in this new region (Fig. 5.4c). Since the change from the ordered phase to this new region is not marked by any change in symmetry but is distinguished by the percolation of domain walls, we have yet another example of a Kertesz line scenario in the present model.

5.1.5 Suppression of $\pm 2\pi/3$ Domain Walls

By suppressing the different types of defects one after the other, we have nearly exhausted the set of defects supported by the \mathbb{Z}_6 model. The only defects remaining are the domain walls which separate angles differing by $\pm\pi/3$ and $\pm 2\pi/3$. The energy cost of the latter type had been made degenerate to that of the former type artificially in the Hamiltonian (Eq. 5.4). We remove this degeneracy and, instead, suppress the formation of the $\pm 2\pi/3$ domain walls by increasing their energy cost by an amount $\delta\epsilon_{\pm 2\pi/3}$. The new

Hamiltonian becomes

$$\mathcal{H} = \mathcal{H}' + \delta\epsilon_{\pm 2\pi/3} \sum_{\langle i,j \rangle} \delta([\theta_i - \theta_j]_{2\pi}, \pm 2\pi/3) + \lambda_3 \sum_{e' \in \Lambda'} |\omega_{3e'}| \quad (5.6)$$

For $\delta\epsilon_{\pm 2\pi/3} = 100$, the proliferation of the $\pm 2\pi/3$ domain walls recedes to a very high temperature and the model is essentially left with $\pm\pi/3$ domain walls only. In effect, the neighboring spins can either orient along the same direction or differ by $\pm\pi/3$. This is precisely the situation encountered for the \mathbb{Z}_3 ferromagnet with $\lambda = 100$ and the \mathbb{Z}_4 clock ferromagnet with $\lambda = 100$ and $\delta\epsilon_{\pm\pi}$. In all these cases, the \mathbb{Z}_n spins were allowed to differ in orientation within a range of $\pm 2\pi/n$. In a manner similar to those cases, we find that in the current case: a single transition from the ordered phase to a partially symmetry broken phase (Fig. 5.4c) where domain walls of type $(0 | 1)$ percolate on their own (Fig. 5.4f) and a \mathbb{Z}_2 symmetry gets restored.

5.2 \mathbb{Z}_3 Antiferromagnet on the Simple Cubic Lattice

We have discussed (Sec. 3.8) how the \mathbb{Z}_3 antiferromagnet can be equivalently written as a \mathbb{Z}_6 ferromagnet. This mapping holds true on the simple cubic lattice because the lattice is bipartite. Using the information obtained about the different phases from our study of the \mathbb{Z}_6 ferromagnet, we can now embark on exploring the phase diagram of the \mathbb{Z}_3 antiferromagnet as well.

The antiferromagnet on the simple cubic lattice is known to undergo a single order-disorder transition, although there have been suggestions for a rotationally symmetric phase, which is similar to the symmetry enhanced phase suggested for \mathbb{Z}_n ferromagnets [142–146]. However, the ordered phase of the \mathbb{Z}_3 antiferromagnet is not a conventional one. In this phase, one of the sublattices picks up a spin state while the other two spins states are arbitrarily distributed on the other sublattice. Therefore, the phase exhibits a broken sublattice symmetry (BSS). What drives the transition from the BSS phase to the

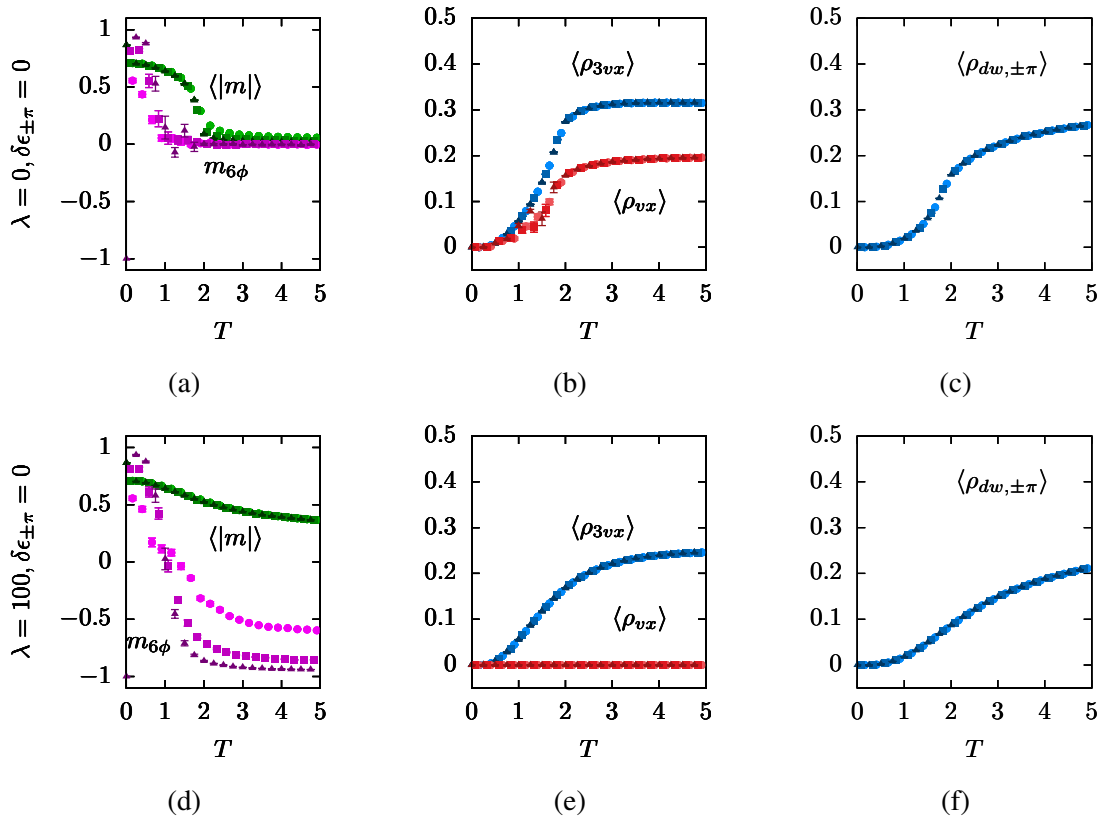


Figure 5.5: Top panel: The \mathbb{Z}_3 antiferromagnet on the simple cubic lattice exhibits a single transition from the BSS phase to the disordered phase, which is accompanied by the proliferation of \mathbb{Z}_6 vortex strings, \mathbb{Z}_3 vortex strings and $\pm\pi$ domain walls. Bottom panel: Upon suppressing the formation of the \mathbb{Z}_6 vortex strings, the system shows a partially symmetry broken phase due to the proliferation of the $\pm\pi$ domain walls.

disordered phase?

We have simulated the effective \mathbb{Z}_6 ferromagnet which is equivalent to the \mathbb{Z}_3 antiferromagnet as described in Sec. 3.8. We find that the order-disorder transition, captured by the decay of the magnetization, is accompanied by the simultaneous proliferation of \mathbb{Z}_6 vortex strings, \mathbb{Z}_3 vortex strings and $\pm\pi$ domain walls (Fig. 5.5a). When we suppress the formation of the \mathbb{Z}_6 vortex strings, the transition changes to one between the BSS phase and a partially symmetry broken phase (Fig. 5.5d). When the $\pm\pi$ domain walls are suppressed as well, the system exhibits a BSS phase throughout. We find that the \mathbb{Z}_3 vortex strings are not able to drive any transitions on their own because they get suppressed when the $\pm\pi$ domain walls are suppressed.

Chapter 6

Melting of Vortex-Antivortex Lattice

The method of raising the core energy of vortices and suppressing their formation has not only allowed us to demonstrate their role in driving phase transitions but has also assisted us in uncovering a rich variety of phases. Can we also uncover new phases by lowering the core energy of vortices and enhancing their formation?

The effect of vortex enhancement has been studied in models with continuous symmetries and rich phase diagrams have been obtained wherein a new vortex-antivortex lattice phase appears for strong enhancement [53, 147–152]. Another approach involves a modification to the potential of the XY model, in order to make it more steep like the Kronecker delta potential of the Potts model. In doing so, the infinite order BKT transition of the two dimensional XY model has been shown to become first-order in nature [153]. This change has been attributed to a sudden proliferation of vortices due to their enhancement [60, 154]. However, the effect of enhancing the formation of vortices has not been studied for models with discrete symmetries.

6.1 \mathbb{Z}_3 Clock Ferromagnet on the Square Lattice

As a first case, we revisit the \mathbb{Z}_3 clock ferromagnet on the square lattice. We consider the Hamiltonian

$$\mathcal{H} = \sum_{\langle i,j \rangle \in \Lambda} 1 - \cos(\theta_i - \theta_j) + \lambda \sum_{i' \in \Lambda} |\omega_{i'}| \quad (6.1)$$

with negative values of λ . We have measured the magnetization $|m|$ and the number densities of domain walls ρ_{dw} and vortices ρ_{vx} at each temperature. For reasons, to be clarified soon, we have also measured the specific heat $c_v = (\langle \mathcal{H}^2 \rangle - \langle \mathcal{H} \rangle^2)N/T^2$. For $\lambda = 0$, the model exhibits a order-disorder transition at $T = 1.49$ which is driven by the simultaneous proliferation of vortices and domain walls. For weak suppression with $\lambda > 0$, we found that the fall of the order parameter appears to become smoother (Sec. 2.2.2). Therefore, we can expect the fall to become sharper as we make λ negative.

6.2 Weak Enhancement of Vortices

For $\lambda = -1.5$, the rise in vortex density shifts to a lower temperature $T \approx 1.1$ and becomes sharper as compared to the $\lambda = 0$ case (Fig. 6.1e). The rise in domain wall density also sharpens and shifts to the same temperature. This behavior is also observed in the decay of the magnetization and the peak of specific heat, both of which shift to $T \approx 1$. The rapid growth of the specific heat and the sharper decay of the magnetization suggests that the transition is becoming stronger. With increasingly negative values of λ , the decay of the magnetization and the rise of defect densities continue to grow sharper, while shifting to lower temperatures. This trend continues upto $\lambda \approx 2$. Below this λ , the shift of the magnetization continues but a qualitative change is observed in the rise of the defect densities.

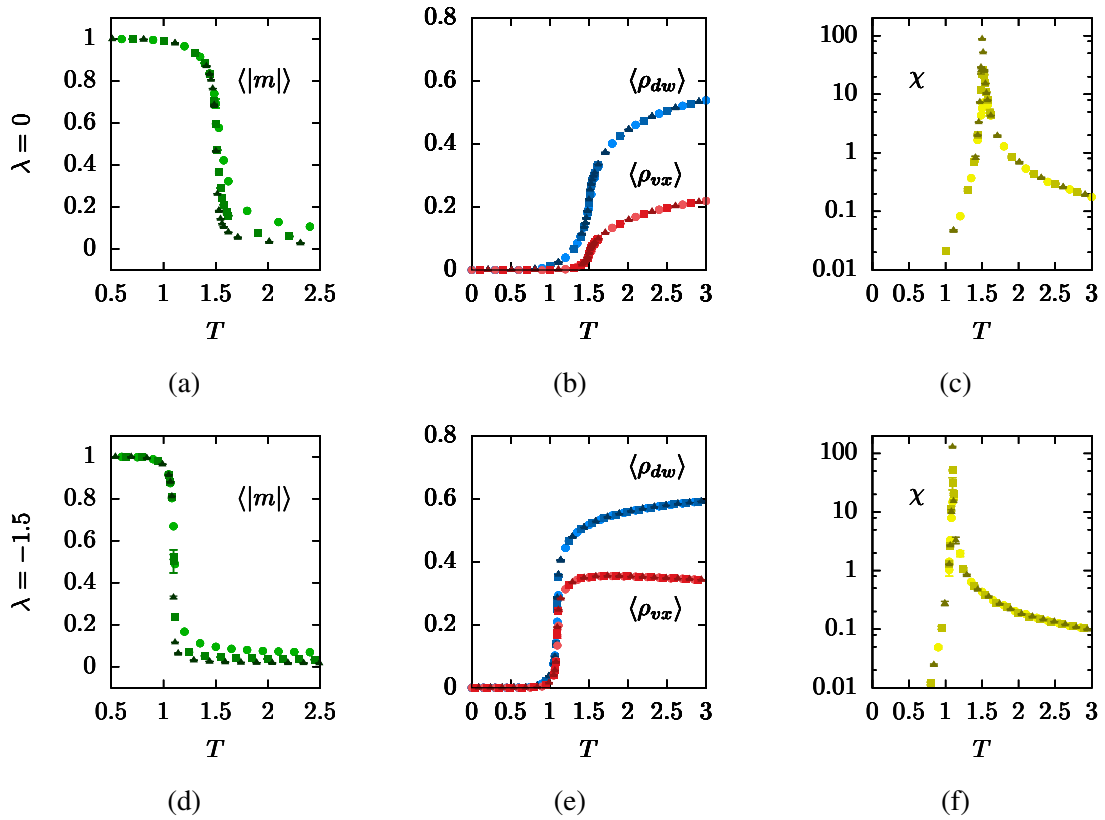


Figure 6.1: The order-disorder transition of the \mathbb{Z}_3 clock ferromagnet on the square lattice, which is accompanied by a simultaneous proliferation of vortices and domain walls (top panel), shifts to a lower temperature when the vortices are weakly enhanced (bottom panel). The rise in the defect densities and the decay of magnetization becomes sharper as well. Data has been obtained for system sizes $L = 16$ (circle), $L = 32$ (square) and $L = 64$ (triangle).

6.2.1 Strong Enhancement of Vortices

In the data for $\lambda = -2.1$, however, the vortex density rises above the domain wall density across an intermediate range of temperatures (Fig. 6.2b). This is interesting because for $\lambda > -2.1$, the vortex density was always smaller than the domain wall density, even in the disordered phase. In addition to the change in the intermediate region, the rise in both densities appear to be discontinuous. With stronger enhancement using $\lambda = -3$, this intermediate region appears to increase in extent (Fig. 6.2e). Additionally, the discontinuous rise of the densities as well as the decay in magnetization shifts to a lower temperature $T \approx 0.3$ (Fig. 6.1d). Surprisingly, however, the specific heat peak shifts to a higher temperature $T \approx 1.2$ (Fig. 6.1f), which appears close to the point where the vortex density returns below the domain wall density. The intermediate region marked out by the defect densities, is therefore, of significant interest.

6.3 Vortex-Antivortex Lattice

A visual inspection of the spin configurations obtained in the intermediate region reveals that the vortices and antivortices have arranged themselves in alternate sublattice sites, i.e. they have formed a vortex-antivortex lattice ($v\bar{v}l$) (Fig. 6.2h). The $v\bar{v}l$ structure also exhibits a few vacancies. The number of these vacancies grows with increasing temperature and becomes considerable in the disordered phase, where the $v\bar{v}l$ structure appears to melt away (Fig. 6.2i). At the low temperature side, on the other hand, we find a completely ordered configuration devoid of domain walls or vortices (Fig. 6.2g) upto the point marked by the discontinuous jump in the defect densities.

The formation of the $v\bar{v}l$ structure is justified because by lowering the core energy, we have made the formation of vortices quite favorable and the sublattice ordering of the defects is the only space-filling pattern allowed by the orientation of the spins. However, with such a negative value of λ , the $v\bar{v}l$ should also be the minimum energy configuration which

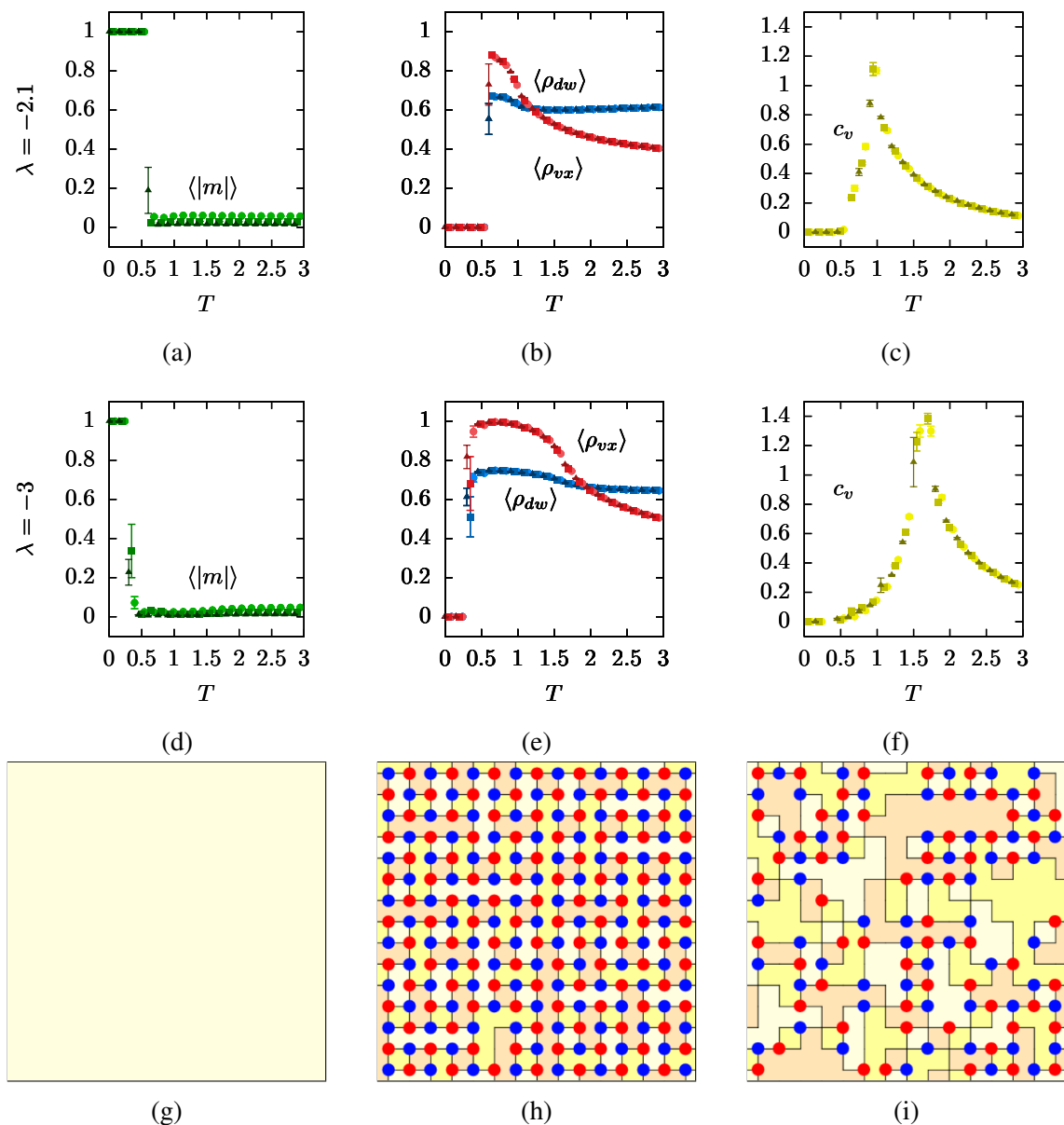


Figure 6.2: For strong suppression of vortices, the decay of magnetization shifts to lower temperatures but the specific heat reverses its trend and starts shifting to higher temperatures. The density of vortices is observed to rise sharply to a value higher than that of domain walls before coming down to a lower value at a higher temperature. In the intermediate region, the vortices and antivortices are found to display a sublattice ordering. System sizes correspond to those in Fig. 6.1.

can be realized at zero temperature. Instead, we find a completely ordered configuration, which has a higher energy, at zero temperature for this λ (Fig. 6.2g).

6.3.1 Non-ergodic Nature of Single Spin-Flip Algorithm

The reason behind this discrepancy lies in the use of a single spin-flip algorithm for the Monte Carlo simulation. If we initialize the system to a completely ordered configuration, the first candidate spin state proposed for the update will be surrounded by spins all belonging to a different state. This configuration never generates a non-zero winding number and therefore, the candidate spin can never utilize the strongly negative values of λ to get accepted as a energy lowering flip. On the contrary, it gets surrounded by four domain walls which have a high energy cost. Therefore, the candidate never gets accepted at low temperatures and the system remains stuck in a completely ordered configuration. This continues till the system is provided a temperature large enough to accept the cost of creating a few domain walls. In such cases, a few candidate spins start getting accepted. Once in a while, two candidate spin flips can get accepted next to each other, which might prove to be sufficient for generating a non-zero winding number. Once a vortex defect has been generated, it begins to seed vortices in its neighborhood, which in turn seed newer vortices. In this process, the system gets covered soon, by a tiling of vortices and antivortices.

In order to alleviate the problem of non-ergodicity at low temperatures, we have repeated the simulation with a complete $v\bar{v}l$ as the initial configuration. For $\lambda = -3$, the $v\bar{v}l$ appears at zero temperature and continues upto the disordering point, as evidenced by the density of vortices reaching unity (Fig. 6.3h). However, our initial condition is found to distort the results for lower values of λ . At $\lambda = -1.5$, where we obtained a single order-disorder transition, the system now shows a $v\bar{v}l$ phase at low temperatures (Fig. 6.2b). For $\lambda = -2.1$, it is difficult to interpret the data as the defect densities show a two step jump towards zero temperature (Fig. 6.2e). We have observed that this behavior at intermediate

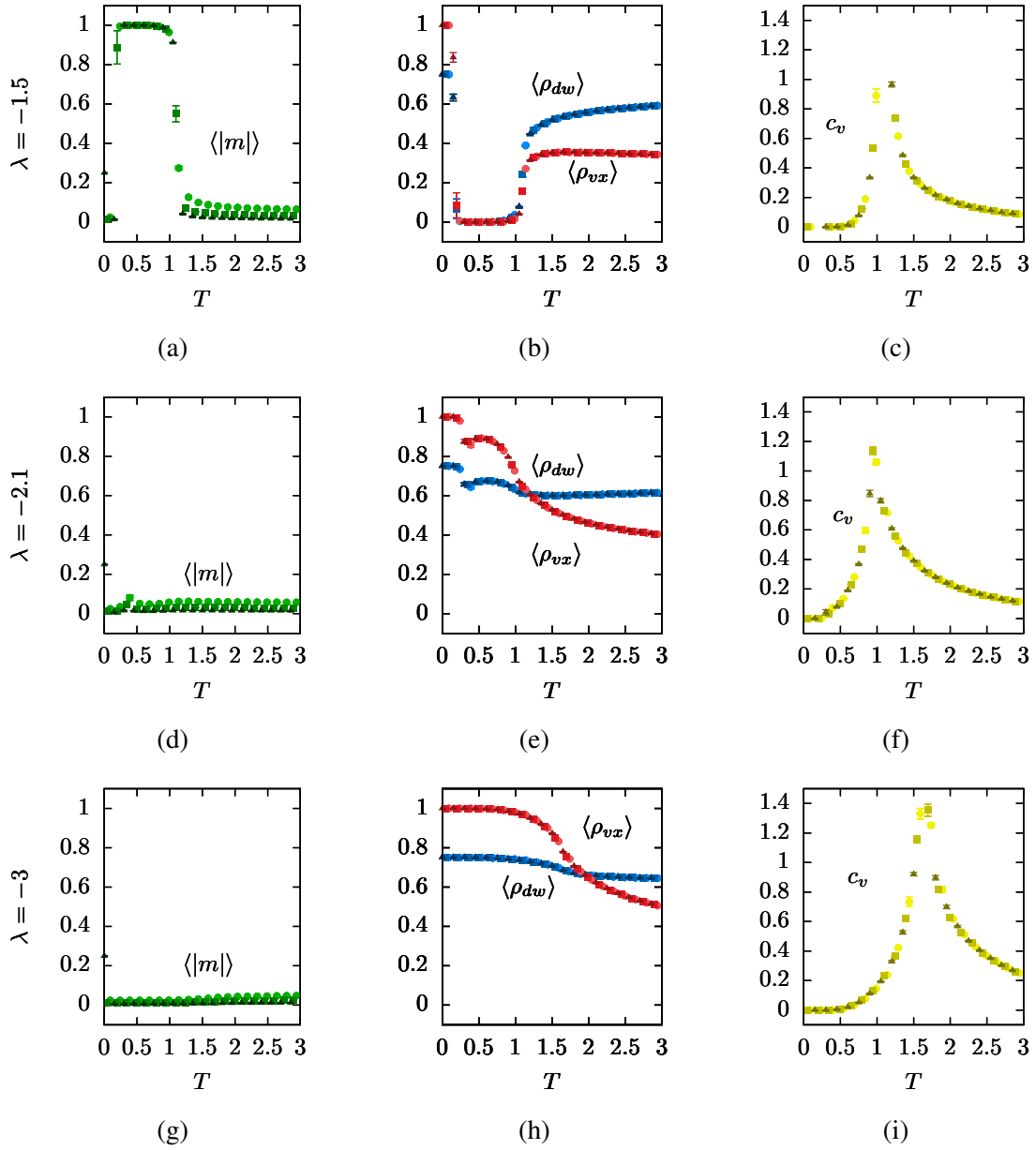


Figure 6.3: Values of the thermodynamic observables obtained by simulating the model with a $\bar{v}l$ as the initial spin configuration at each temperature. System sizes correspond to those in Fig. 6.1.

values of λ occurs because the system starts from the $v\bar{v}l$ configuration and gets jammed while trying to reach an ordered configuration. In other words, there are no local spin moves available to take the system out of the jammed configuration. We conclude that while the ordered configuration is a justifiable starting condition at small negative values of λ and the $v\bar{v}l$ is justified as a starting condition for large negative values of λ , the intermediate region cannot be reliably simulated using the single spin-flip algorithm. In addition, we have already discussed that cluster algorithms cannot take into account the plaquette based winding number calculation required for the λ term.

6.3.2 Wang-Landau Algorithm for Defects

In order to obtain reliable information about this intermediate region, we have simulated the model using the Wang-Landau algorithm [155, 156]. This algorithm directly solves for the density of states and does not suffer from the jamming problem. We note that Hamiltonian (Eq. 6.1) can be written as

$$\mathcal{H} = N_{dw} + \lambda N_{vx} \quad (6.2)$$

where N_{dw} and N_{vx} are the number of domain walls and vortices, respectively, in a given configuration. We have estimated the density of states $g(N_{dw}, N_{vx})$ in terms of these two variables.

For a system of size $L = 16$, we started with a uniform density of states $g(N_{dw}, N_{vx}) = 1$ as the initial condition and maintained a histogram $h(N_{dw}, N_{vx})$ which counts the number of times a particular combination of the two variables is visited in course of the simulation. We visited each vertex i of the lattice Λ , proposed a candidate value θ'_i to update the angle θ_i and noted the values N'_{dw} and N'_{vx} for the configuration which would be generated if θ'_i is accepted. We compared these values to the existing values N_{dw} and N_{vx} . The candidate was accepted with a probability $\min[1, g(N_{dw}, N_{vx})/g(N'_{dw}, N'_{vx})]$. If the candidate was

accepted, we multiplied the value $g(N'_{dw}, N'_{vx})$ by a factor f and incremented $h(N_{dw}, N_{vx})$ by one. The initial value of f was chosen to be $f = e^1 \approx 2.718$. After every 10^3 lattice sweeps, we checked for the flatness of $h(N_{dw}, N_{vx})$ by demanding that the count in any bin of $h(N_{dw}, N_{vx})$ is not less than 80% of the average count. Odd values of N_{dw} and N_{vx} do not occur on the square lattice with periodic boundary conditions. We were careful not to include these bins while checking for the flatness of the histogram. If the histogram was found to be sufficiently flat, we reduced the modification factor as $f \rightarrow \sqrt{f}$. The simulation was terminated when f reached $O(10^{-8})$.

6.4 Phase Diagram of the \mathbb{Z}_3 Ferromagnet on the Square Lattice

Using the density of states generated in this manner, we calculated the values of a few thermodynamic observables as

$$\langle O \rangle = \frac{\sum_{N_{dw}, N_{vx}} O g(N_{dw}, N_{vx}) e^{-\mathcal{H}/T}}{\sum_{N_{dw}, N_{vx}} g(N_{dw}, N_{vx}) e^{-\mathcal{H}/T}} \quad (6.3)$$

In particular, we measured the density of domain walls $\langle N_{dw}/L^2 \rangle$, the density of vortices $\langle N_{vx}/L^2 \rangle$ and the specific heat $c_v = (\langle H^2 \rangle - \langle H \rangle^2) L^2 T^{-2}$. Since the same density of states is used to calculate the observables at different parameters λ and T , we were able to sweep through a large area of the parameter space with fine-grained increments.

Our simulation shows that the density of vortices and domain walls increases drastically across $\lambda \approx -2.2$ along the zero temperature axis (Fig. 6.4). While the region $\lambda > -2.2$ has been addressed correctly using a completely ordered initial configuration, the region $\lambda < -2.2$ is where the single spin-flip algorithm runs the risk of becoming non-ergodic. For large negative λ , however, even the results obtained using the Wang-Landau algorithm indicate the presence of $v\bar{v}l$ at low temperatures and the disordered phase at high

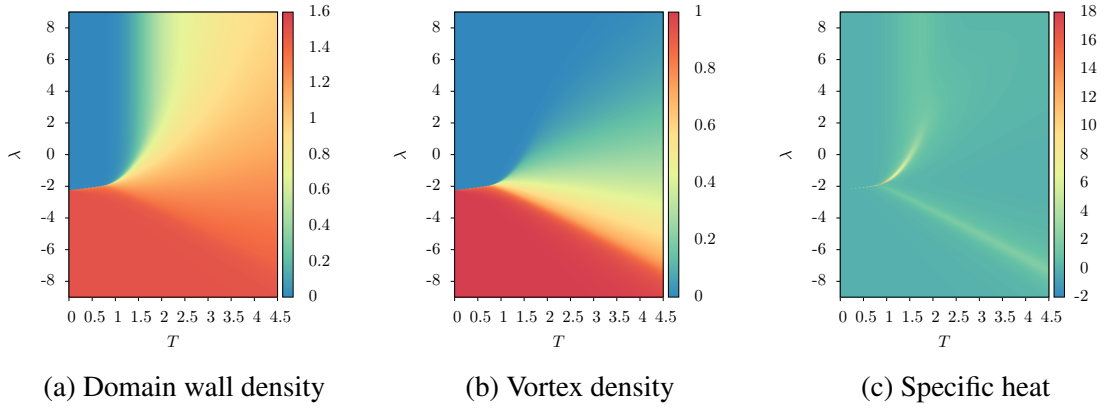


Figure 6.4: Densities of domain walls and vortices and the specific heat obtained using Wang-Landau algorithm for a $L = 16$ system is shown over the parameter space of temperature T and suppression strength λ .

temperatures. This is also reflected in the way the specific heat peaks. For $\lambda < -2.2$, the peak moves gradually towards higher temperatures as λ grows more negative. We also note that the data also vindicates the phase diagram obtained for $\lambda > 0$.

6.5 Defect Based Order Parameter

Independent of the specific location where the $v\bar{v}l$ transitions to the disordered phase or the ordered phase, it is interesting to note that the magnetization is unable to capture the difference between the disordered phase and $v\bar{v}l$ (Fig. 6.3h). This is because the spin configuration in the latter phase displays a weave pattern with all the three states present in a nearly equal proportion (Fig. 6.2h). The symmetry based order parameter is, therefore, unable to capture the melting of the lattice structure and a different order parameter is required to characterize it. We also note that since the magnetization cannot distinguish between the two phases, the use of magnetic susceptibility for locating the transition is unreliable. It is for this reason that we have shifted from the measurement of susceptibility to the measurement of specific heat in this chapter.

The defects exhibit only two types of winding number: +1 and -1. If the +1 defects occupy sublattice A, the -1 defects occupy sublattice B. This is precisely the ordering

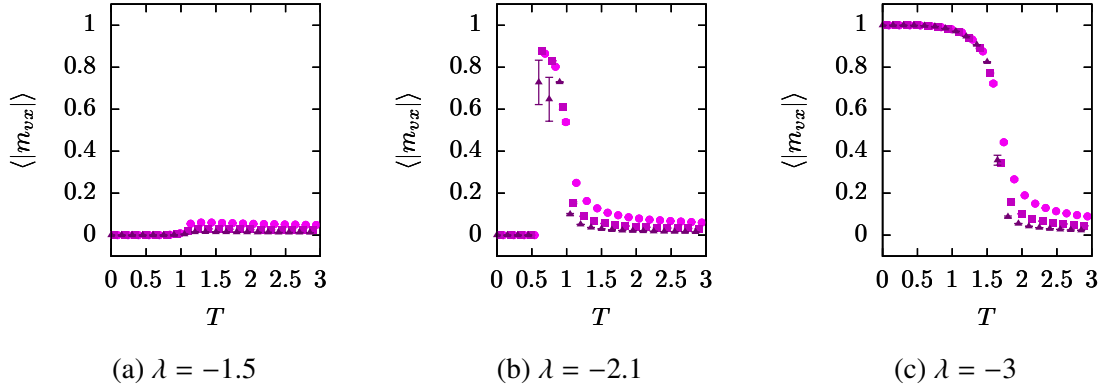


Figure 6.5: Variation of the $v\bar{v}l$ order parameter across temperature for different values of λ . In cases (a) and (b), the initial configuration at each temperature was a completely ordered one, while a complete $v\bar{v}l$ was used for (c). System sizes correspond to those in Fig. 6.1.

pattern displayed by an Ising antiferromagnet. In addition, the $v\bar{v}l$ lattice displays voids, which are characteristic of dilute systems. Therefore, the diluted antiferromagnetic Ising order parameter [147, 157] is a natural choice for characterizing the $v\bar{v}l$ phase. In terms of the winding numbers, the order parameter is defined as:

$$m_{v_x} = \sum_{i' \in \Lambda'} p_{i'} \omega_{i'} / L^2 \quad (6.4)$$

where $p_{i'} = \pm 1$ depending upon the sublattice to which the dual vertex i' belongs. We find that the equivalent of magnetization for this order parameter $\langle |m_{v_x}| \rangle$ takes on zero value in the ordered phase, rises to unity in the $v\bar{v}l$ phase and goes down to zero in the disordered phase (Fig. 6.5).

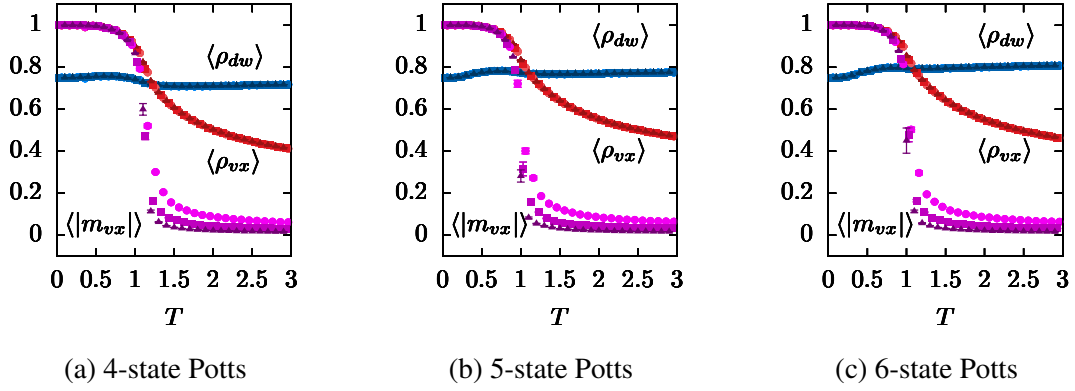


Figure 6.6: Melting transition from the $v\bar{v}l$ phase to the disordered phase obtained with $\lambda = -2$ for n -state Potts models on the square lattice. System sizes correspond to those in Fig. 6.1.

6.6 Melting in n -state Potts Ferromagnets on the Square Lattice

The three-state ferromagnet is not the only one which displays a $v\bar{v}l$ structure. We have considered n -state Potts ferromagnets described by the Hamiltonian

$$\mathcal{H} = \sum_{\langle i,j \rangle \in \Lambda} 1 - \delta(s_i, s_j) + \lambda \sum_{i' \in \Lambda'} |\omega_{i'}| \quad (6.5)$$

where each spin at vertex $i \in \Lambda$ can be in one of n states $s_i \in \{0, 1, \dots, n-1\}$. We have simulated these models for some values of n on the square lattice with negative values of λ . For strong enhancement of vortices with $\lambda = -2$, we find that the Potts models also exhibit a $v\bar{v}l$ phase which melts into the disordered phase at high temperatures (Fig. 6.6).

6.7 \mathbb{Z}_3 Ferromagnet on the Simple Cubic Lattice

As a next step, we have studied the effects of vortex enhancement on the \mathbb{Z}_3 Potts ferromagnet on the simple cubic lattice. Before simulating the model using the single spin-flip algorithm, we have obtained the values of the thermodynamic observables over the pa-

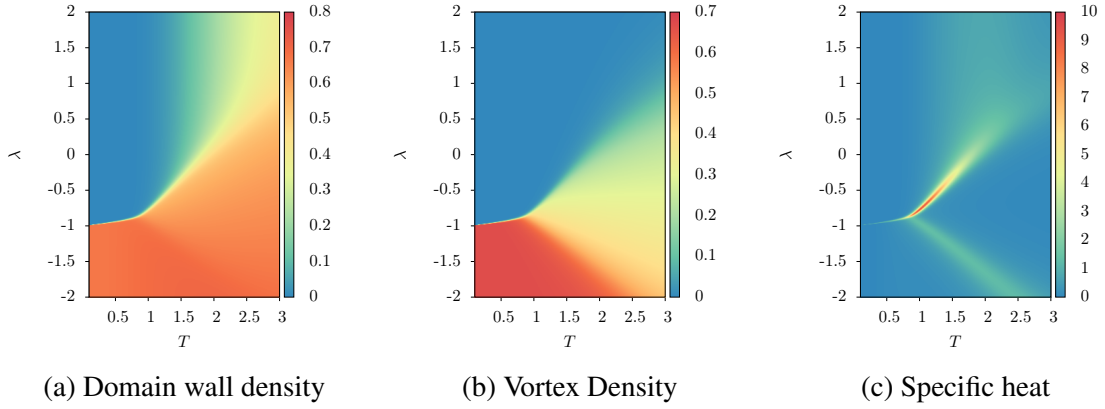


Figure 6.7: Densities of domain walls and vortex strings and the specific heat obtained using Wang-Landau algorithm for the \mathbb{Z}_3 ferromagnet on a $L = 4$ simple cubic lattice is shown over the parameter space of temperature T and suppression strength λ .

parameter space of λ and T using the Wang-Landau algorithm.

We find that similar to the two dimensional case, the three dimensional model exhibits a sudden increase in the densities of domain walls and vortices at large negative values of λ along the zero temperature axis (Fig. 6.7). In addition, the specific heat shows a stronger peak which shifts to higher temperatures as λ grows more negative. Although the observables show the presence of a phase transition from a low temperature phase at large negative λ to the disordered phase, we have not been able to characterize the phase using a vortex based sublattice order parameter as we did in the two dimensional case. This is because the vortex strings in the low temperature phase do not show complete sublattice ordering (Fig. 6.8b). However, they do not form a random tangle in this phase either. We have attempted to sustain a sublattice ordering by initializing the system with a flux lattice structure (Fig. 6.8a). However, over the course of our Monte Carlo simulation, the structure disintegrates, but only in patches. Formulating a suitable order parameter which captures the transition from this vortex condensate phase to the disordered phase therefore remains as an open problem.

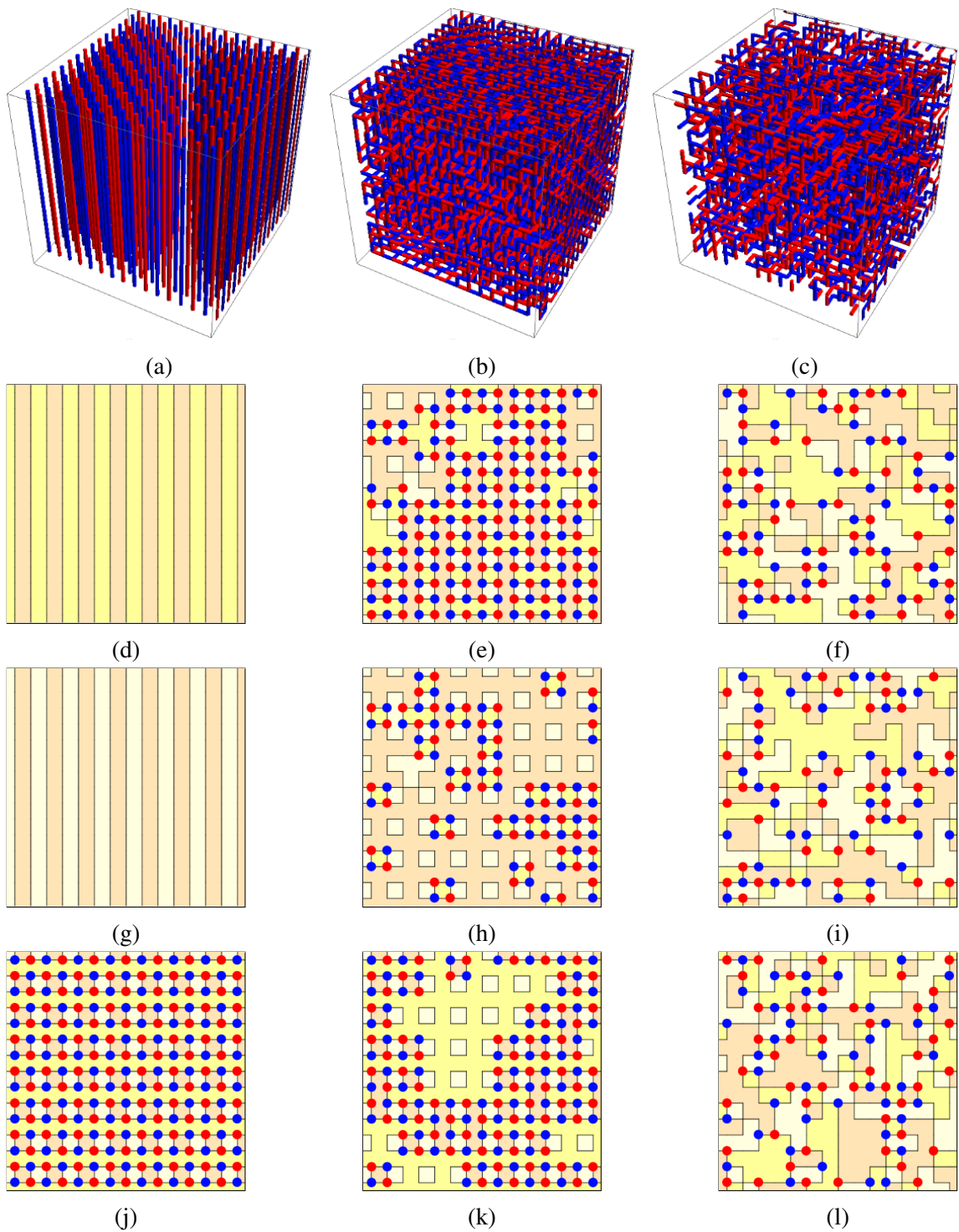


Figure 6.8: Upon initializing the three dimensional \mathbb{Z}_3 ferromagnet on the simple cubic lattice in a manner such that it exhibits a flux lattice structure for the vortex strings (a), the lattice structure breaks down into a vortex condensate (b) over the course of Monte Carlo simulation at $T = 0.5$ with $\lambda = -1.2$. The vortex condensate clearly has more structure than the arrangement of vortex strings at $T = 2.0$ in the disordered phase (c). The panels below the configurations show two dimensional slices along the three different axes of the corresponding configurations.

Chapter 7

Conclusion

The existence of various phases characterized by different signatures of manifested symmetry, which has been the main topic of discussion in this thesis, appear ubiquitously across statistical, quantum condensed matter and high energy physics. By considering a minimal model which exhibits these phases, we have investigated the underlying mechanism that drives the phase transitions and leads to the formation of these phases. While previous attempts to understand the nature of these phases have relied on techniques based on symmetry and mappings onto random cluster models, we have approached the problem using the role played by topological defects as a guiding principle.

We have shown that the order-disorder transitions in simple models, like the three-state Potts, Ashkin-Teller and six-state clock models, are driven by a coupled proliferation of domain walls and vortices. By decoupling the transition using vortex suppression, we have uncovered intermediate phases which are either symmetry enhanced, symmetry broken or partially symmetry broken. Some of the phases that have been discussed in this work are summarized here.

Model	Defect Manipulated	Phases	Sec.
2D \mathbb{Z}_3	none	order-disorder	2.1.5
	vortex weak suppress	order-disorder	2.2.2
	vortex strong suppress	order-QLRO-disorder	2.2.3
	vortex full suppress	order-QLRO	2.2.3
	vortex weak enhance	order-disorder	6.2
	vortex strong enhance	order- $v\bar{v}l$ -disorder	6.2.1
	vortex full enhance	$v\bar{v}l$ -disorder	6.2.1
2D \mathbb{Z}_4	none	order-disorder	3.4
	vortex full suppress	order-partial order	3.4
	vortex + $d w_{\pm\pi}$ full suppress	order-QLRO	3.6
2D \mathbb{Z}_5	none	order-QLRO-disorder	3.5
	vortex full suppress	order-QLRO	3.5
2D \mathbb{Z}_6	none	order-QLRO-disorder	3.7
	vortex full suppress	order-partial order	3.7
	vortex + $d w_{\pm\pi}$ full suppress	order-QLRO	3.7
2D \mathbb{Z}_3 antiferro	none	disorder	3.8
	ferro \mathbb{Z}_6 vortex full suppress	partial order	3.8
	ferro \mathbb{Z}_6 vortex + $d w_{\pm\pi}$ full suppress	QLRO	3.8

Model	Defect Manipulated	Phases	Sec.
3D \mathbb{Z}_3	none	order-disorder	4.2.1
	vortex weak suppress	order-disorder	4.3.1
	vortex strong suppress	order-partial order-disorder	4.3.2
	vortex full suppress	order-partial order	4.3.2
	vortex weak enhance	order-disorder	6.7
	vortex weak enhance	order-vortex cond.-disorder	6.7
	vortex full enhance	vortex cond.-disorder	6.7
3D \mathbb{Z}_4	none	order-disorder	4.5
	vortex + $d w_{\pm\pi}$ full suppress	order-partial order	4.5

We have shown that symmetry enhancement in two dimensions, which is associated with quasi-long-range order, is driven by the percolation of domain walls. However, none of the individual types of domain walls percolate on their own in the quasi-long-range ordered phase. We have discovered that the standard method for calculating vortex winding number contains a flaw which stems from its adherence to modular arithmetic. We have proposed a modified calculation which remedies the flaw. Using the modified method we have correctly identified the role of defects in systems with even number of spin states. This correction has turned out to be crucial for ferromagnets as well as antiferromagnets. In particular, it has revealed that the transition from quasi-long-range order to disorder is not driven solely by vortices, but by a combination of vortices and $\pm\pi$ domain walls.

We have found that symmetry enhancement is replaced by partial symmetry breaking in three dimensions. We have observed that individual types of domain walls percolate on their own in these partial symmetry broken phases. In addition, the proliferation of defects belonging to subgroups of the model's symmetry has been found to play a crucial role in the formation of intermediate phases.

While our results have focussed on the nature of the phases, we have not been able to ascertain the nature of the phase transitions due to computational difficulties. One factor

contributing to this difficulty has been the calculation of winding number at all the vertices of the lattice in each step of the update algorithm. Due to the irregular location of the vertices, which contribute to the winding number calculation, vectorization [158] of the update algorithms has proven to be difficult. This implementation-based slowdown has been amplified by the critical slowing down related to large autocorrelation times observed at the transition and throughout the quasi-long-range ordered phase. The issue of critical slowing down, in particular, is generally avoided by using cluster algorithms. However, we are not aware of any cluster algorithm which can take into account plaquette based computation, like the one required for the winding number calculation at each vertex. Meron cluster algorithms appear to incorporate plaquette interactions [159]. It would, therefore, be interesting to study how such an algorithm can be adapted to the problem of vortex suppression. Such an algorithm would not only allow better characterization of the phases, but also allow simulation of larger systems which are required for finite size scaling and reliable calculation of critical exponents.

The interesting feature of vortex suppression is that it can, in turn, suppress defects in models with other symmetries. Models with $O(3)$ symmetries sustain monopole defects in three dimensions and skyrmion defects in two dimensions. A discrete version of the $O(3)$ model is the tetrahedron model or simply the four-state Potts model. This model would exhibit the discrete versions of monopole and skyrmion defects. However, suppression of extended defects like skyrmions is difficult. Since the plaquette based suppression of discrete vortices effectively suppresses discrete skyrmions, we can obtain insights into the physics of these defects indirectly by using vortex suppression techniques. This, in turn, can provide insights into the behavior of skyrmions in quantum antiferromagnets. For example, can the Heisenberg antiferromagnet exhibit an emergent $U(1)$ phase when skyrmions are suppressed? Similar methods of suppression can be used to search for symmetry enhancement in models with non-Abelian discrete symmetries [160–164]. The dodecahedron model, for example, shows a symmetry enhanced intermediate phase, the physics of which is closely related to the existence of asymptotic freedom in the Yang-

Mills theory [160–162]. A closely related model, the icosahedron model does not show such an intermediate phase [162]. Can vortex suppression in this model open up such a phase?

We have considered the behavior of defects in the equilibrium regime. Non-equilibrium behavior of defects is an equally important topic [165, 166]. It is surprising that a substantial amount of work has gone into studying the coarsening behavior of domains and the evolution of domain walls in spin models with discrete states [167–170]. However, the non-equilibrium behavior of vortices in these models has not been studied. We have shown that the phase diagram of these models in the equilibrium regime is governed by the proliferation of domain walls and vortices. Therefore, research into the evolution of these defects in the non-equilibrium regime is a natural step forward. The non-equilibrium behavior of vortex strings during quenching in multiferroics has become a topic of interest [8, 9, 171]. Our results suggest that an investigation into the behavior of three-fold vortex strings, apart from that of six-fold vortex strings, will be able to shed light on the nature of intermediate phases in these systems.

This work demonstrates that the study of defects responsible for driving phase transitions combined with the study of symmetries used for characterizing the transitions provides a powerful toolkit for understanding the behavior of systems across condensed matter and high energy physics. It is our hope that this toolkit will be used to, not only discover but also, synthesize new phases of matter with interesting properties and beneficial applications.

Bibliography

- [1] Lev Davidovich Landau. On the theory of phase transitions. i. *Zh. Eksp. Teor. Fiz.*, 11:19, 1937.
- [2] Sidney Coleman. *Aspects of Symmetry: Selected Erice lectures*. Cambridge University Press, 1988.
- [3] Benjamin Svetitsky and Laurence G Yaffe. Critical behavior at finite-temperature confinement transitions. *Nuclear Physics B*, 210(4):423–447, 1982.
- [4] Tammay Vachaspati and Alexander Vilenkin. Formation and evolution of cosmic strings. *Physical Review D*, 30(10):2036, 1984.
- [5] T Senthil, Ashvin Vishwanath, Leon Balents, Subir Sachdev, and Matthew PA Fisher. Deconfined quantum critical points. *Science*, 303(5663):1490–1494, 2004.
- [6] R Ganesh, Jeroen van den Brink, and Satoshi Nishimoto. Deconfined criticality in the frustrated heisenberg honeycomb antiferromagnet. *Physical Review Letters*, 110(12):127203, 2013.
- [7] Sumiran Pujari, Kedar Damle, and Fabien Alet. Néel-state to valence-bond-solid transition on the honeycomb lattice: Evidence for deconfined criticality. *Physical Review Letters*, 111(8):087203, 2013.

- [8] SC Chae, N Lee, Y Horibe, M Tanimura, S Mori, B Gao, S Carr, and S-W Cheong. Direct observation of the proliferation of ferroelectric loop domains and vortex-antivortex pairs. *Physical Review Letters*, 108(16):167603, 2012.
- [9] Shi-Zeng Lin, Xueyun Wang, Yoshitomo Kamiya, Gia-Wei Chern, Fei Fan, David Fan, Brian Casas, Yue Liu, Valery Kiryukhin, Wojciech H Zurek, et al. Topological defects as relics of emergent continuous symmetry and higgs condensation of disorder in ferroelectrics. *Nature Physics*, 2014.
- [10] Jorge V José, Leo P Kadanoff, Scott Kirkpatrick, and David R Nelson. Renormalization, vortices, and symmetry-breaking perturbations in the two-dimensional planar model. *Physical Review B*, 16(3):1217, 1977.
- [11] Jürg Fröhlich and Thomas Spencer. Massless phases and symmetry restoration in abelian gauge theories and spin systems. *Communications in Mathematical Physics*, 83(3):411–454, 1982.
- [12] Cintia M Lapilli, Peter Pfeifer, and Carlos Wexler. Universality away from critical points in two-dimensional phase transitions. *Physical Review Letters*, 96(14):140603, 2006.
- [13] Z Ding, DW Bullock, PM Thibado, VP LaBella, and Kieran Mullen. Atomic-scale observation of temperature and pressure driven preroughening and roughening. *Physical Review Letters*, 90(21):216109, 2003.
- [14] Seung Ki Baek, Petter Minnhagen, and Beom Jun Kim. True and quasi-long-range order in the generalized q-state clock model. *Physical Review E*, 80(6):060101, 2009.
- [15] Oleg Borisenko, Gennaro Cortese, Roberto Fiore, Mario Gravina, and Alessandro Papa. Numerical study of the phase transitions in the two-dimensional z (5) vector model. *Physical Review E*, 83(4):041120, 2011.

- [16] O Borisenko, V Chelnokov, G Cortese, R Fiore, M Gravina, and A Papa. Phase transitions in two-dimensional $z(n)$ vector models for $n > 4$. *Physical Review E*, 85(2):021114, 2012.
- [17] Yuta Kumano, Koji Hukushima, Yusuke Tomita, and Masaki Oshikawa. Response to a twist in systems with $z(p)$ symmetry: The two-dimensional p -state clock model. *Physical Review B*, 88(10):104427, 2013.
- [18] Seung Ki Baek, Harri Mäkelä, Petter Minnhagen, and Beom Jun Kim. Residual discrete symmetry of the five-state clock model. *Physical Review E*, 88(1):012125, 2013.
- [19] Christophe Chatelain. Dmrg study of the berezinskii–kosterlitz–thouless transitions of the 2d five-state clock model. *Journal of Statistical Mechanics: Theory and Experiment*, 2014(11):P11022, 2014.
- [20] Daniel Blankschtein, M Ma, A Nihat Berker, Gary S Grest, and CM Soukoulis. Orderings of a stacked frustrated triangular system in three dimensions. *Physical Review B*, 29(9):5250, 1984.
- [21] PD Scholten and LJ Irakliotis. Critical behavior of the q -state clock model in three dimensions. *Physical Review B*, 48(2):1291, 1993.
- [22] Seiji Miyashita. Nature of the ordered phase and the critical properties of the three dimensional six-state clock model. *Journal of the Physical Society of Japan*, 66(11):3411–3420, 1997.
- [23] Masaki Oshikawa. Ordered phase and scaling in $z(n)$ models and the three-state antiferromagnetic potts model in three dimensions. *Physical Review B*, 61(5):3430, 2000.
- [24] Jie Lou, Anders W Sandvik, and Leon Balents. Emergence of $u(1)$ symmetry in the 3d xy model with zq anisotropy. *Physical Review Letters*, 99(20):207203, 2007.

- [25] Christian Maes and Senya Shlosman. Rotating states in driven clock-and xy-models. *Journal of Statistical Physics*, 144(6):1238–1246, 2011.
- [26] Aernout CD Van Enter, Christof Külske, and Alex A Opoku. Discrete approximations to vector spin models. *Journal of Physics A: Mathematical and Theoretical*, 44(47):475002, 2011.
- [27] Oleg Borisenko, Volodymyr Chelnokov, Gennaro Cortese, Mario Gravina, Alessandro Papa, and Ivan Surzhikov. Phase transitions in the three-dimensional z(n) models. *arXiv preprint arXiv:1311.0471*, 2013.
- [28] Koos Rommelse and Marcel den Nijs. Preroughening transitions in surfaces. *Physical Review Letters*, 59(22):2578, 1987.
- [29] Peter B Weichman and Anoop Prasad. Zippering and intermeshing: Novel phase diagrams for interfaces and films. *Physical Review Letters*, 76(13):2322, 1996.
- [30] Hideo Shioda and Yohtaro Ueno. An incompletely-ordered phase in the two-dimensional 6-state general clock model with next-nearest-neighbor interactions. *Journal of the Physical Society of Japan*, 62(12):4224–4232, 1993.
- [31] Ruth V Ditzian, Jayanth R Banavar, GS Grest, and Leo P Kadanoff. Phase diagram for the ashkin-teller model in three dimensions. *Physical Review B*, 22(5):2542, 1980.
- [32] P Pawlicki, G Kamieniarz, and L Debski. Monte carlo analysis of the extended ashkin-teller model. *Physica A: Statistical Mechanics and its Applications*, 242(1):290–298, 1997.
- [33] C Fan. On critical properties of the ashkin-teller model. *Physics Letters A*, 39(2):136, 1972.

- [34] Norikazu Todoroki, Yohtaro Ueno, and Seiji Miyashita. Ordered phase and phase transitions in the three-dimensional generalized six-state clock model. *Physical Review B*, 66(21):214405, 2002.
- [35] Frithjof Karsch and Sven Stickan. The three-dimensional, three-state potts model in an external field. *Physics Letters B*, 488(3):319–325, 2000.
- [36] Pierre Ramond and HM Fried. Field theory: A modern primer. *Physics Today*, 35:57, 1982.
- [37] Leo P Kadanoff. Multicritical behavior at the kosterlitz-thouless critical point. *Annals of Physics*, 120(1):39–71, 1979.
- [38] Yohtaro Ueno. Description of ordering and phase transitions in terms of local connectivity: Proof of a novel type of percolated state in the general clock model. *Journal of Statistical Physics*, 80(3-4):841–873, 1995.
- [39] Yohtaro Ueno and Katsumi Kasono. Incompletely ordered phases and phase transitions in the three-dimensional general clock model. *Physical Review B*, 48(22):16471, 1993.
- [40] Norikazu Todoroki. Generalized cubic model for batio₃-like ferroelectric substance. *Journal of the Physical Society of Japan*, 76(1):015002, 2007.
- [41] N David Mermin. The topological theory of defects in ordered media. *Reviews of Modern Physics*, 51(3):591, 1979.
- [42] Paul M Chaikin and Tom C Lubensky. *Principles of condensed matter physics*, volume 1. Cambridge Univ Press, 2000.
- [43] David R Nelson. *Defects and geometry in condensed matter physics*. Cambridge University Press, 2002.
- [44] Alexander Vilenkin and E Paul S Shellard. *Cosmic strings and other topological defects*. Cambridge University Press, 2000.

- [45] Lars Onsager. Statistical hydrodynamics. *Il Nuovo Cimento (1943-1954)*, 6:279–287, 1949.
- [46] RP Feynman. Progress in low temperature physics. *Vol. I North-Holland, Amsterdam*, page 17, 1955.
- [47] VL Berezinskii. Destruction of long-range order in one-dimensional and two-dimensional systems having a continuous symmetry group i. classical systems. *Sov. Phys. JETP*, 32(3):493–500, 1971.
- [48] John Michael Kosterlitz and David James Thouless. Ordering, metastability and phase transitions in two-dimensional systems. *Journal of Physics C: Solid State Physics*, 6(7):1181, 1973.
- [49] H Kleinert. Gauge field theory of vortex lines in 4 he and the superfluid phase transition. *Physics Letters A*, 93(2):86–90, 1982.
- [50] Greg Kohring, Robert E Shrock, and Peter Wills. Role of vortex strings in the three-dimensional o (2) model. *Physical Review Letters*, 57(11):1358, 1986.
- [51] Greg Kohring and Robert E Shrock. Properties of a generalized 3d o (2) model with suppression/enhancement of vortex strings. *Nuclear Physics B*, 288:397–418, 1987.
- [52] Subodh R Shenoy. Vortex-loop scaling in the three-dimensional xy ferromagnet. *Physical Review B*, 40(7):5056, 1989.
- [53] Subodh R Shenoy. Enhancement and suppression of the transition temperature of a three-dimensional xy ferromagnet by control of vortex-loop fugacity. *Physical Review B*, 42(13):8595, 1990.
- [54] Biplab Chattopadhyay, Mangal C Mahato, and Subodh R Shenoy. Vortex-loop crinkling in the three-dimensional xy model: Numerical evidence in support of an ansatz. *Physical Review B*, 47(22):15159, 1993.

- [55] Subodh R Shenoy and Biplab Chattopadhyay. Anisotropic three-dimensional xy model and vortex-loop scaling. *Physical Review B*, 51(14):9129, 1995.
- [56] VMH Ruutu, VB Eltsov, AJ Gill, TWB Kibble, M Krusius, Yu G Makhlin, B Placais, GE Volovik, and Wen Xu. Vortex formation in neutron-irradiated superfluid ^3He as an analogue of cosmological defect formation. 1996.
- [57] Gary A Williams. Vortex-loop phase transitions in liquid helium, cosmic strings, and high- T_c superconductors. *Physical Review Letters*, 82(6):1201, 1999.
- [58] Nicole Bontemps, Yvan Bruynseraede, Guy Deutscher, and Aharon Kapitulnik. *The vortex state*. Springer, 1994.
- [59] Elmar Bittner, Axel Krinner, and Wolfhard Janke. Vortex-line percolation in the three-dimensional complex $|\psi|^4$ model. *arXiv preprint cond-mat/0510347*, 2005.
- [60] Suman Sinha and Soumen Kumar Roy. Role of topological defects in the phase transition of a modified x y model: A monte carlo study. *Physical Review E*, 81(4):041120, 2010.
- [61] Philip W Anderson. *Basic notions of condensed matter physics*, volume 55. Addison Wesley Publishing Company, 1984.
- [62] Je Phillips. *Physics of high- T_c superconductors*. Elsevier, 2012.
- [63] MR Beasley, JE Mooij, and TP Orlando. Possibility of vortex-antivortex pair dissociation in two-dimensional superconductors. *Physical Review Letters*, 42(17):1165, 1979.
- [64] CHANDAN Dasgupta and BI Halperin. Phase transition in a lattice model of superconductivity. *Physical Review Letters*, 47(21):1556, 1981.
- [65] Biplab Chattopadhyay and Subodh R Shenoy. Kosterlitz-thouless signatures from 3d vortex loops in layered superconductors. *Physical Review Letters*, 72(3):400, 1994.

- [66] Zlatko Tesanović. Extreme type-ii superconductors in a magnetic field: A theory of critical fluctuations. *Physical Review B*, 59(9):6449, 1999.
- [67] AK Nguyen and A Sudbø. Topological phase fluctuations, amplitude fluctuations, and criticality in extreme type-ii superconductors. *Physical Review B*, 60(22):15307, 1999.
- [68] J Hove and A Sudbø. Anomalous scaling dimensions and stable charged fixed point of type-ii superconductors. *Physical Review Letters*, 84(15):3426, 2000.
- [69] BI Halperin and David R Nelson. Theory of two-dimensional melting. *Physical Review Letters*, 41(2):121, 1978.
- [70] David R Nelson and BI Halperin. Dislocation-mediated melting in two dimensions. *Physical Review B*, 19(5):2457, 1979.
- [71] AP Young. Melting and the vector coulomb gas in two dimensions. *Physical Review B*, 19(4):1855, 1979.
- [72] CA Murray and DH Van Winkle. Experimental observation of two-stage melting in a classical two-dimensional screened coulomb system. *Physical Review Letters*, 58(12):1200, 1987.
- [73] Klaus Zahn, R Lenke, and Georg Maret. Two-stage melting of paramagnetic colloidal crystals in two dimensions. *Physical Review Letters*, 82(13):2721, 1999.
- [74] MR Sadr-Lahijany, P Ray, and HE Stanley. Melting driven by particle size-dispersity: a study in two dimensions. *Physica A: Statistical Mechanics and its Applications*, 270(1):295–300, 1999.
- [75] Paul E Lammert, Daniel S Rokhsar, and John Toner. Topology and nematic ordering. *Physical Review Letters*, 70(11):1650, 1993.
- [76] Paul E Lammert, Daniel S Rokhsar, and John Toner. Topology and nematic ordering. i. a gauge theory. *Physical Review E*, 52(2):1778, 1995.

- [77] John Toner, Paul E Lammert, and Daniel S Rokhsar. Topology and nematic ordering. ii. observable critical behavior. *Physical Review E*, 52(2):1801, 1995.
- [78] Gregory Kohring and Robert E Shrock. Generalized isotropic-nematic phase transitions: Critical behavior of 3d p n models. *Nuclear Physics B*, 285:504–518, 1987.
- [79] NV Priezjev and Robert A Pelcovits. Disclination loop behavior near the nematic-isotropic transition. *Physical Review E*, 64(3):031710, 2001.
- [80] TC Lubensky, David Petey, Nathan Currier, and Holger Stark. Topological defects and interactions in nematic emulsions. *Physical Review E*, 57(1):610, 1998.
- [81] OD Lavrentovich. Topological defects in dispersed words and worlds around liquid crystals, or liquid crystal drops. *Liquid crystals*, 24(1):117–126, 1998.
- [82] Maurice Kleman and Oleg D Lavrentovich. Topological point defects in nematic liquid crystals. *Philosophical Magazine*, 86(25-26):4117–4137, 2006.
- [83] Man-hot Lau and Chandan Dasgupta. Numerical investigation of the role of topological defects in the three-dimensional heisenberg transition. *Physical Review B*, 39(10):7212, 1989.
- [84] Michael Kamal and Ganpathy Murthy. New o (3) transition in three dimensions. *Physical Review Letters*, 71(12):1911, 1993.
- [85] Olexei I Motrunich and Ashvin Vishwanath. Emergent photons and transitions in the o (3) sigma model with hedgehog suppression. *Physical Review B*, 70(7):075104, 2004.
- [86] Martin B Einhorn and Robert Savit. Topological excitations in the abelian higgs model. *Physical Review D*, 17(10):2583, 1978.
- [87] Michael E Peskin. Mandelstam-'t hooft duality in abelian lattice models. *Annals of Physics*, 113(1):122–152, 1978.

- [88] Graham Vincent, Nuno D Antunes, and Mark Hindmarsh. Numerical simulations of string networks in the abelian-higgs model. *Physical Review Letters*, 80(11):2277, 1998.
- [89] Sandro Wenzel, Elmar Bittner, Wolfhard Janke, and Adriaan MJ Schakel. Percolation of vortices in the 3d abelian lattice higgs model. *Nuclear physics B*, 793(1):344–361, 2008.
- [90] G't Hooft. Topology of the gauge condition and new confinement phases in non-abelian gauge theories. *Nuclear Physics B*, 190(3):455–478, 1981.
- [91] N_K Nielsen and P Olesen. An unstable yang-mills field mode. *Nuclear Physics B*, 144(2):376–396, 1978.
- [92] Jan Ambjørn and Poul Olesen. On the formation of a random color magnetic quantum liquid in qcd. *Nuclear Physics B*, 170(1):60–78, 1980.
- [93] M Hindmarsh and A Rajantie. Defect formation and local gauge invariance. *Physical Review Letters*, 85(22):4660, 2000.
- [94] Arttu Rajantie. Defect formation in the early universe. *Contemporary Physics*, 44(6):485–502, 2003.
- [95] Martin B Einhorn, Robert Savit, and Eliezer Rabinovici. A physical picture for the phase transitions in z_n symmetric models. *Nuclear Physics B*, 170(1):16–31, 1980.
- [96] Cornelis Marius Fortuin and Piet W Kasteleyn. On the random-cluster model: I. introduction and relation to other models. *Physica*, 57(4):536–564, 1972.
- [97] A Coniglio and W Klein. Clusters and ising critical droplets: a renormalisation group approach. *Journal of Physics A: Mathematical and General*, 13(8):2775, 1980.

- [98] Wolfhard Janke and Adriaan MJ Schakel. Geometrical phase transitions. *Computer Physics Communications*, 169(1):222–225, 2005.
- [99] Wolfhard Janke and Adriaan MJ Schakel. Fractal structure of spin clusters and domain walls in the two-dimensional ising model. *Physical Review E*, 71(3):036703, 2005.
- [100] Abbas Ali Saberi. Thermal behavior of spin clusters and interfaces in the two-dimensional ising model on a square lattice. *Journal of Statistical Mechanics: Theory and Experiment*, 2009(07):P07030, 2009.
- [101] T Blanchard. Wrapping probabilities for ising spin clusters on a torus. *Journal of Physics A: Mathematical and Theoretical*, 47(34):342002–342012, 2014.
- [102] R André, Paulo Murilo C de Oliveira, and Jeferson J Arenzon. Domain-size heterogeneity in the ising model: Geometrical and thermal transitions. *Physical Review E*, 91(4):042113, 2015.
- [103] MN Najafi. Observation of schramm–loewner evolution on the geometrical clusters of the ising model. *Journal of Statistical Mechanics: Theory and Experiment*, 2015(5):P05009, 2015.
- [104] Wolfhard Janke and Adriaan MJ Schakel. Geometrical vs. fortuin–kasteleyn clusters in the two-dimensional q-state potts model. *Nuclear Physics B*, 700(1):385–406, 2004.
- [105] K Lukierska-Walasek and K Topolski. Statistical description of magnetic domains in the two dimensional ising model. *Computational Methods in Science and Technology*, 16(2):173–176, 2010.
- [106] K Lukierska-Walasek and K Topolski. Statistical description of domains in the potts model. *arXiv preprint arXiv:0901.0315*, 2009.

- [107] Jérôme Dubail, Jesper Lykke Jacobsen, and Hubert Saleur. Bulk and boundary critical behaviour of thin and thick domain walls in the two-dimensional potts model. *Journal of Statistical Mechanics: Theory and Experiment*, 2010(12):P12026, 2010.
- [108] Jérôme Dubail, Jesper Lykke Jacobsen, and Hubert Saleur. Critical exponents of domain walls in the two-dimensional potts model. *Journal of Physics A: Mathematical and Theoretical*, 43(48):482002, 2010.
- [109] Frank Winter, Wolfhard Janke, and Adriaan MJ Schakel. Geometric properties of the three-dimensional ising and x y models. *Physical Review E*, 77(6):061108, 2008.
- [110] Abbas Ali Saberi and Horr Dashti-Naserabadi. Three-dimensional ising model, percolation theory and conformal invariance. *EPL (Europhysics letters)*, 92(6):67005, 2010.
- [111] Eduardo Fradkin and Leonard Susskind. Order and disorder in gauge systems and magnets. *Physical Review D*, 17(10):2637, 1978.
- [112] Rudolf Peierls. On ising's model of ferromagnetism. In *Mathematical Proceedings of the Cambridge Philosophical Society*, volume 32, pages 477–481. Cambridge Univ Press, 1936.
- [113] AI Belousov and Yu E Lozovik. Topological phase transition in 2d quantum josephson array. *Solid State Communications*, 100(6):421–426, 1996.
- [114] Cristian Rojas and Jorge V José. Critical properties of two-dimensional josephson-junction arrays with zero-point quantum fluctuations. *Physical Review B*, 54(17):12361, 1996.
- [115] G Ortiz, E Cobanera, and Z Nussinov. Dualities and the phase diagram of the p-clock model. *Nuclear Physics B*, 854(3):780–814, 2012.

- [116] N David Mermin and Ho Wagner. Absence of ferromagnetism or antiferromagnetism in one-or two-dimensional isotropic heisenberg models. *Physical Review Letters*, 17(22):1133, 1966.
- [117] Wolfgang Bietenholz, Urs Gerber, and Fernando G Rejón-Barrera. Berezinskii–kosterlitz–thouless transition with a constraint lattice action. *Journal of Statistical Mechanics: Theory and Experiment*, 2013(12):P12009, 2013.
- [118] Hikaru Kawamura and Macoto Kikuchi. Free-vortex formation and topological phase transitions of two-dimensional spin systems. *Physical Review B*, 47(2):1134, 1993.
- [119] Fa-Yueh Wu. The potts model. *Reviews of Modern Physics*, 54(1):235, 1982.
- [120] David P Landau and Kurt Binder. *A guide to Monte Carlo simulations in statistical physics*. Cambridge university press, 2014.
- [121] Robert H Swendsen and Jian-Sheng Wang. Nonuniversal critical dynamics in monte carlo simulations. *Physical Review Letters*, 58(2):86, 1987.
- [122] Ulli Wolff. Collective monte carlo updating for spin systems. *Physical Review Letters*, 62(4):361, 1989.
- [123] Dietrich Stauffer and Amnon Aharony. *Introduction to percolation theory*. CRC press, 1994.
- [124] L Chayes and J Machta. Graphical representations and cluster algorithms i. discrete spin systems. *Physica A: Statistical Mechanics and its Applications*, 239(4):542–601, 1997.
- [125] L Chayes, D McKellar, and B Winn. Percolation and gibbs states multiplicity for ferromagnetic ashkin-teller models on. *Journal of Physics A: Mathematical and General*, 31(45):9055, 1998.

- [126] P Archambault, ST Bramwell, and PCW Holdsworth. Magnetic fluctuations in a finite two-dimensional model. *Journal of Physics A: Mathematical and General*, 30(24):8363, 1997.
- [127] JM Kosterlitz. The critical properties of the two-dimensional xy model. *Journal of Physics C: Solid State Physics*, 7(6):1046, 1974.
- [128] Rodney J Baxter. *Exactly Solved Models in Statistical Mechanics*. Courier Corporation, 2007.
- [129] John L Cardy. Antiferromagnetic clock models in two dimensions. *Physical Review B*, 24(9):5128, 1981.
- [130] Jayanth R Banavar, GS Grest, and David Jasnow. Ordering and phase transitions in antiferromagnetic potts models. *Physical Review Letters*, 45(17):1424, 1980.
- [131] RJ Baxter. Critical antiferromagnetic square-lattice potts model. In *Proceedings of the Royal Society of London A: Mathematical, Physical and Engineering Sciences*, volume 383, pages 43–54. The Royal Society, 1982.
- [132] MP Nightingale and M Schick. Three-state square lattice potts antiferromagnet. *Journal of Physics A: Mathematical and General*, 15(1):L39, 1982.
- [133] Ikuo Ono. Occurrence of kosterlitz-thouless-like phase transition in antiferromagnetic potts models. *Journal of the Physical Society of Japan*, 53(12):4102–4105, 1984.
- [134] Jiii Kolafa. Monte carlo study of the three-state square potts antiferromagnet. *Journal of Physics A: Mathematical and General*, 17(14):L777, 1984.
- [135] Cristopher Moore, Mats G Nordahl, Nelson Minar, and Cosma Shalizi. Vortex dynamics and entropic coulomb forces in ising and potts antiferromagnets and ice models. *arXiv preprint cond-mat/9902200*, 1999.

- [136] Junseong Heo and Tanmay Vachaspati. Z_3 strings and their interactions. *Physical Review D*, 58(6):065011, 1998.
- [137] AM Allega. Vortices in potts models. *Physics Letters A*, 155(2):169–173, 1991.
- [138] AM Allega. Phase diagram by frustrated vortices in potts models. *Physics Letters A*, 167(4):405–410, 1992.
- [139] Wolfhard Janke and Ramon Villanova. Three-dimensional 3-state potts model revisited with new techniques. *Nuclear Physics B*, 489(3):679–696, 1997.
- [140] Alain Billoire, Robert Lacaze, and André Morel. The z_3 three dimensional potts model with anti-ferromagnetic admixture. *Nuclear Physics B-Proceedings Supplements*, 17:230–233, 1990.
- [141] Richard Zallen. Polychromatic percolation: coexistence of percolating species in highly connected lattices. *Physical Review B*, 16(4):1426, 1977.
- [142] Roman Kotecký. Long-range order for antiferromagnetic potts models. *Physical Review B*, 31(5):3088, 1985.
- [143] Jian-Sheng Wang, Robert H Swendsen, and Roman Kotecký. Antiferromagnetic potts models. *Physical Review Letters*, 63(2):109, 1989.
- [144] Aloysius P Gottlob and Martin Hasenbusch. Three-state anti-ferromagnetic potts model in three dimensions: universality and critical amplitudes. *Physica A: Statistical Mechanics and its Applications*, 210(1):217–236, 1994.
- [145] Miroslav Kolesik and Masuo Suzuki. On the low-temperature ordering of the 3d antiferromagnetic three-state potts model. *Journal of Physics A: Mathematical and General*, 28(23):6543, 1995.
- [146] Ralf K Heilmann, Jian-Sheng Wang, and Robert H Swendsen. Rotationally symmetric ordered phase in the three-state antiferromagnetic potts model. *Physical Review B*, 53(5):2210, 1996.

- [147] Shou-Cheng Zhang. Vortex-antivortex lattice in superfluid films. *Physical Review Letters*, 71(13):2142, 1993.
- [148] Jun Hu and AH MacDonald. Two-dimensional vortex lattice melting. *Physical Review Letters*, 71(3):432, 1993.
- [149] Marc Gabay and Aharon Kapitulnik. Vortex-antivortex crystallization in thin superconducting and superfluid films. *Physical Review Letters*, 71(13):2138, 1993.
- [150] W Vincent Liu and Congjun Wu. Atomic matter of nonzero-momentum bose-einstein condensation and orbital current order. *Physical Review A*, 74(1):013607, 2006. staggered vortex-antivortex lattice found on an optical lattice.
- [151] M Zehetmayer. How the vortex lattice of a superconductor becomes disordered: a study by scanning tunneling spectroscopy. *Scientific Reports*, 5, 2015.
- [152] Somesh Chandra Ganguli, Harkirat Singh, Garima Saraswat, Rini Ganguly, Vivas Bagwe, Parasharam Shirage, Arumugam Thamizhavel, and Pratap Raychaudhuri. Disordering of the vortex lattice through successive destruction of positional and orientational order in a weakly pinned $\text{Co}_0.0075\text{NbSe}_2$ single crystal. *Scientific Reports*, 5, 2015.
- [153] Aernout CD Van Enter and Senya B Shlosman. First-order transitions for n-vector models in two and more dimensions: Rigorous proof. *Physical Review Letters*, 89(28):285702, 2002.
- [154] JE Van Humbergen. From continuous to first-order transition in a simple xy model. *Physical Review Letters*, 53(1):5, 1984.
- [155] Fugao Wang and DP Landau. Efficient, multiple-range random walk algorithm to calculate the density of states. *Physical Review Letters*, 86(10):2050, 2001.

- [156] Fugao Wang and DP Landau. Determining the density of states for classical statistical models: A random walk algorithm to produce a flat histogram. *Physical Review E*, 64(5):056101, 2001.
- [157] Yup Kim and A Brooks Harris. Hysteretic behavior of the site-diluted ising anti-ferromagnet in uniform applied fields. *Physical Review B*, 32(7):4676, 1985.
- [158] D Barkai, KJM Moriarty, and C Rebbi. A highly optimized vectorized code for monte carlo simulations of su (3) lattice gauge theories. *Computer Physics Communications*, 32:1–9, 1984.
- [159] Shailesh Chandrasekharan and Uwe-Jens Wiese. Meron-cluster solution of fermion sign problems. *Physical Review Letters*, 83(16):3116, 1999.
- [160] Adrian Patrascioiu and Erhard Seiler. Is the 2d o (3) nonlinear σ model asymptotically free? *Physics Letters B*, 430(3):314–319, 1998.
- [161] Adrian Patrascioiu and Erhard Seiler. Discrete symmetry enhancement in non-abelian models and the existence of asymptotic freedom. *Physical Review D*, 64(6):065006, 2001.
- [162] Adrian Patrascioiu and Erhard Seiler. Testing asymptotic scaling and nonabelian symmetry enhancement. *Physics Letters B*, 532(1):135–140, 2002.
- [163] Roman Krcmar, Andrej Gendiar, and Tomotoshi Nishino. Phase diagram of truncated tetrahedral model. *arXiv preprint arXiv:1512.09059*, 2015.
- [164] Oleg Borisenko, Volodymyr Chelnokov, Francesca Cuteri, and Alessandro Papa. Bkt phase transitions in two-dimensional non-abelian spin models. *arXiv preprint arXiv:1512.05737*, 2015.
- [165] Kyozi Kawasaki. Topological defects and non-equilibrium. *Progress of Theoretical Physics Supplement*, 79:161–190, 1984.

- [166] Yuriy M Bunkov and Henri Godfrin. *Topological defects and the non-equilibrium dynamics of symmetry breaking phase transitions*, volume 549. Springer Science & Business Media, 2012.
- [167] Gary S Grest, Michael P Anderson, and David J Srolovitz. Domain-growth kinetics for the q-state potts model in two and three dimensions. *Physical Review B*, 38(7):4752, 1988.
- [168] Elizabeth A Holm, James A Glazier, David J Srolovitz, and Gary S Grest. Effects of lattice anisotropy and temperature on domain growth in the two-dimensional potts model. *Physical Review A*, 43(6):2662, 1991.
- [169] Clément Sire and Satya N Majumdar. Correlations and coarsening in the q-state potts model. *Physical review letters*, 74(21):4321, 1995.
- [170] Clément Sire and Satya N Majumdar. Coarsening in the q-state potts model and the ising model with globally conserved magnetization. *Physical Review E*, 52(1):244, 1995.
- [171] SM Griffin, M Lilienblum, KT Delaney, Y Kumagai, M Fiebig, and NA Spaldin. Scaling behavior and beyond equilibrium in the hexagonal manganites. *Physical Review X*, 2(4):041022, 2012.